ESTROGEN-INDUCED NEUROPROTECTION IS MEDIATED BY AN INCREASE IN CASPASE-12-ASSOCIATED APOPTOSIS FOLLOWING MCAO

A Thesis

Submitted to the Graduate Faculty

In Partial Fulfillment of the Requirements

For the Degree of

Master of Science

In the Department of Biomedical Sciences

Faculty of Veterinary Medicine

University of Prince Edward Island

Karen M. Crosby

Charlottetown, P.E.I.

Your file Votre référence
ISBN: 978-0-494-22825-8
Our file Notre référence
ISBN: 978-0-494-22825-8

CONDITIONS FOR USE OF THESIS

The author has agreed that the Library, University of Prince Edward Island, may make this thesis freely available for inspection. Moreover, the author has agreed that permission for extensive copying of this thesis for scholarly purposes may be granted by the professor or professors who supervised the thesis work recorded herein or, in their absence, by the Chair of the Department or the Dean of the Faculty in which the thesis work was done. It is understood that due recognition will be given to the author of this thesis and to the University of Prince Edward Island in any use of the material in this thesis. Copying or publication or any other use of the thesis for financial gain without approval by the University of Prince Edward Island and the author's written permission is prohibited.

Requests for permission to copy or to make any other use of material in this thesis in whole or in part should be addressed to:

Chair of the Department of Biomedical Sciences

Faculty of Veterinary Medicine

University of Prince Edward Island

Charlottetown, P. E. I.

Canada C1A 4P3

SIGNATURE PAGES

iii-iv

REMOVED

ABSTRACT

Estrogen has received considerable attention over the past decade as a potential therapeutic agent against various forms of neurodegenerative diseases including stroke. Experimental data in animal models of stroke have provided exhaustive evidence of the neuroprotective properties of this steroid hormone. Our laboratory in particular has demonstrated that estrogen significantly reduces (~50%) ischemic cell death resulting from permanent occlusion of the middle cerebral artery (MCAO). However, the cellular and molecular mechanisms implicated in the protective actions of estrogen in this experimental model have yet to be elucidated. Accumulating evidence suggests that endoplasmic reticulum stress-induced apoptosis is linked to ischemic cell death and that estrogen interacts with various components of the endoplasmic reticulum stress response. We therefore hypothesized that estrogen enhances endoplasmic reticulum stress-associated apoptosis via activation of caspase-12 to decrease necrotic cell death, thus limiting infarct volume. Estrogen significantly decreased procaspase-12 expression in both the infarct and peri-infarct regions at 1 hour post-MCAO and this corresponded with an increase in active caspase-12 at 2 and 3 hours post-MCAO. An increase in m-calpain expression was observed in the infarct region at 1 hour post-MCAO with estrogen treatment, suggesting m-calpain may play a role in activating caspase-12 following MCAO. TUNEL staining of brain sections showed a significantly higher number of TUNEL positive cells in estrogen treated animals at 4 hours post-MCAO compared to those treated with saline. The amount of necrotic cell death following MCAO was assessed by the presence of lactate dehydrogenase (LDH) in the cerebrospinal fluid (CSF) surrounding the frontal cortex and the results indicated a significant elevation in LDH levels following MCAO compared to sham occlusion. However, estrogen treatment did not decrease the concentration of LDH in the CSF following MCAO when compared to saline treatment. Overall, these data are consistent with the hypothesis that the protective actions of estrogen observed following permanent MCAO in male rats involve an increase in caspase-12 mediated apoptotic cell death.

ACKNOWLEDGEMENTS

The author wishes to thank Dr. Tarek Saleh, Dr. Alastair Cribb, Dr. Cathy Chan, and Dr. Alfonso Lopez for their guidance and support. The author would also like to thank Mr Barry Connell, MSc for his assistance. This work was supported by a grant from the Heart and Stroke Foundation of Prince Edward Island and the Canadian Institutes of Health Research.

TABLE OF CONTENTS

LIST OF TABLES

LIST OF FIGURES

List of Abbreviations

aCSF – artificial cerebrospinal fluid
AF – activation function
AMPA – α-amino-3-hydroxy-5-methyl-4-isoxazolepropionic acid
Apaf-1 – apoptotic protease activating factor 1
ATF6
ATP – adenosine triphosphate
Bcl-2
BDNF – brain-derived neurotrophic factor
CAD – caspase-activated DNase
cAMP – cyclic adenosine monophosphate
CARD – caspase-activation recruitment domain
CED-3 ??
CLM – caveolar-like microdomain
CREB – cAMP-response-element-binding protein
CSF – cerebrospinal fluid
CVD – cardiovascular disease
DAB – 3,3'diaminobenzidine
dATP
DFF - deoxyribonucleic acid fragmentation factor
DISC – death inducing signaling complex
DNA – deoxyribonucleic acid
DNA-PK - deoxyribonucleic acid protein kinase
ECG – electrocardiogram
eIF-2α – eukaryotic translation initiation factor-2-alpha
EnR – endoplasmic reticulum
ER – estrogen receptor
ER-α – estrogen receptor alpha
ER-β – estrogen receptor beta
ERAD – endoplasmic reticulum-associated degradation
ERE – estrogen response element
ER-X – estrogen receptor-X
FADD – Fas-associated death domain protein
GADD153 – growth arrest and DNA damage 153
GAP43
GRP78 – glucose regulated protein 78
GRP94 – glucose regulated protein 94
IC – insular cortex
IP_3R – inositol 1,4,5-triphosphate receptor
IRE1 –
LBD – ligand binding domain
LDH – lactate dehydrogenase
MAPK – mitogen-activated protein kinase
MCA – middle cerebral artery
MCAO – middle cerebral artery occlusion

mRNA – messenger ribonucleic acid
NGF – nerve growth factor
NMDA –
NT/N – neurotensin/neuromedin
OGD – oxygen glucose deprivation
PARP – poly-adenosine diphosphate-ribose polymerase
PBS – phosphate buffered saline
PDI – protein disulfide isomerase
PERK – PKR-like endoplasmic reticulum kinase
PS – phosphatidylserine
RyR – ryanodine receptor
SCD – sudden cardiac death
SERCA – sarco-endoplasmic reticulum Ca^{2+}-ATPase
SOD – superoxide dismutase
tBid – truncated bid
TIA – transient ischemic attack
TNF – tumor necrosis factor
TNFR – tumor necrosis factor receptor
TRADD – tumor necrosis factor receptor-associated death domain protein
TRAF2 – tumor necrosis factor receptor –associated factor 2
TTC – 2,3,5-triphenoltetrazolium chloride
TUNEL – terminal deoxynucleotidyl transferase-mediated deoxyuridine triphosphate nick end-labeling
UPR – unfolded protein response
XBP1 – x-box binding protein 1

CHAPTER 1. INTRODUCTION

1.1 *Cardiovascular disease*

Cardiovascular disease refers to the class of diseases that affect the heart, the vasculature of the heart, and the arterial and venous systems throughout the body and within the brain. Cardiovascular diseases (CVD) such as coronary artery disease, stroke, myocardial infarction and atherosclerosis account for the death of more Canadians than any other disease. In 2002 alone, CVD accounted for 74, 626 Canadian deaths, of those approximately 20 % were due to stroke (1).

1.2 *Cerebrovascular Disease (Stroke)*

Cerebrovascular disease (stroke), when considered separately from other cardiovascular diseases, ranks fourth among all causes of death in Canada (1). In 1999, stroke accounted for 7% of all Canadian deaths. Stroke is a leading cause of serious, long-term disability in Canada. The high mortality and morbidity rate associated with stroke costs the Canadian economy an estimated $2.7 billion annually (1).

Stroke refers to the neurological dysfunction that results from a sudden or gradual disruption in blood flow to certain regions of the brain (2). The inadequate perfusion causes hypoxia and hypoglycemia, leading to cellular death and cerebral infarction if the flow of blood is not immediately restored (3, 4).

Strokes are classified according to their pathophysiology and can be grouped in two categories: hemorrhagic and ischemic strokes (5). Hemorrhagic strokes have a relatively low incidence, accounting for approximately 12% of all strokes. They occur when a cerebral blood vessel in the subarachnoid space (subarachnoid) or within the

brain (intracerebral) ruptures (1). The subsequent bleeding interrupts the normal flow of blood, and causes edema and compression of surrounding brain tissue (6, 7).

The more common type of stroke is ischemic or occlusive, which accounts for approximately 88% of strokes, and occurs when there is an interruption in blood flow due to obstruction of a cerebral blood vessel. The occlusion most frequently develops as a result of a buildup of atherosclerotic plaque and subsequent clot formation in a cerebral artery, referred to as a thrombotic stroke (6). An embolic stroke is caused by a moving blood clot or plaque broken off from an atherosclerotic vessel that travels from its origin, often lodging at arterial bifurcations within the brain (6). A transient ischemic attack (TIA) is similar to an ischemic stroke in that it involves occlusion of a cerebral artery. However, the neurologic deficit associated with a TIA lasts less than 24 hours and the disturbance in cerebral blood flow is restored before infarction occurs (4). Although only minor damage may result, a transient ischemic attack may provide warning of a subsequent ischemic stroke (6).

The majority of ischemic strokes involve the middle cerebral artery (MCA), a major cerebral vessel that is a direct continuation of the carotid artery (8). The MCA is the most frequent site for embolic strokes (6). This is most likely due to the large territory of the vessel and the position of the MCA at the end of the internal carotid artery, causing it to offer the path of least resistance compared to the anterior and posterior cerebral arteries (6). The MCA supplies a portion of the prefrontal cortex known as the insular cortex (IC) (9). The IC is a forebrain nucleus involved in the regulation of autonomic and visceral (including cardiovascular) function (9). The IC receives taste, gastrointestinal, respiratory and cardiovascular afferent inputs, and has rich

reciprocal connections with a variety of regions including the contralateral insular cortex, adjacent cortical regions, and the parabrachial nucleus in the pons (10).

1.2.1 *Cardiovascular consequences of stroke*

Accumulated evidence from both animal and human studies suggests that the insular cortex plays a major role in the abnormalities in cardiac function that commonly result from stroke. The involvement of the insular cortex in the regulation of cardiovascular function was demonstrated in rats by Oppenheimer and colleagues (11). In their study, stimulation of the IC resulted in electrocardiographic (ECG) changes including alteration of the P wave, widening of the QRS complex and depression of the ST segment (11). Stimulation of the IC also resulted in an increase in the plasma catecholamine, norepinephrine, indicating increased activation of the sympathetic nervous system (12). These autonomic and cardiac consequences have been shown to frequently occur following permanent occlusion of the middle cerebral artery (MCAO) in animals, which results in a focal lesion primarily involving the insular cortex (13). Following MCAO in cats, an elevation in both plasma epinephrine and norepinephrine were reported (14), and this corresponded with myocardial damage (14, 15). Myocardial lesions and necrotic cell death, as indicated by elevated levels of serum cardiac enzymes including creatine phosphokinase, have been shown to occur following stroke (16, 17). Evidence from animal models of stroke also suggests that an asymmetry of sympathetic and subsequent cardiac consequences exists. Hachinski et al. (18) demonstrated that occlusion of the right, but not left, MCA resulted in a prolonged increase in sympathetic nerve activity, an elevation in plasma norepinephrine, and abnormalities in ECG recordings.

Similar results have been observed in humans: Goldstein et al. (19) reported that 92 % of the 150 patients with acute stroke in their study showed ECG abnormalities, the most common changes being prolongation of the QT interval, abnormal U waves, tachycardia, and atrial fibrillation. Other studies have reported similar findings with tachycardia, and atrial and ventricular fibrillation being among the cardiac arrhythmias that most often resulted from stroke (20, 21). A hemispheric lateralization in sympathetic activity following MCAO, similar to what has been shown in animals, has also been demonstrated in humans. Elevated plasma catecholamines resulted from a right, but not left, hemispheric stroke involving the insular cortex (22). The most important consequence of these stroke-induced cardiovascular disturbances in humans is sudden cardiac death (SCD). With an annual mortality of 5-10% in stroke victims, SCD represents the most frequent cause of death following stroke (23). SCD, as well as cardiac arrhythmias and stroke, have been reported to occur less frequently in women compared to men (24), as will be discussed in detail below.

1.3 *Gender difference in stroke incidence*

It is well recognized that pre-menopausal women have a lower incidence of cardiovascular disease (25, 26), including stroke (27), compared to men. However, this protection diminishes as women approach menopause, such that after the age of 45, a greater percentage of women than men die from a stroke each year. In 2001, 8.4% of female deaths in Canada resulted from stroke, compared to 5.7% for men (28). The fact that this protection from stroke-induced mortality is lost by the perimenopausal years, suggests that female reproductive hormones may play a role in this sex difference. Pre-menopausal females have higher levels of circulating estrogens, principally 17β-estradiol

(29). However, estrogen levels diminish as females approach menopause due to the cessation in production of this steroid hormone in the ovarian follicles (29). The fact that declining levels of plasma estrogen correspond with an increasing incidence of stroke in females has led researchers to speculate and investigate the possible neuroprotective effects of estrogen in animal models of stroke.

1.4 *Estrogen neuroprotection and gender*

A similar beneficial effect of estrogen has been observed in animal studies in which cerebral ischemia has been experimentally induced. Studies have reported that female animals experience substantial protection from stroke compared with their male counterparts (30, 31), and this benefit disappears upon removal of plasma estrogen following ovariectomy (32). Alkayed et al. (33) observed that female rats had a smaller infarct size and higher cerebral blood flow in a transient MCAO/reperfusion model of ischemia compared with male and ovariectomized female rats. The effect of fluctuating endogenous estrogen levels on ischemic brain injury in female animals was also investigated: rats in proestrus (high estrogen levels) had a significant reduction in infarct volume following permanent MCAO in comparison with those in metestrus (low estrogen levels) (34).

The effect of exogenous estrogen has been well documented to provide protection in a variety of animal models of cerebral ischemia. The beneficial effects of this steroid hormone are consistent across different stroke models, including transient MCAO followed by reperfusion, and permanent MCAO (reviewed in (35)). Both chronic (7-10 day) and acute (30-120 minute) pretreatments of estrogen significantly reduce infarct volume in both ovariectomized female and intact male rats (33, 35-40). Post ischemic

treatment of estrogen is also beneficial: Yang and colleagues (41) reported a therapeutic window of approximately 3 hours following permanent MCAO during which estrogen could be administered and still exert neuroprotective effects.

Our laboratory has demonstrated that the intravenous administration of 17β-estradiol 30 minutes prior to permanent MCAO significantly reduced the lesion size by approximately 50% (see Figure 1) (42). This protection was observed within the first 4 hours following the stroke. Specifically, at 3 and 4 hours post-MCAO, estrogen dramatically reduced the size of the infarct in comparison to the saline treated group (see Figure 2) (43). Further, injection of estrogen directly into the insular cortex prior to MCAO resulted in a similar decrease in infarct volume (44). However, coinjection of estrogen with the potent estrogen receptor (ER) antagonist ICI-182,780, prevented the estrogen-induced reduction in infarct volume (44). This suggests that the protective effects of estrogen in this stroke model are mediated through an ER.

1.4.1 *Estrogen receptors*

Estrogen may mediate its effects by binding to an ER, a member of the steroid hormone nuclear receptor superfamily (29). ERs function as ligand-activated transcription factors that, when bound to an agonist such as 17β-estradiol, interact with specific DNA sequences to modulate transcription of estrogen-regulated genes (45).

Two subtypes of the estrogen receptor have been identified thus far: the classical ER-α and the more recently cloned ER-β (46). ER-α and ER-β share similar structural organization: they both consist of a central DNA binding domain, an activation function domain (AF-1) in the amino terminus, and a ligand binding domain (LBD) in the carboxy-terminal region, in which a second activation function (AF-2) resides (45, 47).

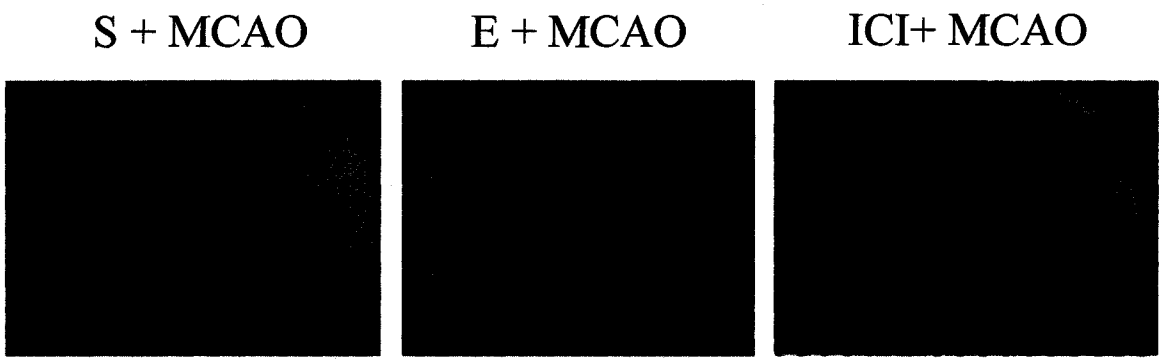

Figure 1. Representative digital photographs of coronal brain slices illustrating the extent of the infarct size within the cortex after MCAO following either saline (S), estrogen (E) (30 minutes prior to MCAO) or ICI-182,780 (ICI) injections into the insular cortex. (Reproduced with permission from Saleh et al. (42)).

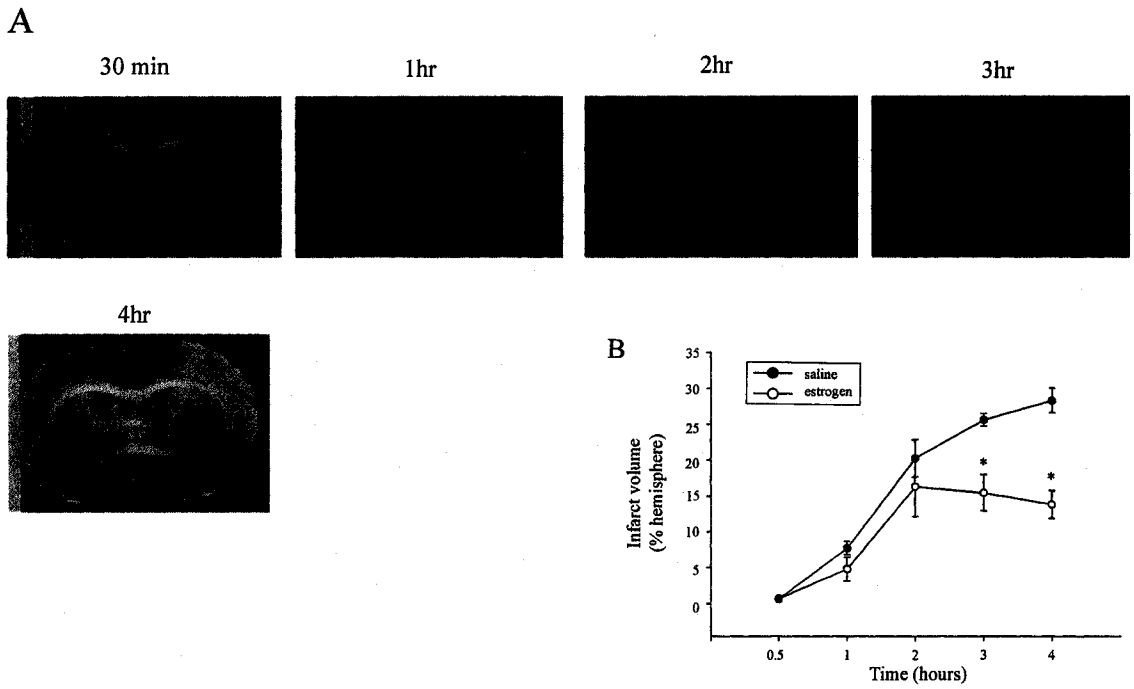

Figure 2. (A) Representative digital photographs illustrating the extent of the infarct size within the cortex at progressive time points following MCAO with saline pretreatment. (B) Graphic representation of the change in infarct volume (measured as percentage of the hemisphere) following MCAO with either saline or estrogen pretreatment. (Reproduced with permission from Saleh et al. (43)).

Both AF-1 and AF-2 are responsible for the activation of gene transcription following binding of the ligand (48).

Estrogen is found in the circulation bound to sex-hormone-binding globulin. When free from this glycoprotein, estrogen can freely diffuse across the plasma membrane (40), or be actively transported by megalin, a recently characterized transport protein localized on the surface of the cell (49). Once inside the cell, estrogen binds to the ER, thus liberating the receptor from its inhibitory chaperone complex consisting of heat shock proteins and immunophilins (45, 50). This leads to receptor dimerization and subsequent binding of the hormone-receptor complex to specific sequences of DNA, referred to as estrogen response elements (EREs) (51, 52). EREs are localized in the promoter region of target estrogen responsive genes. The resulting effect is a modulation, either enhancement or suppression, of transcription of the ERE-containing genes. Although estrogen receptors can directly interact with the transcriptional machinery (47), other factors such as co-activators and co-repressors are also thought to play a role in the process (50).

Besides the "classical" genomic action, there is a growing body of evidence that the rapid effects of estrogen may be mediated through other signaling mechanisms. Such effects are characterized by their rapid onset (within seconds to minutes) and insensitivity to inhibitors of DNA transcription and protein synthesis (53). Evidence is accumulating that ER-α and ER-β may mediate some rapid effects of estrogen. For example, the estrogen-ER-α complex has been shown to associate with phosphatidylinositol 3-kinase, resulting in activation of the Akt serine/threonine kinase (54). Both ER-α and ER-β have

been shown to rapidly activate the mitogen-activated protein kinase (MAPK) signal transduction pathway in a variety of cell types including neurons (55, 56).

It has also been proposed that the rapid effects of estrogen are mediated through receptors with pharmacological properties distinct from those of the "classical" nuclear receptors. Evidence is accumulating that a plasma membrane ER may mediate the rapid effects of estrogen that cannot be explained by transcriptional mechanisms (53). This membrane-bound ER, designated ER-X (57) has yet to be completely characterized, but appears to be structurally related to ER-α and β. Evidence suggests that this plasma membrane receptor is concentrated within caveolar-like microdomains (CLMs) of neuronal plasma membranes, the neuron-specific homologs of caveolae (57, 58). CLMs also contain a variety of proteins that have been implicated in signal transduction pathways, therefore it is likely that ER-X may mediate some of the rapid effects of estrogen through the initiation of various signaling pathways.

ERs have been proposed to exist within the endoplasmic reticulum (EnR) (for a review, see (59)). Parikh et al (60) identified high affinity binding sites for estrogen in calf uterine microsomes. Estrogen binding sites within the EnR have also been characterized in the rabbit (61) and rat uterus (62, 63). While little is known about these microsomal ER-like proteins, Muldoon et al. (62) suggested some possible roles including modulation of estrogen's access to nuclear receptors and formation of functional complexes that may translocate to extranuclear sites to alter non-genomic cellular processes. More recently, protein disulfide isomerase (PDI) has been shown to be an extensive estrogen binding protein within the EnR, which may facilitate binding of estrogen to the ER (64).

1.4.2 *The role of ER-α and ER-β in neuroprotection*

ER-α and ER-β mRNA and protein are widely distributed throughout the central nervous system (CNS) of the rat (46). Although striking differences exist in the abundance and distribution of the expression of these receptor subtypes throughout the CNS, there is also a significant overlap (46). In the rat brain, both ER-α and β have been identified in the cerebral cortex, however there appears to be a temporal distribution of these receptor subtypes in this region. ER-α is expressed in the cerebral cortex in developing female rats, whereas ER-β is not detected at this early stage (65). At later stages of development, both receptor subtypes are expressed, and finally, ER-β appears to be the predominant estrogen receptor in the cerebral cortex in adult rats (46, 66). Zhang et al. (67) have detected high levels of ER-β in the cerebral cortex of both male and female adult rats.

To date, the issue about which ER subtype plays a predominant role in estrogenic neuroprotection has not been resolved. Despite the minimal presence of ER-α mRNA in the cerebral cortex (46), several laboratories have demonstrated that this receptor subtype plays a critical role in estrogen-mediated neuroprotection in animal models of cerebral ischemia (68-70). For example, Merchenthaler and colleagues (68) noted that ER-α was responsible for mediating the neuroprotective actions of estrogen following permanent MCAO. They showed that the penumbra (detailed in section 1.5) contained a large number of ER-α mRNA-expressing and ER-α-immunoreactive cells and this was only observed on the ipsilateral, and not the contralateral side. Dubal et al. (69) reported that deletion of ER-β in ER-β knockout mice had no effect on the estrogen–induced protection following ischemia in mice, whereas the protective actions of estrogen were

completely abolished in ER-α knockout mice. In a more recent study, Dubal et al. (70) investigated the temporal expression of ER-α following permanent MCAO and reported a significant ER-α mRNA induction in the ischemic region early in the development of the infarct. Although a great deal of evidence supports the role of ER-α in estrogen-induced neuroprotection in animal models of ischemia, ER-β has also been shown to mediate the beneficial effects of estrogen. Wang et al. (71) indicated the importance of ER-β in neuronal survival as developmental abnormalities occurred in ER-β knockout mice. In addition, activation of ER-β was shown to promote neuroprotection against glutamate excitotoxicity in hippocampal neurons (72). Although the exact role of the ER subtypes in estrogen neuroprotection has not yet been determined, there is unquestionable evidence that genomic mechanisms of action play a significant role in the protective actions of estrogen.

1.4.3 *Mechanisms of estrogen-induced neuroprotection mediated by genomic actions*

The genomic neuroprotective actions of estrogen involve promoting neuronal survival through the induction of axonal and dendritic sprouting (73, 74), and the promotion of synaptogenesis (75). These actions are accomplished through an induction in transcription of genes that code for structural proteins such as neurofilament proteins, microtubules (76), and GAP43, a phosphoprotein that has been implicated in both axonal elongation and synaptogenesis in the rat hypothalamus (77). Estrogen has also been documented to increase the expression of numerous neurotrophins including nerve growth factor (NGF) (78) and brain-derived neurotrophic factor (BDNF) (79), which directly support the vital functions of neurons. Other neuroprotective target genes include apoptotic/anti-apoptotic genes. Evidence suggests that the protective actions of

estrogen may be mediated through modulation of the Bcl-2 family of genes, to which both apoptotic and anti-apoptotic genes belong (78, 80) and this has been proposed as a mechanism of estrogen-induced protection following cerebral ischemia (81, 82).

The transcriptional effects of estrogen are not limited to genes that contain EREs, because several studies have indicated that estrogen may promote gene transcription through cross-talk with intracellular signaling mechanisms to exert its neuroprotective effects. Estrogen may promote survival and plasticity through interaction with MAPK signaling pathway (52). For example, activation of the MAPK pathway has been implicated in estrogen-induced neuroprotection against glutamate toxicity in cortical neurons (58, 83). The indirect transcriptional effects of estrogen may also involve interaction with cAMP pathways via the cAMP-response-element-binding protein (CREB). Watters et al. (84) reported an estrogen-induced increase in transcription of the neurotensin/neuromedin (NT/N) gene that was mediated through an interaction with the cAMP/protein kinase A signal transduction cascade in the mouse brain. By interacting with various signaling cascades, estrogen can indirectly activate the transcription of genes that play a role in neuronal survival.

1.4.4 *Mechanisms of estrogen-induced neuroprotection mediated by non-genomic actions*

In addition to the genomic actions of estrogen, there is considerable evidence for non-genomic mechanisms of estrogen-induced neuroprotection. Following ischemia, estrogen has been reported to have vasodilatory (85), antioxidant (86) and anti-inflammatory (87) protective effects. A growing body of evidence indicates that estrogen alters glutamatergic neuronal activity and therefore may attenuate the glutamate

excitotoxicity (detailed in section 1.5) that is an important mechanism of injury in stroke. Both *in vitro* (88, 89) and *in vivo* (90) studies have shown that a rapid non-genomic action of estrogen protects neurons from glutamate excitotoxicity and subsequent cell death. *In vitro*, estrogen was found to preserve cortical neuronal viability and function in a glutamate toxicity model (89). *In vivo* microdialysis revealed a rapid and significant reduction in extracellular levels of glutamate with acute estrogen treatment following transient MCAO (90).

Taken together, the above evidence suggests that estrogen provides neuroprotection by decreasing cell death following stroke. As previously stated, our laboratory has demonstrated that estrogen significantly reduces ischemia-induced cell death (by ~50%) following permanent MCAO. In order to understand the possible mechanism for this estrogen-induced neuroprotection, the cellular and molecular events involved during ischemia will be briefly described.

1.5 *Cellular and molecular effects of ischemia*

Focal ischemia by MCAO results in the development of two main regions defined by the degree of cerebral blood flow: the core and the penumbra (91). Within the core, blood flow is reduced to less than 15% of normal perfusion (91). As the brain has a very high demand for oxygen and glucose, the disruption in circulation in the areas affected by the stroke leads to their rapid depletion. The residual oxygen within the brain is consumed within a few seconds, and within 2 minutes, glucose is reduced by over 80% (3). As a result, the mitochondria are no longer able to produce ATP and the cell resorts to anaerobic metabolism as a means of producing cellular energy (92). However, in the absence of oxygen, lactic acid accumulates via anaerobic glycolysis and causes a

decrease in cellular pH (93). If the much-needed oxygen and glucose are not quickly restored, permanent damage and cell death typically occur within 5-6 minutes. The molecular and cellular effects of ischemia are outlined in Figure 3.

Due to the lack of ATP within the infarct core, there is an abrupt and dramatic redistribution of ions across the plasma membrane, associated with membrane depolarization. K^+, Na^+ and Ca^{2+} are the main contributors to this "anoxic depolarization" (91). A massive efflux of K^+ from neurons occurs in the infarct core, mediated initially by the opening of voltage-dependent K^+ channels and later by failure of the Na^+/K^+ ATPase, an energy-dependent enzyme that pumps 2 K^+ in and 3 Na^+ out of the cell. The resultant increase in extracellular K^+ causes depolarization of surrounding neurons (94). Because Na^+ efflux is prevented due to the loss of ATP required for the Na^+/K^+ ATPase, a large increase in intracellular Na^+ results, leading to a marked increase in cellular water content and cerebral edema (95). In addition, a large influx of Ca^{2+} occurs early in ischemia. These ionic changes and the resulting depolarization of neurons lead to the excessive vesicular release of neurotransmitters, in particular, glutamate.

Glutamate is the major excitatory neurotransmitter in the central nervous system. Under non-ischemic conditions, the low level of extracellular glutamate (1-5 μM) is maintained by a presynaptic or astrocytic glutamate reuptake (91). However, following an ischemic insult, glutamate accumulates in the extracellular space and can reach a concentration of several hundred micromolar, resulting in overstimulation of ionotropic and metabotropic glutamate receptors (96). The ionotropic glutamate receptors, mainly NMDA and AMPA receptors, act as ligand gated Na^+ and Ca^{2+} channels and their

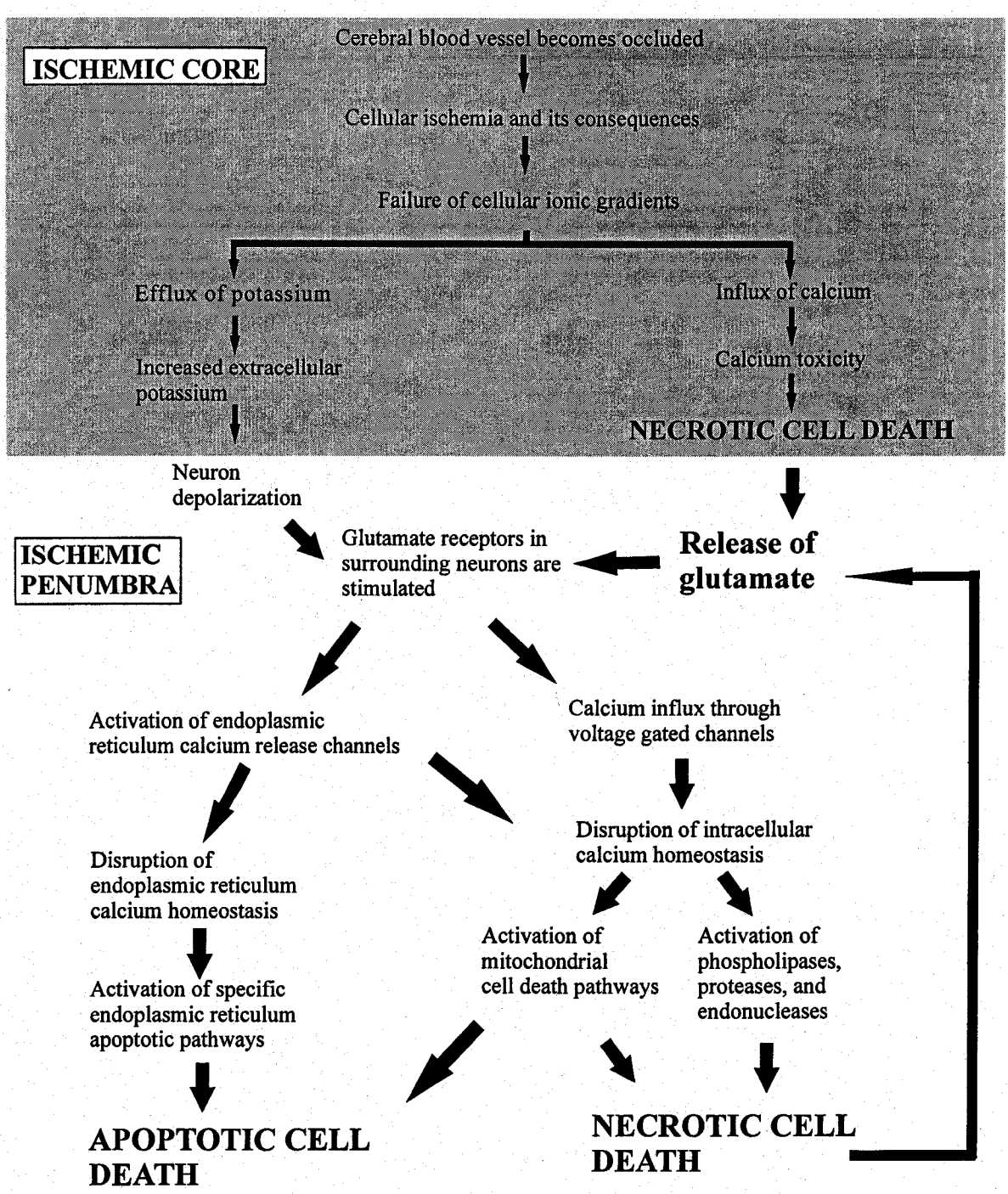

Figure 3. Molecular and cellular events proposed for the involvement of the endoplasmic reticulum in apoptotic and necrotic cell death following ischemic stroke. Other pathways may also be involved but are not illustrated here. Excitotoxicity following activation of glutamate receptors may directly and indirectly lead to disruption of endoplasmic reticulum calcium homeostasis, activating apoptotic and necrotic pathways. When necrotic pathways are activated, glutamate release and subsequent spreading depression may be enhanced. If cell death pathways are blocked or shifted towards apoptotic pathways, glutamate release and hence spreading depression is likely reduced (97).

prolonged activation results in increased excitability and intracellular calcium overload (91). A large elevation of calcium within the cell can have several consequences: activation of proteases, endonucleases, and phospholipases, the latter of which results in membrane degradation (91); formation of reactive oxygen species; and activation of cell death pathways (91, 93, 98). As this excitation and calcium overload continue, excitotoxic cell death occurs and results in a subsequent massive release of intracellular contents, including glutamate. This wave of depolarization from the ischemic core continues to spread and contributes to the cell death in the surrounding penumbra and is referred to as the "spreading depression" (91).

The penumbra is a region of tissue surrounding the infarct core that is physiologically impaired but potentially salvageable (99). Whether the cells in the penumbra survive depends on a number of factors including the timely return of adequate circulation, and the amount of toxic products released by neighboring necrotic cells. This region has less severely impaired cerebral circulation (approximately 40% of normal blood flow) (91) and as a result, the depletion of ATP is not as profound as in the infarct core. Also, extracellular glutamate levels are generally lower here than in the core, and therefore cells in the penumbra are not as susceptible to excitotoxicity and calcium overload (100). However, cells in the penumbra are "stressed" (see section 1.6.1 for details) by the mild hypoxia and hypoglycemia and therefore typically undergo apoptosis (91). Necrotic cell death has also been shown to occur in the penumbra (91). The glutamate released in the infarct core can stimulate glutamate receptors in the penumbra, resulting in Ca^{2+} influx and the subsequent sequence of events that occur in the core (noted above). Apoptosis can result from an elevation in intracellular calcium, also due

to overstimulation of glutamate receptors. However, this calcium influx is not as significant as that required to activate necrotic cell death pathways (91, 101). Cells that undergo apoptosis do not release their cellular contents as the plasma membrane remains intact, and thus do not contribute to the spreading depression of cell death (102). The EnR is an intracellular organelle involved in calcium homeostasis and therefore disruptions in calcium activates EnR pathways which contribute to the progressive spread of cell death following ischemia.

1.6 *Endoplasmic Reticulum*

The EnR is one of the largest intracellular organelles, constituting at least one-tenth the volume of the cell (103). It is a continuous membranous network of interconnected tubules and vesicles that extends throughout the cytoplasm from the nuclear envelope to the plasma membrane (103). The EnR is a multi-functional organelle that plays a vital role in many intracellular processes including synthesis, folding, and post-translational modification of proteins, synthesis of membrane lipids, as well as regulation of calcium storage and release (104-106).

The EnR is the major calcium storage compartment within the cell and plays a key role in the maintenance of intracellular calcium homeostasis (106). The normal function of the EnR requires a high concentration of calcium within the EnR lumen that typically ranges from 300-400 μM, compared to ~0.1 μM in the cytosol (105, 107). Calcium levels in the EnR are controlled by three transmembrane Ca^{2+} transporters: the inositol 1,4,5-triphosphate receptor (IP_3R) and the ryanodine receptor (RyR) release Ca^{2+} from the EnR, and this is counteracted by the sarco-endoplasmic reticulum Ca^{2+}-ATPase (SERCA) that functions to maintain the internal store of calcium by actively transporting

calcium back into the EnR from the cytosol (108). The maintenance of calcium homeostasis in the EnR is important for many cellular functions including intracellular signal transduction, apoptotic cell death, as well as the synthesis, modification and folding of proteins (104).

In addition to maintaining calcium homeostasis, the EnR also plays a fundamental role in protein synthesis, folding, and post-translational modification (109). Approximately one-third of all cellular proteins are synthesized in ribosomes embedded in the rough EnR (110). Prominent among these proteins are membrane-associated and integral membrane proteins as well as those destined for the secretory pathway (110). Prior to completion of translation, these proteins are translocated across the EnR membrane into the EnR lumen where they are quickly and accurately folded into their tertiary and quaternary structures (108). As these proteins travel through the EnR, a number are targeted for N-linked glycosylation, an event that influences protein folding (104). The unique oxidizing environment of the EnR lumen also promotes the formation of disulfide bonds between cysteine residues in the polypeptide chains. With the protein concentration in the EnR being approximately 100 mg/ml, the EnR demands constantly monitored protein processing to determine that the folding is being performed correctly (109, 111). A number of resident protein chaperones facilitate the protein folding process by preventing protein aggregation, ensuring the proteins are correctly folded before they are transported to their intracellular and extracellular destinations (112), and targeting misfolded proteins for degradation (107). Prominent among these chaperones are glucose regulated protein 78 (GRP78), GRP94, and PDI (108, 110). A disruption in one of the

major functions of the EnR, whether it be a disturbance in intracellular calcium homeostasis or improper protein folding, causes EnR stress (106).

1.6.1 *Endoplasmic reticulum stress*

EnR stress can result from a variety of conditions including hypoxia, glucose deprivation, ischemia, changes in calcium concentration, an over production of proteins, and failure of post-translational modifications in the EnR (reviewed in (107)). An alteration in either of the two key processes of calcium regulation and protein synthesis and modification can have profound effects on each other (106). For example, a disturbance in calcium homeostasis, manifested as a depletion of calcium from the EnR, can disrupt the chaperone and protein folding functions of the EnR. Conversely, an accumulation of unfolded proteins can alter EnR calcium homeostasis. In response to disturbances in calcium homeostasis and protein folding, the cell triggers an EnR stress response, termed the unfolded protein response (UPR) (104). The UPR is an adaptive cellular response that functions to relieve the stress through three different mechanisms: a transient attenuation in the rate of protein synthesis (113), an upregulation of genes encoding the molecular chaperones (113), and activation of EnR-associated degradation (ERAD) (114). These responses collectively minimize the accumulation and aggregation of misfolded proteins by decreasing the protein load on the EnR, thereby increasing the capacity of the EnR machinery for folding and degradation. If these cellular responses are not sufficient in relieving the stress, then specific EnR-associated cell death pathways are activated (115).

1.6.2 *Ischemia-induced endoplasmic reticulum stress*

The notion that EnR dysfunction may be involved in the pathogenesis of neuronal cell injury was first proposed in 1996 (116) where it was reported that the metabolic changes that occur during EnR stress highly resemble those produced during cerebral ischemia. Specifically, Paschen (116) observed that in transient ischemia, protein synthesis is attenuated as a result of phosphorylation and inactivation of the eukaryotic translation initiation factor eIF-2α, a protein specifically inactivated under conditions of EnR stress. During the UPR, eIF-2α is phosphorylated by the PKR-like endoplasmic reticulum kinase (PERK), resulting in an attenuation of protein synthesis to decrease the protein load on the EnR (117). Further evidence has been presented suggesting that PERK is activated in the reperfused brain following transient cerebral ischemia, also indicative of the involvement of EnR dysfunction in ischemic injury (118). Cerebral ischemia also causes an increased expression of certain EnR stress genes such as GRP78, GRP94, PDI and growth arrest and DNA damage 153 (GADD153) (119, 120). In a more recent study, Paschen and colleagues (121) showed that transient global and focal cerebral ischemia triggers processing of x-box protein 1 (xbp1) mRNA, an event necessary for the upregulation of genes involved in the EnR stress response. Once processed, xbp1 mRNA is translated into the XBP1 protein, a transcription factor that induces the expression of GRP78 and other EnR stress genes (121). The events involved in the EnR stress response are shown in Figure 4.

Disruption in EnR calcium homeostasis has also been implicated in cerebral ischemia. Prolonged stimulation of ionotropic glutamate receptors, due to the spreading depression described above, results in significant increases in intracellular calcium

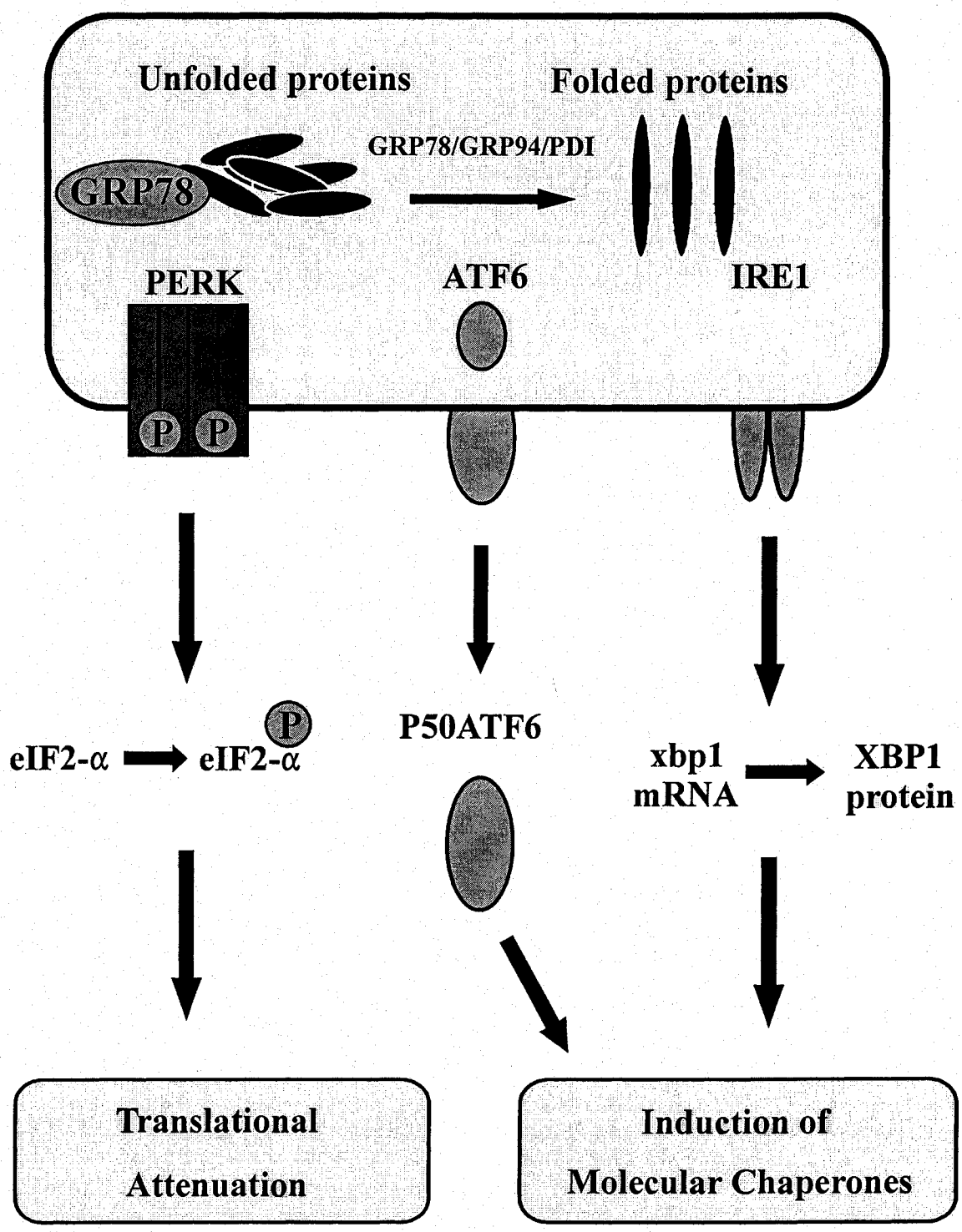

Figure 4. Mechanisms of cell survival in response to endoplasmic reticulum stress. Accumulation of unfolded proteins in the EnR activates the EnR stress sensors, PERK, ATF6, and IRE1 that result in translational attenuation and upregulation of transcription of genes encoding the molecular chaperones. The PERK-eIF2-α pathway and the IRE1-XBP1 pathwayare activated following ischemia, indicating that ER stress is an important event in this condition.

concentrations, thereby inducing EnR stress (95). It has recently been shown that dantrolene, an antagonist of the EnR ryanodine receptor, protects neurons against ischemic damage (122) suggesting that intracellular calcium plays a role in ER stress-induced cell death. In addition, Parsons and colleagues (123) showed a decrease in SERCA activity in the ischemic brain, indicative of dysfunction in ER calcium handling. These disruptions in protein folding and calcium homeostasis that occur during ischemia can result in activation of specific EnR-mediated cell death pathways.

1.7 *Mechanisms of cell death associated with EnR dysfunction*

EnR stress following an ischemic insult, has been shown to activate a number of proteases involved in cell death. Specifically, activation of caspase-12, a cysteine protease central to EnR stress-mediated apoptosis, has been implicated following both transient (124) and permanent (125) ischemia. In addition, increased levels of the cytoplasmic, calcium-dependent protease calpain, have been observed in cerebral ischemia. Once activated, calpains may result in either necrotic or apoptotic cell death, the latter of which may be mediated through activation of caspase-12 (126).

Agents which disrupt EnR function have been associated with the two main mechanisms of cell death: necrosis and apoptosis. Necrosis, or accidental cell death, is characterized by swelling of the cell, rupture of the plasma membrane, and subsequent uncontrolled release of inflammatory cellular contents (126). In contrast, apoptosis is an energy dependent, highly-regulated form of programmed cell death that results in the orderly removal of cellular remnants by phagocytosis before the integrity of the membrane is lost (127). Apoptosis and necrosis are not necessarily independent cell death pathways, but rather are two possible outcomes that may follow an initial common

insult or pathway. The predominant mode of cell death is decided by a number of factors including the intensity of the insult, level of ATP (128), and the time following the insult at which cell death is assessed (128,130). The nature of the injury is not decisive in determining whether the outcome is apoptotic or necrotic, because both types of cell death have been shown to result from the same insult (130). However, the severity and duration of the insult can play a major role in determining the mode of cell death. For example, Unal-Cevik (131) noted that apoptotic features have been shown to be more prevalent in short duration, transient ischemia followed by reperfusion, as well as shortly after permanent occlusion of the MCA. In fact, apoptotic cell death has been identified as early as 1 hour following permanent MCAO (132). Conversely, necrosis becomes the predominant form of cell death as the duration of ischemia increases (131). The level of ATP is also a deciding factor as to whether cells will undergo apoptosis or necrosis, with apoptosis preceding if there is a sufficient supply of ATP. However, depletion of ATP, as is observed in the ischemic core, shifts the mode of cell death from apoptosis to necrosis (91). Following ischemia, these mechanisms of cell death also follow a spatial distribution: necrotic cell death is predominant in the core of the infarct and usually occurs in tracts of contiguous cells (133). Apoptosis, on the other hand, typically occurs in cells scattered throughout the penumbral region (101).

1.7.1 *Necrotic cell death*

Necrosis has been described as a disordered mode of cell death, occurring in cases of severe and acute injuries, such as anoxia and sudden nutrient deprivation, or extreme injuries, such as heat stress and exposure to toxic agents (128). Regardless of the nature of the primary insult, ATP levels in the affected cells decrease to near zero in a matter of

seconds (3). Lowering of intracellular ATP is followed by a disruption in ionic homeostasis. One contributor to this change in the ionic balance is a rise in intracellular Na^+ levels due in large part to impairment of the plasma membrane Na^+/K^+ ATPase (134). This Na^+ overload is associated with an increase in cellular water content, and subsequent cell swelling (91). The intracellular organelles swell, and disruption of the organelle membranes occur (127). In some cases, chromatin condensation occurs along with random and diffuse fragmentation of the DNA (127). The disruption in ionic homeostasis also results in excessive influx of Ca^{2+}, due in part to the Na^+/Ca^{2+} exchanger operating in reverse mode, which leads to activation of cytoplasmic proteases, namely calpains. Upon activation, these proteases play a role in the progressive permeability of the plasma membrane, an event that occurs early in the death process (135). How calpain mediates the increase in plasma membrane permeability during necrotic cell death remains unknown. It was shown, however, that calpain cleaves important cytoskeleton proteins, and that this event is closely associated with increases in membrane permeability (135). Eventually, the activity of calpains, in conjunction with the excessive cellular swelling, results in complete rupture of the plasma membrane, causing uncontrolled release of the intracellular contents and stimulation of an immune response in the surrounding tissue (136).

The presence of lactate dehydrogenase (LDH) in the extracellular fluid is a common marker of cellular degeneration and necrotic cell death. LDH is an enzyme that catalyzes the interconversion of pyruvate and lactate (91). Under normal physiological conditions, LDH is confined to the intracellular environment, thus detection of LDH outside the cell indicates the release of cellular contents as a result of necrosis.

Measurement of LDH release from cells *in vitro* is a well established method to assess necrotic cell death (88, 137-139). In vivo, the presence of LDH in the cerebrospinal fluid (CSF) has been measured following cold-induced brain injury by *in vivo* microdialysis (140) and has been determined to be an appropriate indicator of necrotic cell death. In this study, Kihara and colleagues (140) investigated the effect of the antioxidant, superoxide dismutase (SOD), on neuronal injury resulting from cold-induced brain injury in the frontal cortex of the rat. The cold-induced brain injury was reported to result in a ten-fold increase in LDH activity in comparison to baseline values obtained prior to the injury in saline-treated animals. In animals that had been administered SOD, a significant reduction in LDH activity in the CSF was observed indicating an SOD-induced reduction in necrotic cell death (140).

1.7.2 *Apoptotic cell death*

Apoptosis, or programmed cell death, is an essential physiological process that plays a critical role in normal embryonic development and maintenance of tissue homeostasis. However, excessive or insufficient apoptosis causes a disruption in the homeostasis of tissues and can therefore contribute to the pathogenesis of a wide variety of diseases including acute neurological injuries, neurodegeneration, and cardiovascular diseases (141). The term apoptosis was coined by Kerr, Wyllie, and Currie (142) in 1972 and can be described as a distinct sequence of morphological and biochemical events that lead to a controlled destruction of the cell. This type of cell death is designed specifically to disintegrate cells in an ordered fashion, so as to avoid the pathological release of intracellular contents into the tissue, as observed in necrotic cell death (143). This is accomplished by maintaining the composition of the plasma membrane, with the

exception of subtle changes in the outer leaflet of the membrane that causes their engulfment by neighboring cells (133, 143).

To facilitate their engulfment by macrophages, apoptotic cells must reduce their volume. Thus, the earliest morphological phase of apoptosis is shrinkage of the cell, which is accompanied by little or no change in the structure of intracellular organelles (144). The decrease of up to 60% of the apoptotic cell volume is mainly due to an increase in K^+ and Cl^- efflux from the cell. The resultant accumulation of KCl outside the cell shifts the osmotic balance such that water is drawn from the cell in an attempt to reestablish a normal osmotic gradient (144).

Another early morphological event in the apoptotic cell death process is progressive condensation of the nuclear chromatin into masses that cluster peripherally along the border of the nuclear membrane (145). Chromatin condensation is not an active process, but instead occurs as a result of the loss of structural integrity of the nuclear matrix and nuclear lamina (146). Following chromatin condensation and margination, the entire nucleus condenses and eventually breaks up within the cell (147). The most striking biochemical event that occurs in the apoptotic cell death process is the cleavage of the double-stranded DNA. The DNA is initially cleaved into large fragments of approximately 50-200 kilobases, which are subsequently cleaved between nucleosomes to produce fragments in multiples of approximately 180 base pairs (148). This results in the formation of a characteristic ladder-like pattern when analyzed by agarose gel electrophoresis (149). Nuclear condensation and DNA fragmentation within the nucleus typically occur as early as 1-4 hours after the apoptotic cell death process is stimulated (144).

The plasma membrane and organelles including the mitochondria and EnR remain intact until the later phases of apoptosis. The apoptotic cells lose contact with neighboring cells as a result of cleavage of proteins involved in cell-to-cell attachment sites (104). The microvilli on the plasma membrane are lost and the cells start to show protrusions of the membrane commonly referred to as blebs (127). The blebs eventually separate, forming apoptotic bodies densely packed with cellular organelles and nuclear fragments. A later phase of apoptosis involves the exposure of phosphatidylserine (PS) on the outer leaflet of the plasma membrane (146). PS is one of the four major phospholipids that comprise the membrane, however, there is an uneven distribution of these phopholipids, with PS being exclusively located on the cytoplasmic side of the membrane bilayer in healthy cells (150). When a cell commits to apoptosis, the enzymes that maintain PS on the inner leaflet of the bilayer are inactivated. As a result, the asymmetry is lost and PS rapidly flips to the outer leaflet of the plasma membrane (100). As macrophages are equipped with receptors specific for PS, cells or cellular fragments exposing this phospholipid at their surface are rapidly recognized, engulfed and degraded. Thus, apoptosis allows the elimination of the cells without the release of cellular constituents which would otherwise cause inflammation (151). The anti-inflammatory property of apoptotic cells is instrumental in avoiding disruption of the surrounding tissue (130). For comparison purposes, the morphological and biochemical distinctions between apoptosis and necrosis are outlined in Table 1.

1.8 *Caspases*

The discovery of genes required for execution of the apoptotic cell death process in *Caenorhabditis elegans* prompted further investigation into whether similar genes

Table 1. Distinguishing typical morphological and biochemical features of apoptosis and necrosis

Characteristics	**Apoptosis**	**Necrosis**
Distribution	Affects individual scattered cells	Affects groups of neighboring cells
Cell size	Shrinkage	Swelling
Nuclei	Chromatin condensation	Nuclear membrane disruption
DNA degradation	Early internucleosomal cleavage	Late non-specific fragmentation
Plasma membrane	Remains intact Phosphatidylserine on surface	Ruptures
Organelle shape	Apoptotic bodies	Disrupted
Cell degradation	Phagocytosis	Phagocytosis Inflammation

(See text for references and details)

existed in mammals. Interestingly, CED-3, a cell death gene in *C. elegans* was found to encode a protein highly homologous to the mammalian protease interleukin-β-converting enzyme (ICE), also known as caspase-1 (152). This observation led to the identification and characterization of a growing family of caspases. To date, 14 caspases have been identified in mammals and many, but not all, have been implicated in the apoptotic process (153).

Caspases, or "cysteine aspartate-specific proteases" are proteolytic enzymes that share a unique specificity for cleaving target proteins at sites next to aspartate residues (139). Caspases are synthesized as inactive proenzymes that are comprised of 4 distinct domains: an amino-terminal domain of variable size (termed N-terminal polypeptide or prodomain), a large subunit (17-21 kDa), a small subunit (10-13 kDa) and a short interdomain linker region between the large and small subunits (152). These procaspases are activated by proteolytic cleavage of both the N-terminal domain and the linker segment, resulting in the formation of a heterodimer consisting of the large and small subunits (154). The mature caspase possesses full enzymatic activity when two heterodimers align in a head-to-tail configuration to form a tetramer that contains two catalytic active sites (refer to Figure 5) (153). Caspases may be activated through recruitment into activating complexes, which leads to subsequent autoproteolytic processing, or by direct proteolytic cleavage by another caspase (155, 156).

Once activated, these proteases play important roles in both the apoptotic cell death process (caspase-2,-3,-6,-7,-8,-9,-10, and -12) and inflammation (caspase-1, -4, -5, -11, and -13) (157). The apoptotic caspases are classified as initiators or executors, depending on their point of entry into the apoptotic cascade (158). Initator caspases

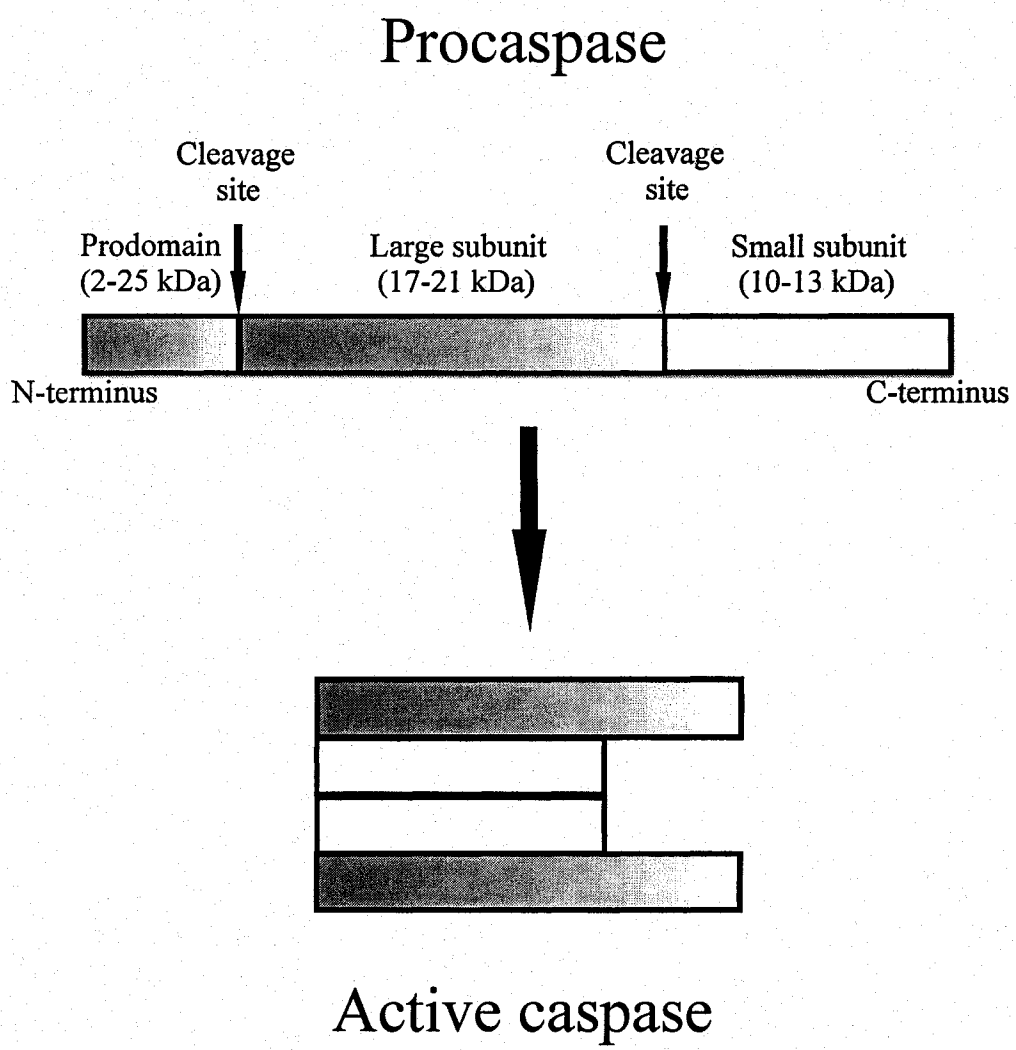

Figure 5. Schematic diagram of a caspase. The procaspase consists of a prodomain, a large subunit, a small subunit, and a linker region between the large and small subunits. Cleavage at the sites indicated above generates the active caspase which consists of a tetramer of two large and two small subunits.

(caspase-2, -8, -9, -10, and -12) are upstream in the apoptotic pathway and respond to apoptotic stimuli by undergoing autoproteolytic activation. Executor caspases (caspase-3, -6, and-7) are processed by the initiator caspases and are responsible for dismantling the cellular structure (158).

The morphological and biochemical changes seen in apoptotic cells result from the cleavage of various proteins by caspases. Shrinkage of apoptotic cells is facilitated by caspase-induced cleavage of the major proteins that comprise the cytoskeleton, including fodrin and G-actin (159). Caspases are responsible for the internucleosomal fragmentation of DNA by cleavage of a variety of substrates involved in DNA repair and replication (105). Among these substrates are caspase-activated DNase (CAD), DNA-protein kinase (DNA-PK), polyADP-ribose polymerase (PARP), and DNA fragmentation factor (DFF) 40 (160). Breakdown of lamin, the major structural protein in the nuclear envelope, causes the nucleus to break up within the cell (159).

Three main caspase-mediated apoptotic pathways have been identified: the extrinsic pathway, the intrinsic pathway, and the endoplasmic reticulum stress signaling pathway. The extrinsic pathway is initiated by binding of ligands to trans-membrane death receptors of the tumor necrosis factor receptor type-1 superfamily (160-162). Cell death signals, such as Fas ligand and tumor necrosis factor (TNF)-2 bind to their respective death receptors Fas and TNF receptor (TNFR) -1, causing receptor autoactivation and subsequent recruitment of the corresponding adaptor molecules, Fas-associated death domain protein (FADD) and TNF-R-associated death domain protein (TRADD), respectively. These adaptor proteins contain death effector domains that mediate their association with the corresponding N-terminal death effector domains in

procaspase-8 and -10. Following recruitment of these procaspases to the cytoplasmic domains of the death receptors, a death inducing signaling complex (DISC) is formed, which leads to autoproteolytic processing of these proenzymes (152). Downstream apoptotic pathways of active caspase-8 and -10 can be elicited in two directions. A cascade of caspase activation can be initiated that includes caspases-3, -6, and -7 (163) or alternatively, the mitochondria-mediated apoptotic pathway can be activated through cleavage of Bid, a pro-apoptotic member of the Bcl-2 family (146). Truncated Bid (tBid) translocates from the cytosol to the mitochondria and alters the mitochondrial membrane permeability leading to release of apoptosis-inducing molecules (153).

A second pathway of caspase activation is initiated through the mitochondria. This pathway, also called the intrinsic pathway, can be activated by multiple stimuli including calcium, reactive oxygen species, and DNA damage (158). In response to apoptotic signals, proapoptotic members of the Bcl-2 family of proteins such as Bax and Bak, translocate to the outer mitochondrial membrane and disrupt the integrity of the membrane, a critical step in the mitochondrial-mediated apoptotic process. This disruption allows the release of pro-apoptotic factors such as cytochrome c from the mitochondrial intermembrane space into the cytosol (152). Upon entering the cytosol, cytochrome c binds to apoptotic protease activating factor 1 (Apaf-1) which, in the presence of dATP, undergoes a conformational change that enhances its ability to associate with procaspase-9 (158). Procaspase-9 is recruited to this apoptosome complex, via its N-terminal caspase-activation recruitment domain (CARD) (158). After cleavage, caspase-9 remains bound to the apoptosome where it is catalytically active and able to cleave effector caspases that will subsequently execute the apoptotic process.

More recently, a third caspase-mediated apoptotic pathway has been identified and involves the EnR. Prolonged EnR stress can lead to activation of apoptosis through two main pathways: a mitochondrial-dependent pathway in which proapoptotic signals are sent from the EnR to the mitochondria; and a caspase-12-dependent pathway (130).

1.8.1 *Caspase-12*

Caspase-12 was first reported to play a role in EnR stress-induced apoptosis in 2000 by Nakagawa and colleagues (164). They demonstrated that caspase-12 is specifically activated both *in vitro* and *in vivo* by molecules that induce EnR stress including tunicamycin (inhibitor of N-linked protein glycosylation), brefeldin A (inhibitor of ER-Golgi transport), as well as thapsigargin (inhibitor of SERCA), and the calcium ionophore A23187 (148). Furthermore, it was shown in this study that caspase-12 was not activated by apoptotic signals that do not induce EnR stress (164). Procaspase-12 is localized on the cytoplasmic side of the EnR membrane and, like other caspases, is synthesized as an inactive proenzyme that consists of a prodomain, a large (~20 kDa) and small (~10 kDa) subunit, and a linker segment between the two subunits (165). Under normal physiological conditions, GRP78 forms a complex with procaspase-12 at the ER membrane, preventing its activation (166). However, under conditions of EnR stress, GRP78 dissociates from caspase-12 to bind with unfolded proteins, allowing the processing of this protease (166). Active caspase-12 typically has a molecular weight of ~30 kDa (124).

Several molecular mechanisms for the processing of procaspase-12 have been reported. TRAF2 (TNF receptor-associated factor 2) has been demonstrated to form a stable complex with procaspase-12 under normal conditions (167). With the induction of

EnR stress, TRAF2 dissociates from procaspase-12 and is recruited to the EnR stress sensor protein IRE-1. IRE-1 is able to recruit TRAF2 following its activation, an event that occurs upon removal of GRP78, which subsequently binds to unfolded proteins accumulating in the EnR lumen. Following dissociation of TRAF2 from procaspase-12, autoproteolytic processing of this protease occurs (167). Caspase-7, a cytoplasmic protease, can activate procaspase-12 by translocating to the ER membrane and cleaving the prodomain to generate active caspase-12 (115). Procaspase-12 can also be converted into the active enzyme following cleavage by m-calpain, a calcium-dependent cytosolic protease that is activated by a rise in the concentration of calcium in the cytosol after disruption in calcium homeostasis (168). There are at least 14 members of the calpain family that can be categorized into two subfamilies: μ-calpains and m-calpains, which are named to reflect their requirements for calcium. μ-calpains are activated by micromolar and m-calpains by millimolar concentrations of cytosolic calcium (169). These proteases are heterodimers, consisting of an 80 kDa subunit and a common 28 kDa regulatory subunit (169). Once activated by calcium, calpains undergo autoproteolytic processing to reduce their mass from ~80 kDa to ~78 kDa (169), at which point they are able to attack a number of cytoskeletal proteins, DNA repair enzymes, as well as other proteases, including procaspase-12 (169, 170). m-calpain can translocate to the ER membrane and directly cleave procaspase-12, resulting in its activation (170). m-calpain has also been shown to activate caspase-3, and cleave caspase-3, -7, -8, and -9 into inactive fragments (125). The mechanisms of caspase-12 activation as well as the caspase-12 mediated apoptotic pathways are described in Figure 6.

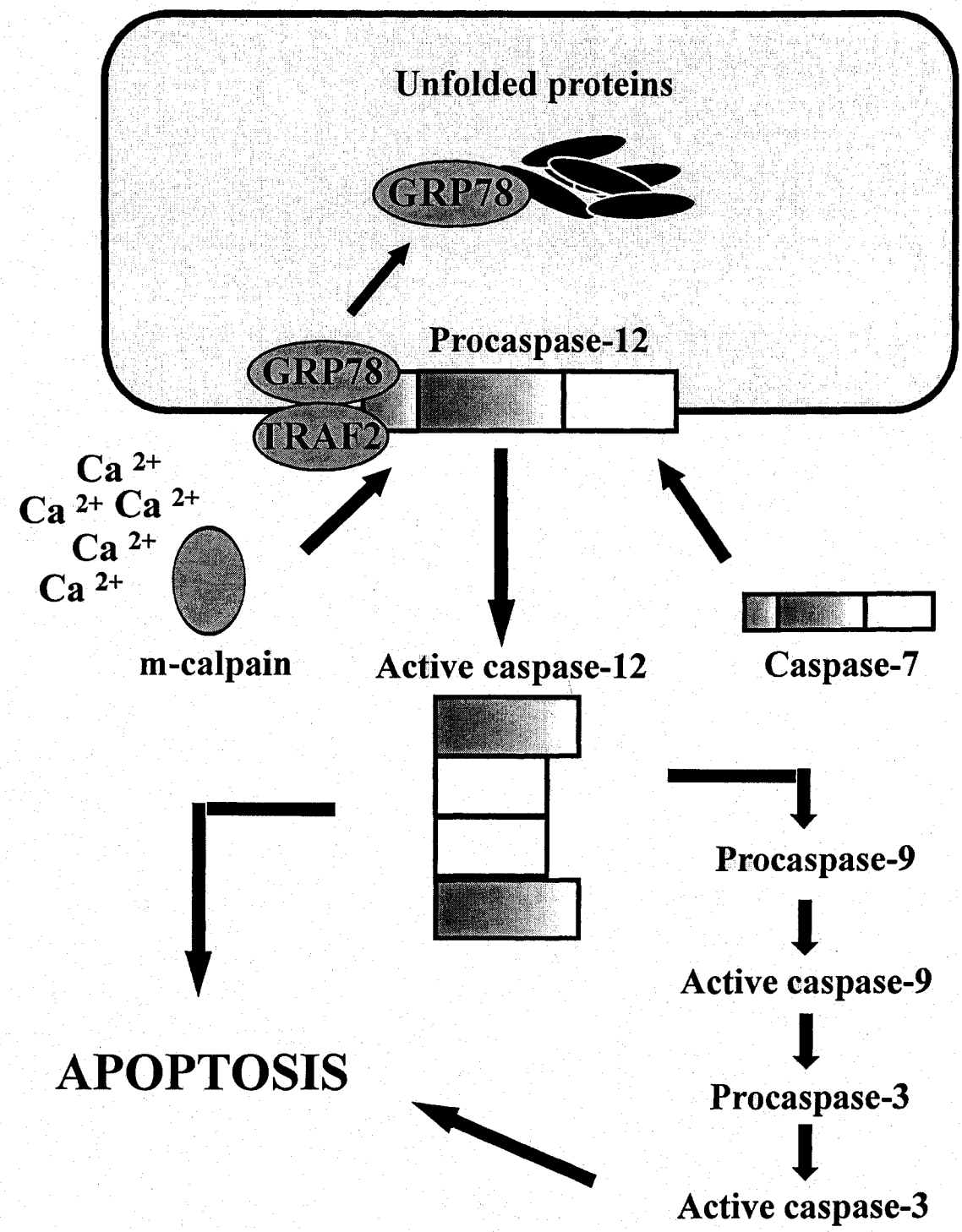

Figure 6. Mechanisms of caspase-12-mediated apoptosis in response to excessive endoplasmic reticulum stress. GRP78 dissociates from procaspase-12 to assist in protein folding. Procaspase-12 can then be cleaved/activated by m-calpain or caspase-7, both of which translocate from the cytosol to the EnR membrane, or it may undergo autoproteolysis upon dissociation from TRAF2. Once activated, caspase-12 can cause apoptosis directly or it may activate a caspase-9/3 cascade.

EnR stress-mediated apoptosis can be executed by a number of pathways following activation of caspase-12 by any of the above mechanisms. In an *in vitro* model of EnR stress, caspase-12 has been shown to translocate to the cytoplasm and cleave procaspase-9 leading to caspase-3 activation (115). Although cytochrome-c released from the mitochondria is hypothesized to be required for activation of caspase-9 during apoptosis, caspase-12 mediated cleavage of procaspase-9 occurs in a cytochrome-c-independent manner (171). Evidence suggests that caspase-12 can lead to apoptotic cell death in the absence of activation of other caspases including caspase-3, which is the main executor caspase in many apoptotic pathways. Fujita et al. (172) demonstrated translocation of processed caspase-12 within the nuclei of apoptotic cells, suggesting that caspase-12 may directly participate in apoptotic events in the nuclei.

The relevance of caspase-12 to EnR stress-induced apoptosis has been questioned because the human caspase-12 gene contains mutations which preclude its function as a normal caspase. However, human caspase-4 and -5 have amino acid sequences that are 48% and 45% identical to rodent caspase-12 respectively (157). Therefore these caspases may perform the functions normally ascribed to rodent caspase-12 in the context of EnR stress. Human caspase-4 is localized to the EnR membrane and is cleaved when cells are treated with EnR stress-inducing agents. Furthermore, knockdown of caspase-4 using small interfering RNA in human neuroblastoma cells has been shown to partially reduce cell death caused by the EnR stress inducers, thapsigargin and tunicamycin (173).

1.8.2 *Caspase-12 and neuronal cell death*

ER stress-induced activation of caspase-12 and subsequent apoptotic cell death has been implicated in neuronal cell death in a number of situations. In a rodent model of

traumatic brain injury, elevated levels of procaspase-12, as well as the processed form, were observed in both the cortex and hippocampus (158). Active caspase-12 rapidly increased within 6 hours of injury, and peaked by 1 day post-injury. Furthermore, the increased caspase-12 expression was predominantly found in neurons in the ipsilateral cortex and hippocampus, but also in cortical astrocytes at the site of the injury (158). There is also evidence of caspase-12 activation in rodent models of stroke. In one study (124), mice were subjected to transient occlusion of the middle cerebral artery (MCAO) for 1 hour followed by reperfusion for 2, 5, 11, 23, or 47 hours. This cerebral ischemia/reperfusion induced EnR stress, confirmed by an upregulation of the EnR-resident molecular chaperone, GRP78, at the site of the insult. This was observed concurrently with caspase-12 activation. Cleavage of caspase-12 was observed at 5-23 hours of reperfusion, and was predominantly localized in neurons that exhibited DNA fragmentation, indicative of apoptosis. Furthermore, it appeared that caspase-7 did not contribute to the processing of procaspase-12, suggesting that other mechanisms of caspase-12 activation were involved in their experimental model. Aoyama and colleagues (174) demonstrated activation of caspase-12 in the peri-infarct region following transient MCAO. Caspase-12 activation was also observed in a permanent model of cerebral ischemia. Mouw et al. (125) investigated caspase-12 mRNA and protein levels 24 hours following permanent MCAO. Both mRNA levels and protein expression for caspase-12 were significantly increased (46% and 40% respectively) compared to sham groups. Furthermore, the localized expression of caspase-12 was investigated immunohistochemically and was found to be localized in neurons in the striatum. However, the caspase-12 found in the cortex was not localized in neurons.

Activation of m-calpain, a well known regulator of caspase-12 activity, has been proposed to play a role in neuronal cell death in ischemic brain injury. Calpain activity, as measured by a breakdown in spectrin, was observed following 1-3 hours of focal ischemia (175). m-calpain has also been reported to activate caspase-12 in neurons. Nakagawa et al. (168) demonstrated caspase-12 activation induced by oxygen glucose deprivation (OGD) in glial cells and amyloid β in neurons that was inhibited by a calpain inhibitor, but not a caspase inhibitor. This suggests that in neuronal cell death, EnR stress-induced apoptosis may occur by the activation of m-calpain first, followed by caspase-12 activation.

1.9 *Hypothesis and specific aims*

From the literature reviewed above, it is evident that estrogen provides protection against stroke in both human and animal studies. In our laboratory, estrogen administered 30 minutes prior to permanent MCAO resulted in a significant reduction (~50%) in infarct volume within the first 4 hours following the stroke (42, 43). However, the mechanism by which estrogen is neuroprotective in this model has yet to be elucidated. Following MCAO, the progressive spread of cell death from the infarct core to the surrounding penumbra occurs primarily as a result of glutamate excitotoxicity resulting in necrotic cell death. Apoptotic cell death also occurs (mainly in the penumbral region), but does not significantly contribute to the expansion of the infarct, because the release of intracellular contents is absent in this mode of cell death. An increase in the ratio of apoptotic to necrotic cell death following ischemia would therefore be protective because this would limit glutamate excitotoxicity and reduce the "spreading depression" of necrotic cell death that is characteristic of ischemia. In

addition, calcium disruption and endoplasmic reticulum stress-induced apoptosis via activation of caspase-12 has recently been identified as an important cell death pathway following ischemia.

Taken together, this evidence has led us to hypothesize that **estrogen increases MCAO-induced apoptosis via activation of caspase-12 to decrease both necrotic cell death and infarct volume**. To provide support for this hypothesis, the following objectives will be tested:

(1) To determine if estrogen enhances apoptosis via caspase-12 activation within 4 hours post-MCAO;

(2) To determine if estrogen decreases necrotic cell death *in vivo* within 4 hours post-MCAO.

CHAPTER 2. MATERIALS AND METHODS

2.1 *Surgical Procedures*

All procedures in this thesis were approved by the UPEI Animal Care Committee Protocol # 04-032. Male Sprague-Dawley rats (225-250g) obtained from Charles River Laboratories (Montreal, QC) were housed in groups of 4-6 with food and water *ad libitum*. All rats were allowed a minimum of 5 days for acclimatization before any experimental procedures were performed. Each animal was anesthetized with sodium thiobutabarbitol (Inactin; Sigma-Aldrich, St. Louis, MO; 100 mg/kg; ip) and when a surgical plane of anesthesia was reached, an incision was made in the right leg exposing the femoral vein. Approximately 15 cm of polyethylene tubing (PE-10; Clay Adams, Parsippany, NJ) connected to a 1 ml syringe (BD Biosciences; Mississauga, Ont) was inserted into the right femoral vein for the administration of 17β-estradiol (Sigma; 0.0125 mg/kg) or heparinized physiological saline (0.9%; 0.2 ml), which occurred 30 minutes prior to occlusion of the middle cerebral artery (see section 2.2 for details). A tracheotomy was performed and a trachea tube placed to facilitate breathing. The rat was then placed in a stereotaxic frame (David Kopf, Tujunga, CA) in the prone position and secured firmly in place. Temperature was monitored with a digital rectal thermometer (Fisher Scientific, Nepean, Ont) and maintained at 37±1 °C using a heated circulating water bath.

2.2 *Middle Cerebral Artery Occlusion*

Following placement of the animal in the stereotaxic frame, a rostro-caudal incision was made in the skin down the midline of the skull. A dorso-ventral incision

was subsequently made through both the skin and frontalis muscle at the level of Bregma (175). The frontalis and temporalis muscles were partially removed exposing the underlying squamosal bone and the area of fusion with the zygoma. A hand-held drill was used to make a small burr hole in the rostro-dorsal portion of the squamosal bone and the squamosal bone was carefully dissected away exposing the right middle cerebral artery (MCA). The dura mater was removed using the bent tip of a 26-gauge hypodermic needle and the right MCA was permanently occluded at three points using bipolar electrical coagulation (Cameron-Miller Inc; Chicago, IL). The first occlusion was made slightly dorsal to the rhinal fissure; the second occlusion was made slightly ventral to the bifurcation of the MCA to the frontal and parietal cortices; and the third occlusion was made just distal to the bifurcation to the parietal cortex (refer to Figure 7). In the sham groups, the experimental procedures were as described above except the MCA was not occluded.

2.3 Determination of infarct size

Initially, 6 animals were used to determine if size and variability of the infarct (measured as a percentage of the hemisphere), as well as the neuroprotective effect of estrogen, were similar to those previously determined in our laboratory (42). Three animals were administered 17β-estradiol (Sigma-Aldrich; 0.0125 mg/kg) and another 3 were administered physiological saline (0.2 ml), and 30 minutes later, all animals had their MCA occluded. At four hours post-MCAO, animals were transcardially perfused with phosphate buffered saline (PBS; 0.1 M; 200 ml) and decapitated. Brains were subsequently removed and placed in a rat brain matrix (Harvard Apparatus, Saint Laurent, QC) and sliced into 1 mm coronal sections and incubated for 10 minutes in a

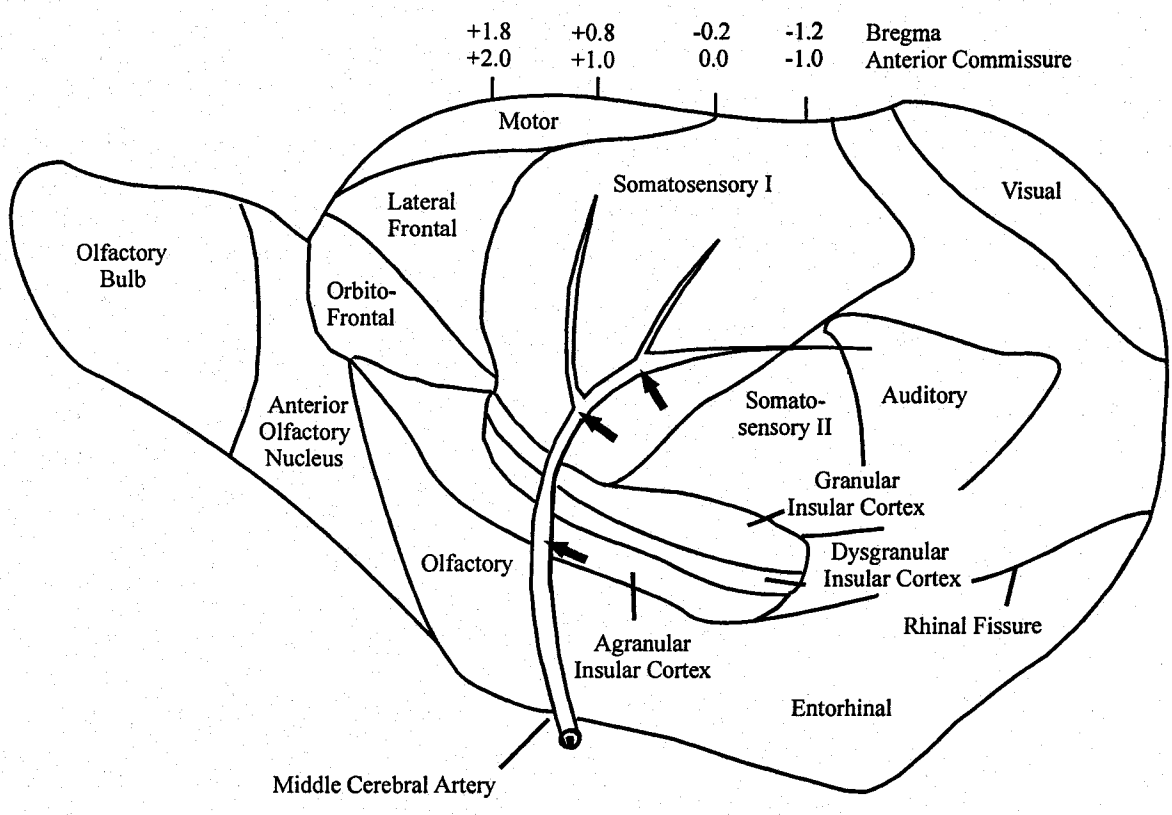

Figure 7. Schematic diagram of the lateral view of the rat forebrain to illustrate the position of the middle cerebral artery. Each point of occlusion in our MCAO model is indicated with an arrow. The distances in millimeters at the top of the drawing are given with respect to bregma according to the atlas of Paxinos and Watsons (176). (Modified from 177).

2% 2,3,5-triphenoltetrazolium chloride (TTC) solution (in PBS). TTC is a marker of mitochondrial oxidative enzyme activity and therefore living tissue will take up the stain (red) while dead tissue will not (absence of stain). The coronal sections were fixed and stored in 10 % formalin at 4°C. Sections at the level of the joining of the anterior commissure (between 0.0 and -0.26 mm from Bregma) were digitally photographed and the infarct size was determined using a computer-based image analysis program (Scion Image; Scion Corporation, Frederick, MD). Both the infarct region (indicated by the lack of TTC staining), and the right hemisphere were outlined and the area of each region was measured 3 times and the average was recorded. The infarct area of each section was calculated as a percentage of the hemisphere. The MCAO model and the quantification of infarct area has been previously used and validated in our laboratory (42, 43).

2.4 *Tissue harvesting and preparation for western blotting*

Brain tissue was collected from separate rats at 0 (immediately following MCAO), 1, 2, 3, and 4 hours after occlusion of the MCA. Six animals were administered 17β-estradiol (Sigma-Aldrich; 0.0125 mg/kg) and 6 were administered saline (0.2 ml) for each time point. At the appropriate post-MCAO time point, animals were perfused as described in section 2.3. Ipsilateral and contralateral cortices were rapidly dissected and biopsy needles (Miltex Inc., York, PA) with internal diameters of 4 and 8 mm were used to collect tissue from the region directly affected by the stroke (infarct core), and the immediately surrounding tissue (peri-infarct or penumbra), respectively. The corresponding tissue regions on the contralateral side were also collected to be used as internal controls (refer to Figure 8). Brain tissue was added to cryovials containing 300 µl of PBS and 3 µl protease inhibitor (Sigma-Aldrich), frozen in liquid nitrogen

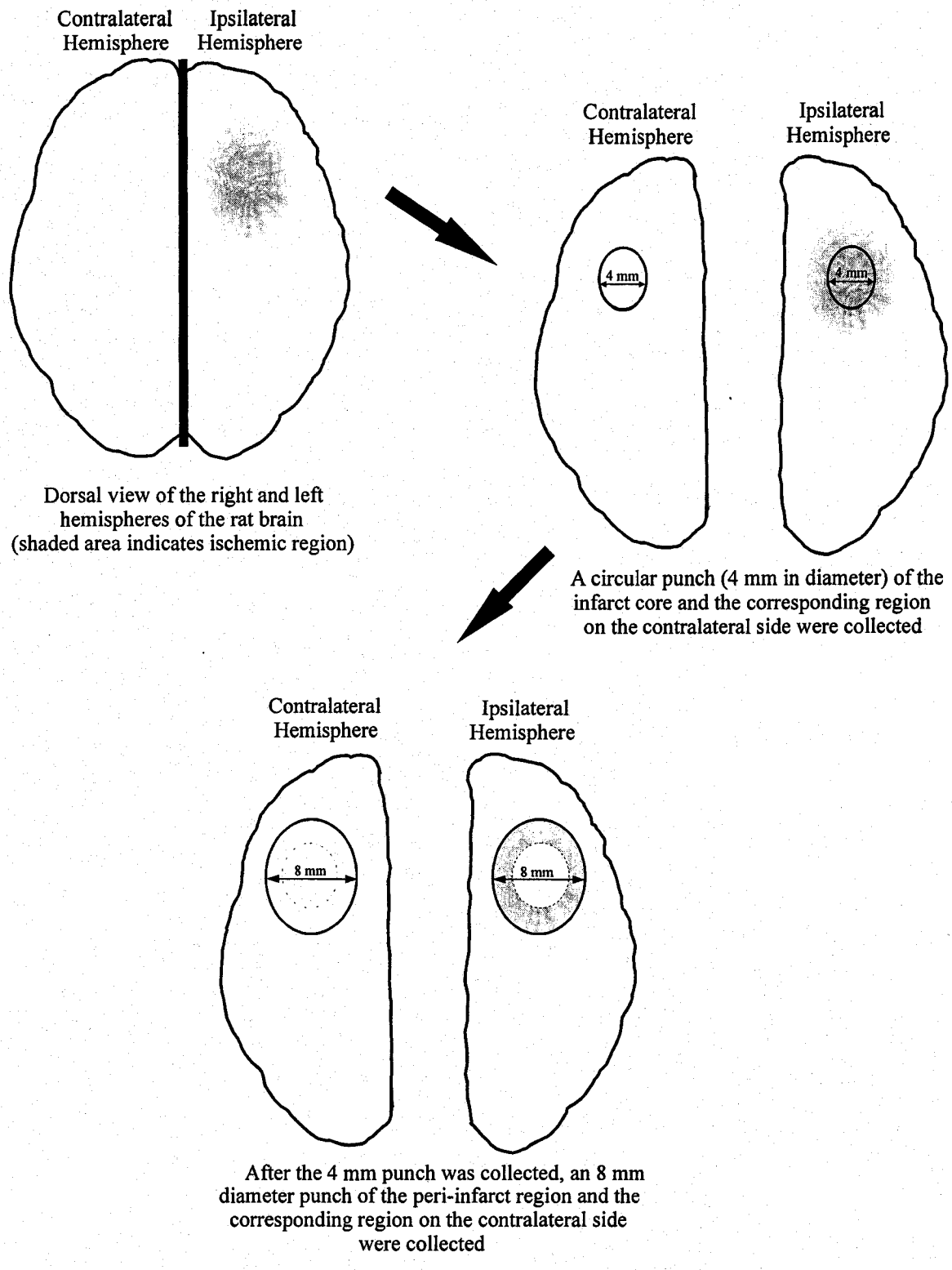

Figure 8. Schematic diagram illustrating the procedure for collecting tissue from the infarct, peri-infarct and the corresponding contralateral regions using 4 and 8 mm biopsy punches.

and stored at -80°C. The samples were homogenized (2 x 10 seconds) and centrifuged at 9000 x g for 10 minutes. The resulting supernatant was collected and protein concentrations were determined using a modified Lowry protein assay (Bio-Rad Laboratories, Mississauga, ON).

2.5 *Western blot analysis*

Aliquots of each sample (50 μg of protein) were added to 4 x Laemmli buffer and PBS. The mixture was boiled for 3 minutes and loaded onto a 15% polyacrylamide gel. Following electrophoresis, the separated proteins were transferred to a nitrocellulose membrane (Bio-Rad Laboratories) using a wet transfer method (Bio-Rad Laboratories). The membranes were blocked for 1 hour in 5% non-fat milk, and incubated overnight at room temperature with a 1:500 dilution of rat monoclonal anti-caspase-12 antibody (Sigma-Aldrich), or a 1:1000 dilution of rabbit anti-m-calpain antibody (Triple Point Biologics, Inc; Forest Grove, OR) in a 5% blocking solution. After washing with PBS, the membranes were incubated with a 1:10,000 dilution of horseradish peroxidase-conjugated anti-rat IgG (for caspase-12) or anti-rabbit IgG (for m-calpain) (both obtained from Sigma-Aldrich). The membranes were again washed, treated with ECL Western blotting detection reagents (General Electric, Piscataway, NJ), and immediately exposed on an image station (Kodak Image Station 440CF; New Haven CT). For active caspase-12, samples from the infarct and peri-infarct regions in estrogen and saline treated animals were run on additional blots and incubated in a 1:100 dilution of rat monoclonal anti-caspase-12 antibody (Sigma-Aldrich). The remainder of the procedure was performed as described above for caspase-12 western blotting. To ensure consistent protein loading, membranes were also immunostained with a 1:2000 dilution of mouse

monoclonal anti-β-actin (Sigma-Aldrich) followed by 1:10,000 dilution of horseradish peroxidase-conjugated anti-mouse IgG (Sigma-Aldrich). The protein band densities were normalized to the density of the β-actin band from the same sample. The density of each protein band was also standardized to the mean density of the protein bands from the contralateral cortex in saline treated animals within each blot to correct for different background intensities between blots.

2.6 *Immunohistochemistry*

2.6.1 *Caspase-12 immunohistochemistry*

The surgical procedures for preparing animals and performing the MCAO protocol were as described above. Three animals were administered 17β-estradiol (Sigma-Aldrich; 0.0125 mg/kg) and 3 were administered saline (0.2 ml) at each of 2 and 4 hours post-MCAO. At 2 or 4 hours post-MCAO, animals were transferred to a fume hood where they were transcardially perfused with PBS (200 ml) and phosphate buffered paraformaldehyde (4%; 200 ml). Brains were rapidly removed and placed on a shaker in 4% phosphate buffered paraformaldehyde at room temperature overnight. The fixed brains were placed in a rat brain matrix (Harvard Apparatus) and cut into 1 mm coronal sections. The sections in which the anterior commissure was observed to join (between 0.0 and -0.26 mm from Bregma) were sent to Diagnostics Services where they were put in a processor (Tissue-Tek® VIP; Sakural Ramsey, MN) for 14 hours. Sections were then embedded in paraffin and cut with a rotary microtome into 5 μm thick sections and mounted onto Superfrost Plus slides (Fisher Scientific Inc). The mounted sections were allowed to dry at room temperature. The selected sections were deparaffinized with

xylene and rehydrated through a series of ethanol solutions (100%, 95%, 90%, 80%, and 70%) each for 5 minutes. Tissue sections were incubated in 0.3% Triton-X (Sigma-Aldrich) in PBS 3 times for 10 minutes each, and then blocked with 4% bovine serum albumin (BSA; Sigma-Aldrich) in PBS for 1 hour at room temperature. Following this, a range of dilutions (1:50, 1:100, 1:500, 1:1000, and 1:2000) of rat monoclonal anti-caspase-12 antibody (Sigma-Aldrich) in PBS were applied to different tissue sections to determine the optimal dilution of primary antibody. The sections were incubated in primary antibody overnight at 4°C. The following day, the slides were washed with PBS, and then incubated in a 1:500 dilution of biotinylated anti-rat secondary antibody (Abcam; Cambridge, MA) overnight at 4°C. Slides were washed the following day with PBS and were incubated in a 1:1500 dilution of ExtrAvidin®-peroxidase (Sigma-Aldrich) in PBS for 4 hours at room temperature. The sections were then washed with PBS and incubated in 3,3'diaminobenzidine (DAB; 10 mg; Sigma-Aldrich) dissolved in 19 ml PBS and 40 µl hydrogen peroxide for approximately 10 minutes. Sections were washed again with PBS and dehydrated with a series of ethanols (70%, 80%, 90%, 95%, and 100%) each for 5 minutes. Slides were then coverslipped with Flo-Texx (Lerner Laboratories; Pittsburgh, PA) and allowed to dry overnight in a fume hood. Negative control sections were prepared as above but with the omission of the primary antibody. The experiments were repeated several times with the protocol slightly altered (ex. different concentrations of Triton-X; different antibody incubation times) to enhance the staining intensity. We eventually tried a different antibody and the protocol was as described above except that sections were incubated in several dilutions (same as those listed above) of rabbit polyclonal anti-caspase-12 antibody (Cell Signaling Technology,

Inc., Danvers, MA) overnight at 4°C. After the PBS washes the following day, sections were incubated in a 1:500 dilution of biotinylated anti-rabbit secondary antibody (Zymed Laboratories, San Francisco, CA) overnight at 4°C. When staining was still not observed, the procedure was repeated with frozen tissue sections to eliminate any damage to the antigen that may have resulted from the paraffin embedding process. The brains were stored overnight in 4% phosphate buffered paraformaldehyde as described above, and were then post-fixed in 30% sucrose (PBS) for 2 days at 4°C. Brains were then placed in a rat brain matrix (Harvard Apparatus) and cut in 1 mm coronal sections. The section from each brain at the level of the joining of the anterior commissure was placed on a cryostat specimen disk and covered by frozen specimen embedding medium (Thermo Shanden; Pittsburgh, PA). 10 μm coronal sections were cut with a cryostat (Leica, CM 1900; Richmond Hill, Ont) and mounted on poly-L-lysine treated slides. Sections were rinsed with PBS and the above protocol was followed beginning with the incubation in 0.3% Triton-X (Sigma-Aldrich) in PBS. Following the 1 hour incubation in 4% BSA, sections were incubated in either rat monoclonal anti-caspase-12 antibody (Sigma-Aldrich) or rabbit polyclonal anti-caspase-12 antibody (Cell Signaling Technology, Inc) followed by incubation with the corresponding secondary antibody (listed above).

2.6.2 *Terminal deoxynucleotidyl transferase-mediated deoxyuridine triphosphate nick end-labeling (TUNEL) staining*

Additional animals were used for the investigation of TUNEL staining in sections from animals undergoing MCAO. Animals were administered either 17β-estradiol (Sigma-Aldrich; 0.0125 mg/kg) or saline (0.2 ml) and at either 2 or 4 hours post-MCAO (n = 3 per treatment group for each time point) animals were perfused and the sections

were embedded in paraffin and mounted on slides as previously described in section 2.6.1. Coronal sections (5 μm) were deparaffinized with xylene and rehydrated as described in section 2.6.1. Tissue sections were then washed with PBS and incubated in proteinase K (Roche Diagnostics; Laval, QC; 20 μg/ml in 10 mM Tris HCl) for 30 minutes in a humidified chamber at 37°C. After washing with PBS, each section was incubated in 50 μl of a TUNEL reaction mixture (In Situ Cell Death Detection Kit, POD; Roche Diagnostics) consisting of terminal deoxynucleotidyl transferase (enzyme solution) and a nucleotide mixture (label solution), for 60 minutes in a humidified chamber at 37°C. The tissue sections were again washed and incubated in 50 μl of a horseradish peroxidase-conjugated anti-fluorescein antibody (In Situ Cell Death Detection Kit, POD; Roche Diagnostics, Inc.; Mississauga, Ont) for 30 minutes at 37°C in a humidified chamber. Sections were then washed and incubated in DAB chromogen (DakoCytomation, Mississauga, ON) for 1 minute at room temperature in a fume hood. Sections were counterstained with hematoxylin for 1 minute and dehydrated as described above. Positive controls were prepared by incubation of one slide in DNase (Grade 1; Roche Diagnostics, Inc.; 3000 U/ml) for 10 minutes prior to incubation in the TUNEL reaction mixture. For a negative control, one slide was incubated with only the label solution (the enzyme solution was omitted).

Tissues were examined using photomicrographs (40 X magnification) which were taken with a digital camera mounted on a microscope connected to a computer. Three different fields from both the ipsilateral and contralateral cortices were analyzed. A grid was taped to the computer screen (see Figure 9) and positive cells were counted in every

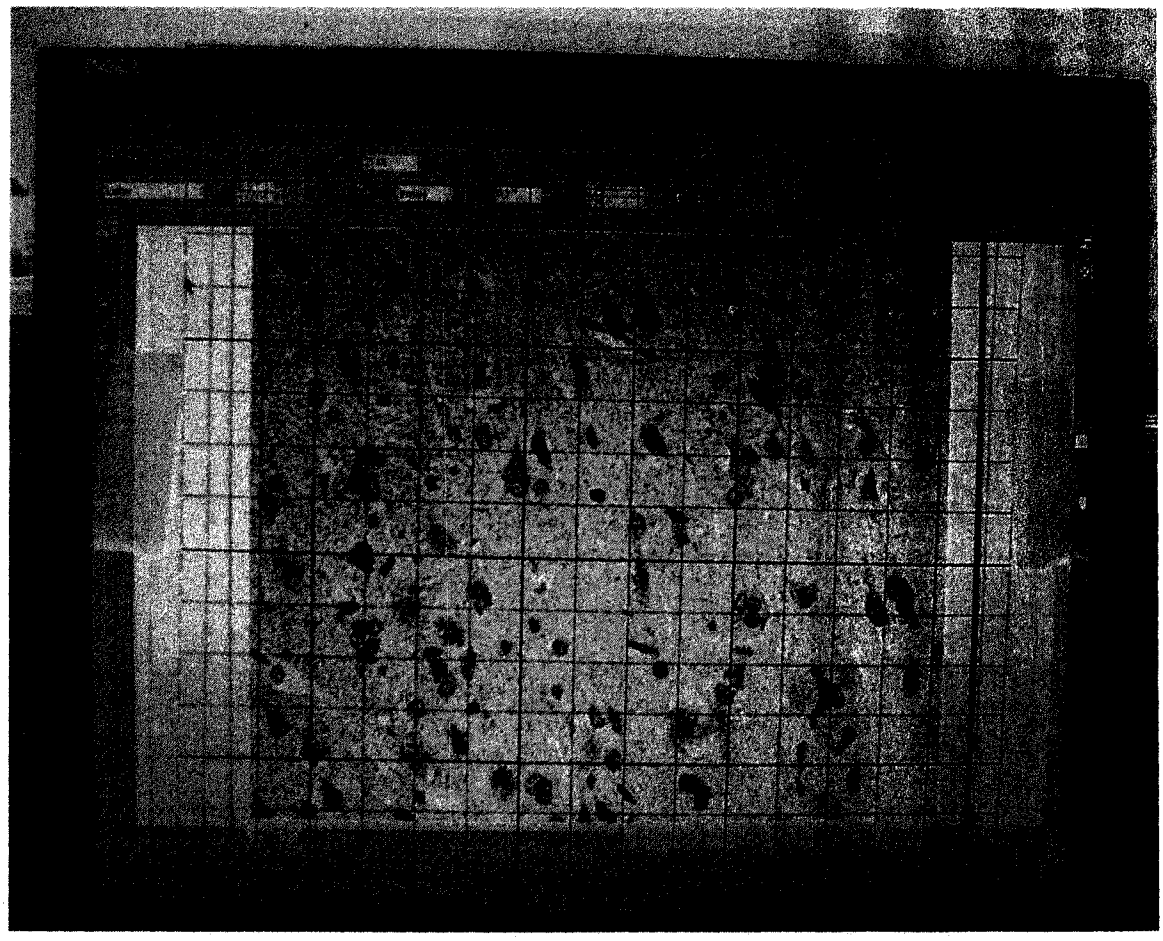

Figure 9. Quantification of TUNEL staining. A grid was taped to a computer screen and the number of TUNEL positive cells in every second square of the grid was counted. Three different fields from both the ipsilateral and contralateral cortices were quantified.

second square of the grid and the average number of cells from the 3 fields was recorded. Cells were considered positive if they were small, round, and dark brown in color. Cells with equivocal definition were counted as negative.

2.7 *DNA laddering*

The surgical procedures in preparation for DNA laddering were as described above except that for the initial experiments, only saline (0.2 ml) was administered to stroke or sham treated animals (n = 3/group). At 2 hours post-MCAO, rats were transcardially perfused with PBS (200 ml), and decapitated. The brains were rapidly removed, placed in a rat brain matrix (Harvard Apparatus), and sliced in 1 mm coronal sections. Infarct tissue and the corresponding region of tissue from the contralateral side (25 mg) were dissected from the coronal section from each brain at the level of the joining of the anterior commissure. The DNA was extracted from the tissue according to the protocol for purification of total DNA from animal tissues from a DNeasy Tissue Kit (Qiagen Inc., Mississauga, ON). Briefly, the tissue was cut into small pieces and placed in a microcentrifuge tube containing 180 µl of a tissue lysis buffer (included in kit). 20 µl of proteinase K (Qiagen; 600 mAU/ml) was added and the mixture was incubated at 55°C for 1 hour. After mixing on a vortex, 200 µl of lysis buffer was added and the mixture was incubated for 10 minutes at 70°C. Then, 200 µl of ethanol was added, and after mixing on a vortex, the mixture was added to a spin column placed in a 2 ml collection tube. The mixture was centrifuged at 6000 x g for 1 minute. The spin column was then placed in a new collection tube and 500 µl of wash buffer was added. The mixture was again centrifuged at 6000 x g for 1 minute and the spin column placed in a new collection tube. 500 µl of wash buffer was added and the mixture was centrifuged at 20,000 x g for

3 minutes. The spin column was then placed in a 1.5 ml microcentrifuge tube and 200 µl of elution buffer was added directly onto the membrane. After incubation for 1 minute at room temperature, the mixture was centrifuged at 6000 x g for 1 minute and the flow-through was collected and stored at -20°C. The concentration of the DNA was determined using a spectrophotometer (NanoDrop®, N-D 1000; Wilmington, DE). The DNA was loaded on a 1% Sybrsafe® agarose gel and visualized under UV illumination. DNA laddering was not observed, so the experiment was repeated and the protocol was slightly altered: half of the elution buffer was added to increase the final concentration of DNA. The DNA was again loaded on a 1% agarose gel and visualized under UV illumination, and again no laddering was observed.

An alternate DNA extraction kit specific for apoptotic DNA (Apoptotic DNA Ladder Kit, Roche Diagnostics, Inc) was then used. Surgical procedures were as described above, and 3 animals were administered 17β-estradiol (Sigma-Aldrich; 0.0125 mg/kg) and 3 were administered saline (0.2 ml). Animals were subjected to MCAO and at 2 or 4 hours post-MCAO, tissue was collected as described previously in this section. To optimize the amount of DNA extracted from the tissue, 200 µl of tissue lysis buffer (4 M urea, 200 mM Tris, 20 mM NaCl, 200 mM EDTA; pH 7.4; 25°C) and 40 µl proteinase K (20 mg/ml) were added to the tissue, which was cut into small pieces. The mixture was placed on a vortex and then incubated for 1 hour at 55°C. 200 µl binding buffer (provided with the kit) was added and the mixture was incubated at 72°C for 10 minutes. The remainder of the procedure was followed directly from the protocol for DNA extraction using the Apoptotic DNA Ladder Kit (Roche Diagnostics, Inc). Briefly, 100 µl of isopropanol was added and the mixture was vortexed. The sample was then

pipetted into a filter tube which was placed in a collection tube, and centrifuged at 5867 x g for 1 minute. The flow-through was discarded and 500 µl of washing buffer was added and the mixture was centrifuged at 5900 x g for 1 minute. This step was repeated and finally, the sample was centrifuged at 15500 x g for 10 seconds. The filter tube was then placed in a 1.5 ml microcentrifuge tube and 200 µl of prewarmed (70°C) elution buffer was added. The mixture was centrifuged at 5900 x g for 1 minute and the flow-through was then stored at -20°C. The concentration of DNA was determined and the DNA was loaded onto an agarose gel as described previously in this section. Further steps were taken to optimize the amount of DNA laddering observed: the amount of starting tissue was increased from 25 to 50 mg, and the volume of elution buffer was decreased by half.

2.8 *Microdialysis and probe recovery efficiency determinations*

To determine the recovery efficiency of the microdialysis probe and the optimal flow rate, an *in vitro* microdialysis experiment was performed. The microdialysis probe was attached to a micro-manipulator and lowered into a beaker containing artificial cerebrospinal fluid (aCSF; pH 7.4; composition, NaCl 126.5 mM; $NaHCO_3$ 27.3 mM; KCl 2.4 mM; KH_2PO_4 0.5 mM; $CaCl_2$ 1.1 mM; $MgCl_2$ 0.85 mM; $NaSO_4$ 0.5 mM; glucose 5.9 mM; 0.8 % bovine serum albumin and 0.03% bacitracin) with a known concentration of lactate dehydrogenase (Sigma-Aldrich; 10,000 ng/ml). Samples were collected in 20 minute intervals at a flow rate of 2 or 5 µl/min and assayed for lactate dehydrogenase immediately following each experiment. It was determined that the probe had a recovery efficiency of ~ 4%.

2.9 *Microdialysis*

Based on the *in vitro* recovery efficiency experiments, there was no difference in the recovery of LDH between the different flow rates tested. Therefore, 5 µl/min was the chosen flow rate as it resulted in a greater sample volume. Once the animal was securely positioned in the stereotaxic frame, a rostro-caudal incision was made down the midline of the skull and the skin was reflected back exposing Bregma. The microdialysis probe attached to a micro-manipulator was centered over Bregma and the coordinates were recorded. The coordinates for the insular cortex were obtained from a stereotaxic atlas of a rat brain (175). The microdialysis probe (CMA/Microdialysis; Montreal, QC) had an inlet cannula and an outlet cannula mounted on a metal shaft (14 mm long) with a polycarbonate membrane (3 mm long, molecular weight cutoff at 100,000 Daltons). (refer to Figure 10). The probe was positioned + 0.8 mm posterior and - 5.3 mm lateral to Bregma, directly over the insular cortex. The probe was connected to a 5 ml syringe (BD Biosciences) via 30 cm of PE-50 inflow tubing. The syringe was filled with aCSF that was filtered with a Millex®-SV 5.0 µm filter unit (Millipore; Cork, Ireland) and hooked up to a syringe pump (Harvard Apparatus). A 20 cm length of PE-50 tubing was connected to the outlet portion of the probe. Prior to insertion into the brain, the probe was perfused with aCSF at a flow rate of 5 µl/min for approximately 20 minutes. The right MCA was exposed and the dura was removed as described above. The probe was lowered until the tip of the probe came in contact with the surface of the brain. The dorsal/ventral coordinates were then recorded and the probe was lowered into the brain (3.3 mm below Bregma).

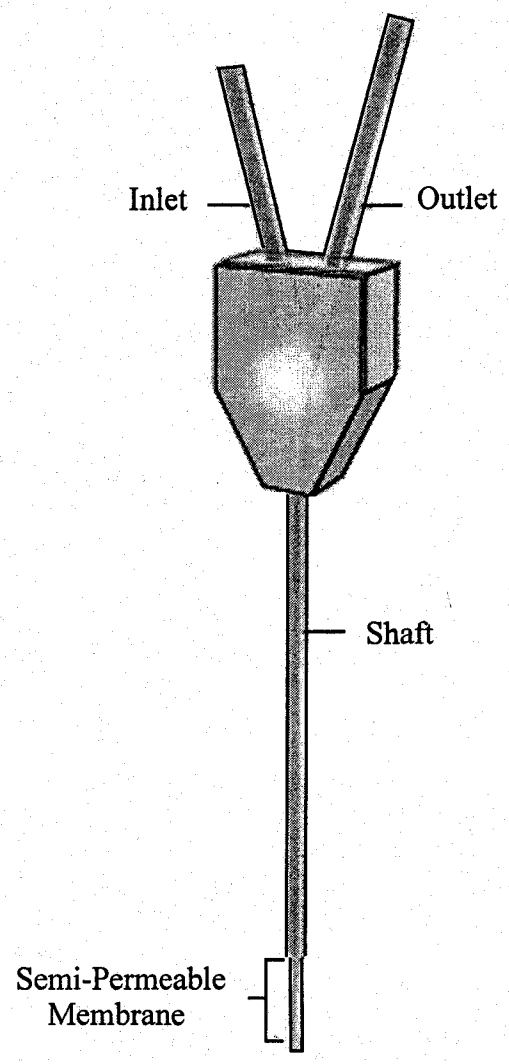

Figure 10. Diagram of a microdialysis probe illustrating the inlet and outlet cannulae, the shaft, and the semi-permeable membrane.

2.10 *Cerebrospinal fluid sample collection*

The samples were collected in 0.6 ml microcentrifuge tubes (Fisher Scientific Inc), at 20 minute intervals for 1 hour prior, and 4 hours post-MCAO or sham occlusion. The first 2 samples collected were discarded. Samples were stored on ice and immediately assayed for LDH at the end of each experiment (refer to section 2.11).

2.11 *Lactate dehydrogenase assay*

At the end of each experiment, LDH release in the cerebrospinal fluid was determined using a CytoTox® Non-Radioactive Cytotoxicity Assay (Promega Corporation, Madison, WI). This assay is a colorimetric enzymatic assay, which, in the presence of LDH, results in the conversion of a tetrazolium salt into a red formazan product. The amount of color formed is proportional to the number of lysed cells. In each well of a 96 well plate, 40 µl of sample and 10 µl aCSF were loaded (Ultident, St. Laurent, Que). The substrate buffer was added (50 µl in each well) and the plate was covered with foil to protect it from light and incubated at room temperature for 30 minutes. Acetic acid was then added (50 µl to each well) to stop the reaction and the plate was placed in a spectrophotometer (SpectraMax 190; Bio-Tek Instruments, Inc; Winooski, VT) and the absorbance was recorded at 490 nm using the SoftMax Pro 4.8 software program.

2.12 *Push-pull perfusion*

All samples obtained using the in vivo microdialysis were below the detection limits for LDH. Therefore, another microdialysis probe with a higher molecular weight cutoff (3 Mega Daltons; Microbiotech; Stockholm, Sweden) was used. The inlet and outlet cannulae of this probe were connected to a flexible shaft (15 mm long) with a

polyethylene membrane (2 mm long) attached at the bottom end of the shaft. The recovery efficiency of this probe was determined as described in section 2.8 and was calculated to be ~10%. A push-pull pumping system was required for proper performance of this high molecular weight cutoff dialysis probe in order to minimize the risk of filtrating the perfusion media into the tissue. The probe was connected to a 10 ml syringe (BD Biosciences) filled with filtered aCSF via 300 cm of PE inflow tubing. The syringe was hooked up to a syringe pump (Harvard Apparatus). The outlet portion of the probe was connected to a 250 µl syringe (Hamilton Co.; Reno, NV) which was hooked up to another syringe pump (Harvard Apparatus) with 20 cm of PE tubing. Prior to insertion into the brain, the probe was placed in a beaker of aCSF, and aCSF was pumped into the inlet cannula of the probe from the 10 ml syringe. Concurrently, aCSF was pulled from the outlet portion of the probe at a flow rate of 5 µl/min. The probe was then inserted into the insular cortex as described in section 2.9. The concentration of LDH was again not sufficient to reach the threshold of detection in the LDH assay, therefore the experiment was repeated with the semi-permeable membrane of the probe removed. The membrane was carefully removed revealing a pull cannula surrounded by an outer push cannula. The pull cannula was shortened using a scalpel until the distance between the pull and push cannulae was 0.5 mm. The *in vitro* recovery efficiency test was performed as detailed in section 2.8 and the recovery efficiency was determined to be ~75%. The push-pull experiment was repeated using animals administered 17β-estradiol (Sigma-Aldrich; 0.0125 mg/kg) or saline (0.2 ml) having underwent MCAO or sham occlusion (n = 5 per group).

2.13 *Cerebrospinal fluid sample collection*

Samples were collected into a 250 µl Hamilton syringe hooked up to a syringe pump (Harvard Apparatus). The samples in the syringe were emptied into 0.6 ml microcentrifuge tubes (Fisher Scientific, Inc.) and these tubes were stored on ice for the duration of the experiment. Samples were collected in 20 minute intervals 1 hour prior to and 4 hours post- MCAO. As in the microdialysis experiments, the first 2 samples were discarded.

2.14 *Determination of probe placement*

At the end of the experimental time course, animals were perfused, brains removed, and 1 mm coronal sections were cut as described in section 2.3. Tissue sections were stored in 4% formalin at 4°C. To verify that the tips of the microdialysis and push-pull probes were inserted in the insular cortex, sections in which the probe had reached its maximum depth were examined under a dissecting microscope. These sections were compared with the corresponding sections obtained from a stereotaxic atlas of the rat brain (175).

2.15 *Statistical analysis*

The statistical analysis was carried out using a statistical software package (SigmaStat and SigmaPlot; Jandel Scientific, Tujunga, CA). All data are presented as a mean ± standard error of the mean. In all cases, differences were considered statistically significant if $p \leq 0.05$. A one-way analysis of variance (ANOVA) and either a paired or unpaired t-test were used to determine if significant differences existed over time and between both treatment groups. Post-hoc analysis was carried out with the Student-

Newman-Keuls test. The paired t-test was used in most of the western blotting analysis because the data were standardized to the mean band density from the contralateral side in saline treated animals. For the active caspase-12 data, an unpaired t-test was used because the blots were run in a different fashion. The data from the push-pull perfusion experiments was sequentially collected and therefore a one-way ANOVA with repeated measures was used. The area under the curve was also determined for the push-pull perfusion experiments and an unpaired t-test was performed to determine if significant differences existed between groups. For the immunohistochemical data, the number of positively stained cells in the ischemic and contralateral regions was determined. A paired t-test was used to determine if significant differences existed between the ipsilateral and contralateral cortices within each animal, whereas an unpaired t-test was used to determine if differences existed between estrogen and saline treated animals.

The letters located in the graphs of the results section indicate significant differences between points:

* = estrogen value is significantly different from saline value at the same time point

= value is significantly different from 0 hour time point in the same treatment group

† = value is significantly different from sham or contralateral value at the same time point

! = value is significantly different from 4 hour time point in the same treatment group

CHAPTER 3. RESULTS

3.1 *Preliminary infarct volume assessment*

The infarct volume was measured from estrogen and saline treated animals at 4 hours post-MCAO to determine if the size and variability of the infarct, as well as the neuroprotective effect of estrogen, were similar to those previously determined in our laboratory (42). Estrogen was observed to significantly decrease ($p < 0.05$; $n = 3$/group; Figure 11) the area of the infarct at 4 hours post-MCAO when compared to saline. The infarct size, (measured as a percentage of the hemisphere), in estrogen treated animals was 24.3 ± 5.4 %, in comparison to 57.0 ± 1.9 % in saline treated animals. This represented an estrogen-induced reduction in infarct volume by 57 %, similar to the ~50% estrogen-induced decrease in infarct size previously demonstrated in our laboratory (42).

3.2 *Levels of procaspase-12 in estrogen and saline treated animals following MCAO*

To determine if the neuroprotective effects of estrogen were mediated through EnR stress-induced apoptotic pathways, the expression of procaspase-12 following MCAO in both estrogen and saline treated animals was investigated by western blotting. Figure 12 contains representative western blots showing the expression of procaspase-12 in the infarct, peri-infarct and corresponding contralateral regions at 0, 1, 2, 3, and 4 hours post-MCAO.

3.2.1 *Changes in procaspase-12 in the infarct region*

Analysis and quantification of western blots showed that estrogen significantly decreased ($p < 0.05$; $n = 6$; Figure 13A) levels of procaspase-12 in the infarct region at 1

A

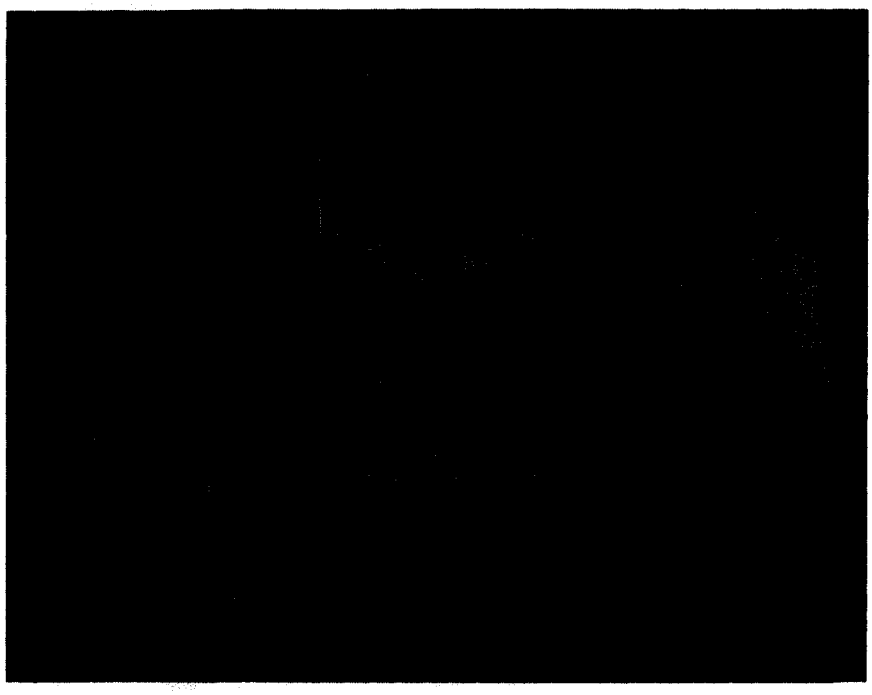

B

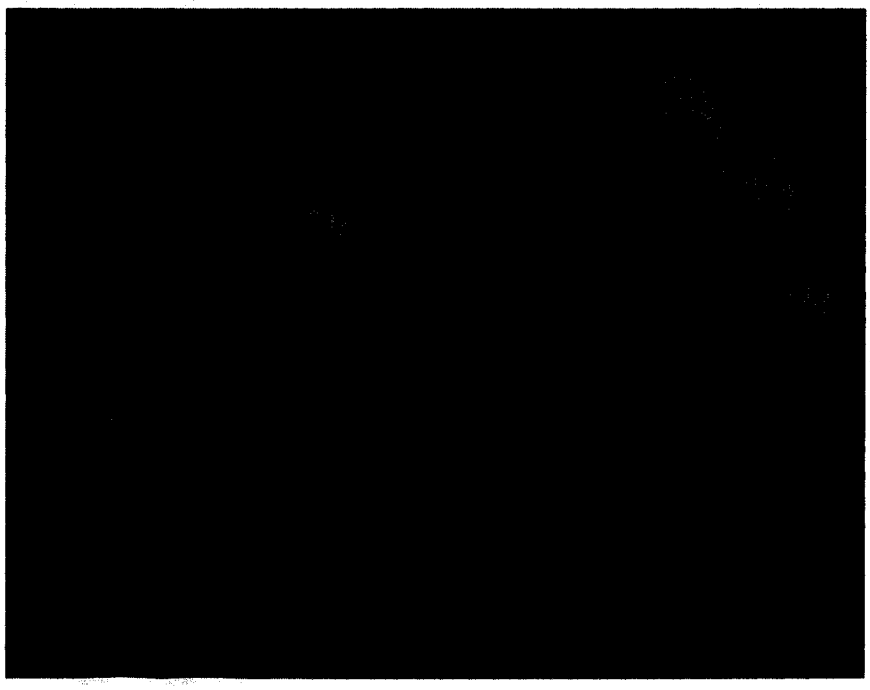

Figure 11. Digital photographs of TTC-stained coronal sections at 4 hours post-MCAO with either estrogen (A) or saline (B) pretreatment. The infarct area is indicated by the unstained region outlined above.

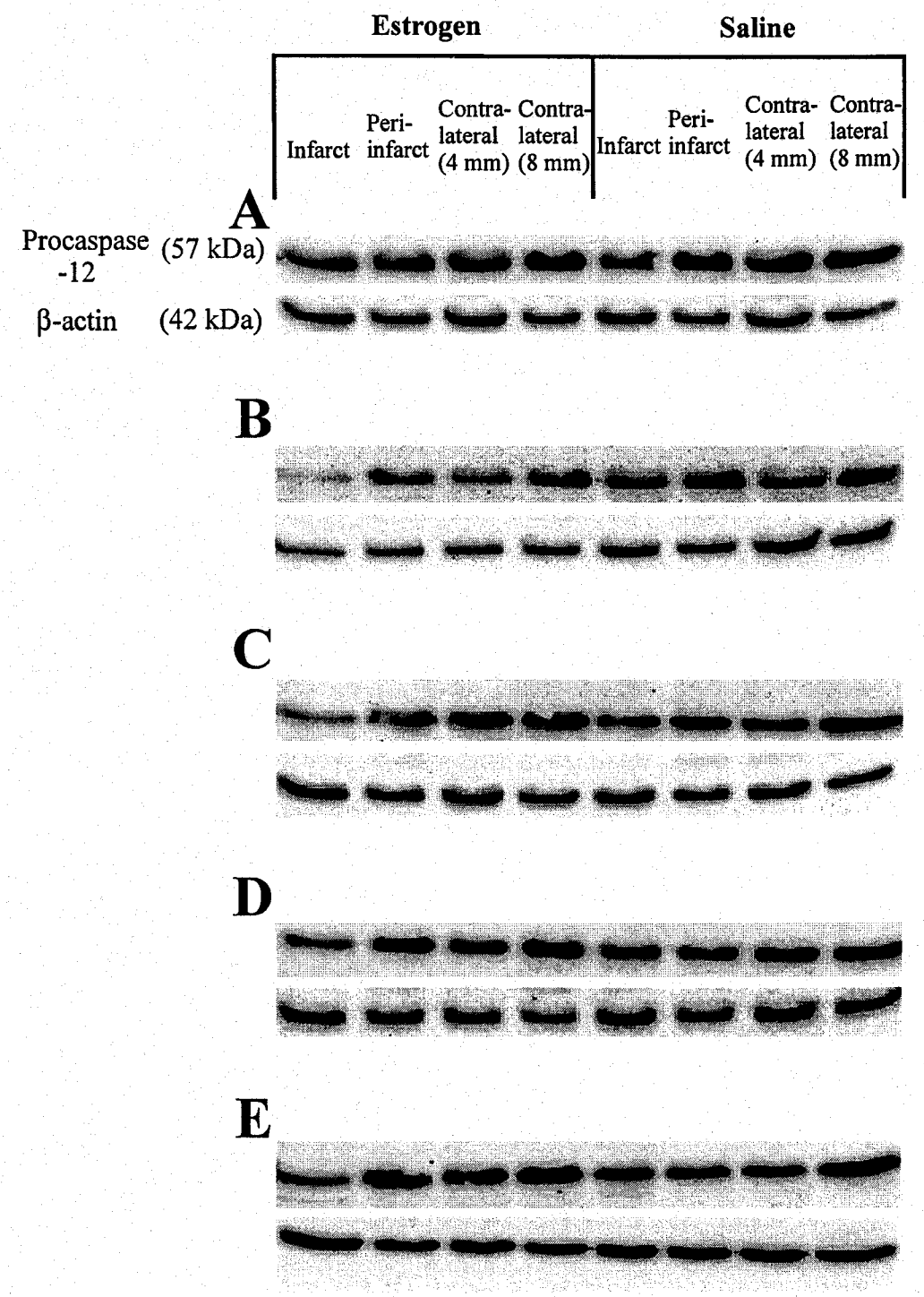

Figure 12. Representative western blots showing procaspase-12 and the corresponding β-actin levels in the infarct, peri-infarct, and corresponding contralateral regions in both estrogen and saline treated animals. A: immediately following MCAO (0 hours), B: 1 hour post-MCAO, C: 2 hours post-MCAO, D: 3 hours post-MCAO, E: 4 hours post-MCAO.

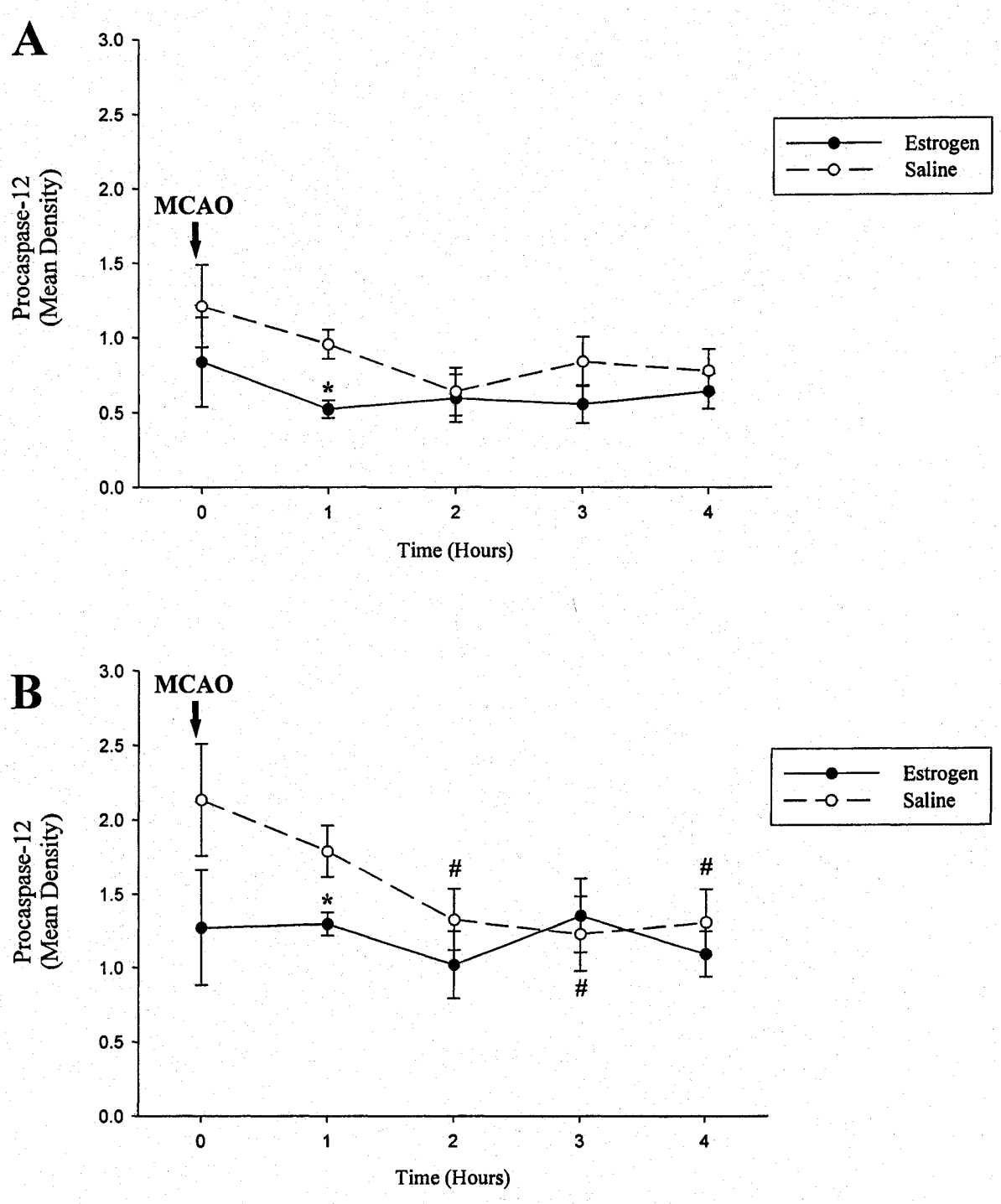

Figure 13. Procaspase-12 expression on the ipsilateral side at 0, 1, 2, 3, and 4 hours post-MCAO with either estrogen or saline pretreatment. A: Infarct (4 mm punch), B: Peri-infarct (8 mm punch). * indicates significant difference ($p < 0.05$) between estrogen and saline treated animals at the same time point; # indicates significant difference ($p < 0.05$) from 0 hours post-MCAO within the same treatment group.

hour post-MCAO. No significant differences ($p > 0.05$) were found at any other time point up to 4 hours post-MCAO when comparisons were made between estrogen and saline treated animals. A one-way ANOVA was performed to determine if procaspase-12 levels changed over time within each treatment group. In both estrogen and saline treated animals, there were no significant differences ($p > 0.05$) over the 4 hour post-MCAO time period.

3.2.2 *Changes in procaspase-12 in the peri-infarct region*

Estrogen treatment was also found to significantly decrease ($p < 0.05$; $n = 6$; Figure 13B) the level of procaspase-12 in the peri-infarct region at 1 hour post-MCAO when compared to saline. Similar to the infarct region, there were no significant differences ($p > 0.05$) in procaspase-12 levels between estrogen and saline treated animals at any other time points.

There was also no significant difference ($p > 0.05$; Figure 13B) over time in the estrogen treatment group. In contrast, in saline treated animals, the level of procaspase-12 in the peri-infarct region significantly decreased ($p < 0.05$) from that observed immediately following MCAO (0 hours). Procaspase-12 expression was found to be lower at 2, 3, and 4 hours post-MCAO compared to the 0 hour post-MCAO time point.

3.2.3 *Changes in procaspase-12 in the contralateral regions*

Tissue from the contralateral cortex corresponding to the infarct (4 mm punch) and peri-infarct (8 mm punch) was collected and used as an internal control and the level of procaspase-12 in these regions was determined. No significant differences in procaspase-12 expression were observed between estrogen and saline treated animals at

any time point in both the 4 mm ($p > 0.05$; $n = 6$; Figure 14A) and 8 mm ($p > 0.05$; $n = 6$; Figure 14B) contralateral regions. There was also no significant difference ($p > 0.05$) over the 4 hour time course within each treatment group in both contralateral regions.

To determine if the expression of procaspase-12 was increased on the ipsilateral side compared to the contralateral side in both estrogen and saline treated animals, a paired t-test was performed. The level of procaspase-12 was significantly decreased ($p < 0.05$; $n = 6$; Table 2) in animals pretreated with estrogen in the infarct region when compared to the corresponding contralateral region immediately following the stroke (0 hours) as well as at 1 and 4 hours post-MCAO.

There was no significant difference ($p > 0.05$; $n = 6$; Table 2) in the level of procaspase-12 at any time point following MCAO in estrogen treated animals when the peri-infarct region was compared to the corresponding contralateral region.

No significant differences ($p > 0.05$; $n = 6$; Table 3) were observed between the infarct core and the corresponding contralateral region in saline treated animals at any time point up to 4 hours post-MCAO.

When the level of procaspase-12 in the peri-infarct was compared to the corresponding contralateral region in saline treated animals, significant differences ($p < 0.05$; $n = 6$; Table 3) were observed. At both the 0 and 1 hour post-MCAO time points, procaspase-12 levels were significantly higher in the peri-infarct region (8 mm punch) in comparison to the contralateral side.

3.3 *Caspase-12 activation following MCAO*

The amount of cleaved caspase-12 (observed at a molecular weight of ~30 kDa), indicating caspase-12 activation, was determined in both estrogen and saline treated

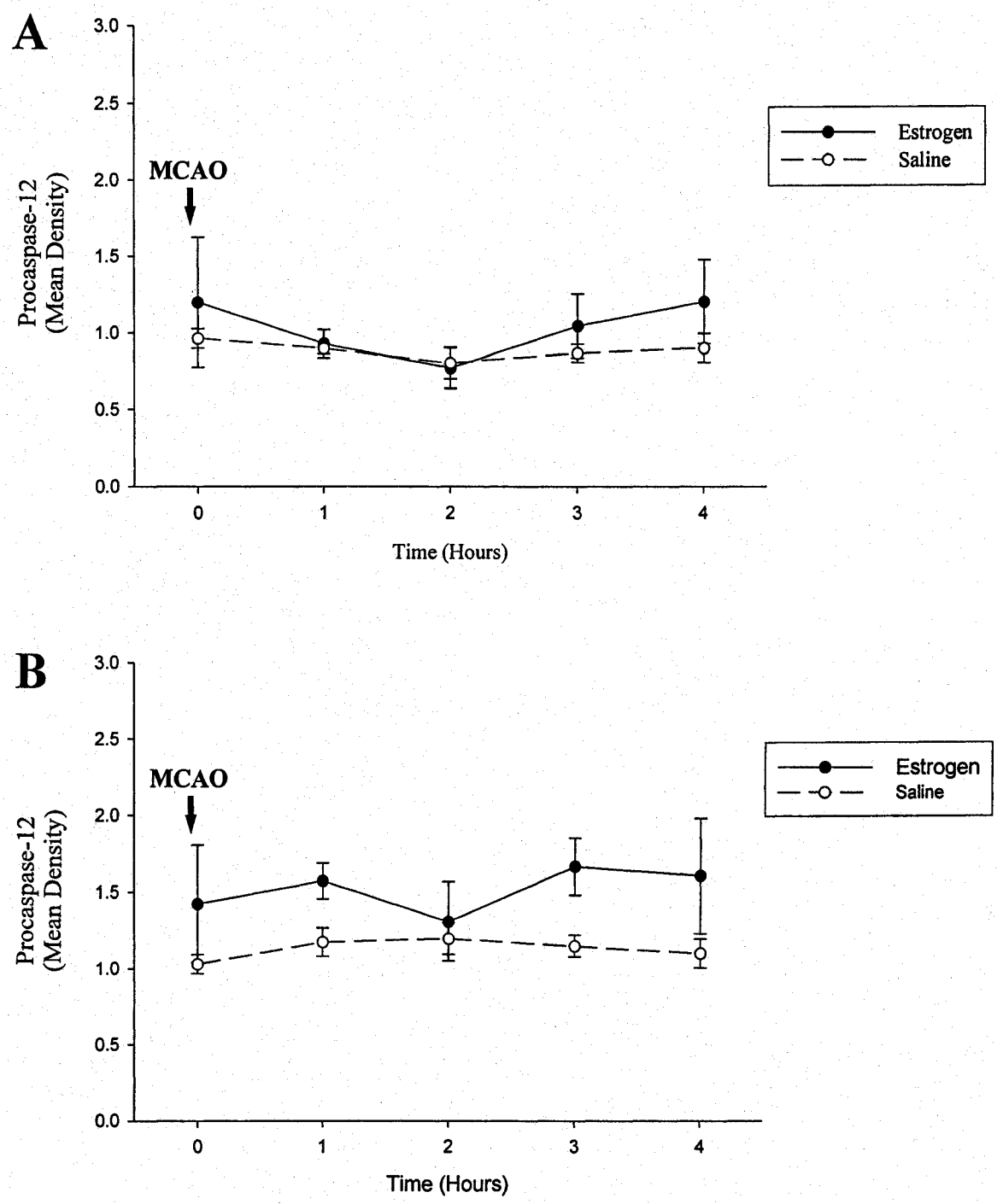

Figure 14. Procaspase-12 expression on the contralateral side at 0, 1, 2, 3, and 4 hours post-MCAO with either estrogen or saline pretreatment. A: Contralateral region corresponding to infarct (4 mm punch), B: Contralateral region corresponding to peri-infarct (8 mm punch).

Table 2. Comparison of the expression of procaspase-12 between the ipsilateral and contralateral cortices in ***estrogen*** treated animals at 0, 1, 2, 3, and 4 hours post-MCAO

Time Following MCAO (Hours)	Mean Density of Protein Bands ± Standard Error					
	Infarct	Contralateral (4 mm)	Comparison Between Groups p-value	Peri-Infarct	Contralateral (8 mm)	Comparison Between Groups p-value
0	0.84 ± 0.30	1.20 ± 0.43	**p = 0.04***	1.74 ± 0.57	1.98 ± 0.64	p = 0.63
1	0.52 ± 0.06	0.93 ± 0.09	**p = 0.003***	1.30 ± 0.08	1.57 ± 0.12	p = 0.09
2	0.60 ± 0.16	0.77 ± 0.13	p = 0.25	1.02 ± 0.23	0.77 ± 0.26	p = 0.07
3	0.56 ± 0.13	1.05 ± 0.21	p = 0.10	1.35 ± 0.25	1.67 ± 0.19	p = 0.26
4	0.64 ± 0.12	1.20 ± 0.27	**p = 0.02***	1.09 ± 0.15	1.61 ± 0.38	p = 0.13

* indicates significant difference between ipsilateral and corresponding contralateral region

Table 3. Comparison of the expression of procaspase-12 between the ipsilateral and contralateral cortices in ***saline*** treated animals 0, 1, 2, 3, and 4 hours post-MCAO

Time Following MCAO (Hours)	Mean Density of Protein Bands ± Standard Error					
	Infarct	Contralateral (4 mm)	Comparison Between Groups p-value	Peri-Infarct	Contralateral (8 mm)	Comparison Between Groups P-value
0	1.21 ± 0.28	0.96 ± 0.06	p = 0.39	2.14 ± 0.38	1.03 ± 0.06	**p = 0.04***
1	0.96 ± 0.10	0.89 ± 0.04	p = 0.63	1.79 ± 0.17	1.17 ± 0.09	**p = 0.02***
2	0.64 ± 0.16	0.80 ± 0.10	p = 0.34	1.33 ± 0.21	1.20 ± 0.10	p = 0.68
3	0.84 ± 0.17	0.87 ± 0.06	p = 0.87	1.23 ± 0.25	1.15 ± 0.07	p = 0.96
4	0.78 ± 0.15	0.90 ± 0.10	p = 0.51	1.31 ± 0.22	1.10 ± 0.10	p = 0.48

* indicates significant difference between ipsilateral and corresponding contralateral region

animals. Activated caspase-12 was observed in the infarct region in the procaspase-12 blots, therefore samples from these regions in animals pretreated with either estrogen or saline were run on additional blots and incubated in a higher concentration of caspase-12 primary antibody (Figures 15 and 16). Activated caspase-12 was not observed on the contralateral side from either estrogen or saline treated animals at any time point post-MCAO (data not shown).

3.3.1 *Caspase-12 activation in the infarct region*

In the infarct region, a t-test revealed that estrogen significantly increased ($p < 0.05$; $n = 4$; Figure 17A) the level of activated caspase-12 at both 2 and 3 hours post-MCAO in comparison to saline treated animals. Significant differences between treatment groups were not observed at any other time point following MCAO.

In addition, the expression of activated caspase-12 was observed to significantly increase ($p < 0.05$) over time. At 2 and 3 hours post-MCAO, the amount of active caspase-12 was significantly elevated compared to the time point immediately following the stroke (0 hours).

3.3.2 *Caspase-12 activation in the peri-infarct region*

Estrogen was also found to significantly increase ($p < 0.05$; $n = 4$; Figure 17B) the level of activated caspase-12 at 2 hours post-MCAO. Significant differences in activated caspase-12 were not observed ($p > 0.05$) at any other post-MCAO time point between estrogen and saline treated animals.

A one-way ANOVA revealed no significant differences ($p > 0.05$) in activated caspase-12 levels over time within the estrogen and saline treatment groups.

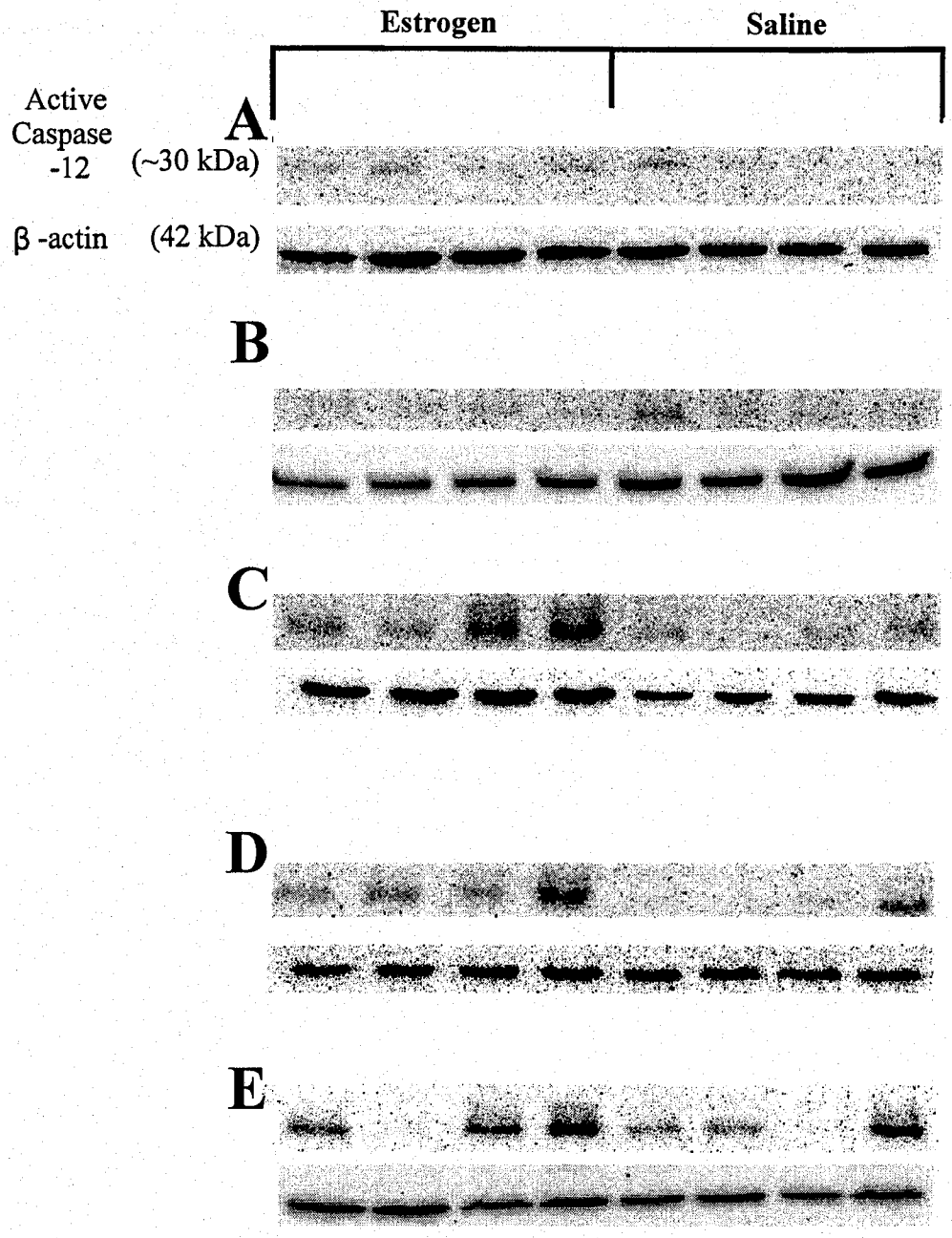

Figure 15. Western blots showing active caspase-12 and the corresponding β -actin levels in the infarct region in both estrogen and saline treated animals. A: immediately following MCAO (0 hours), B: 1 hour post-MCAO, C: 2 hours post-MCAO, D: 3 hours post-MCAO, E: 4 hours post-MCAO.

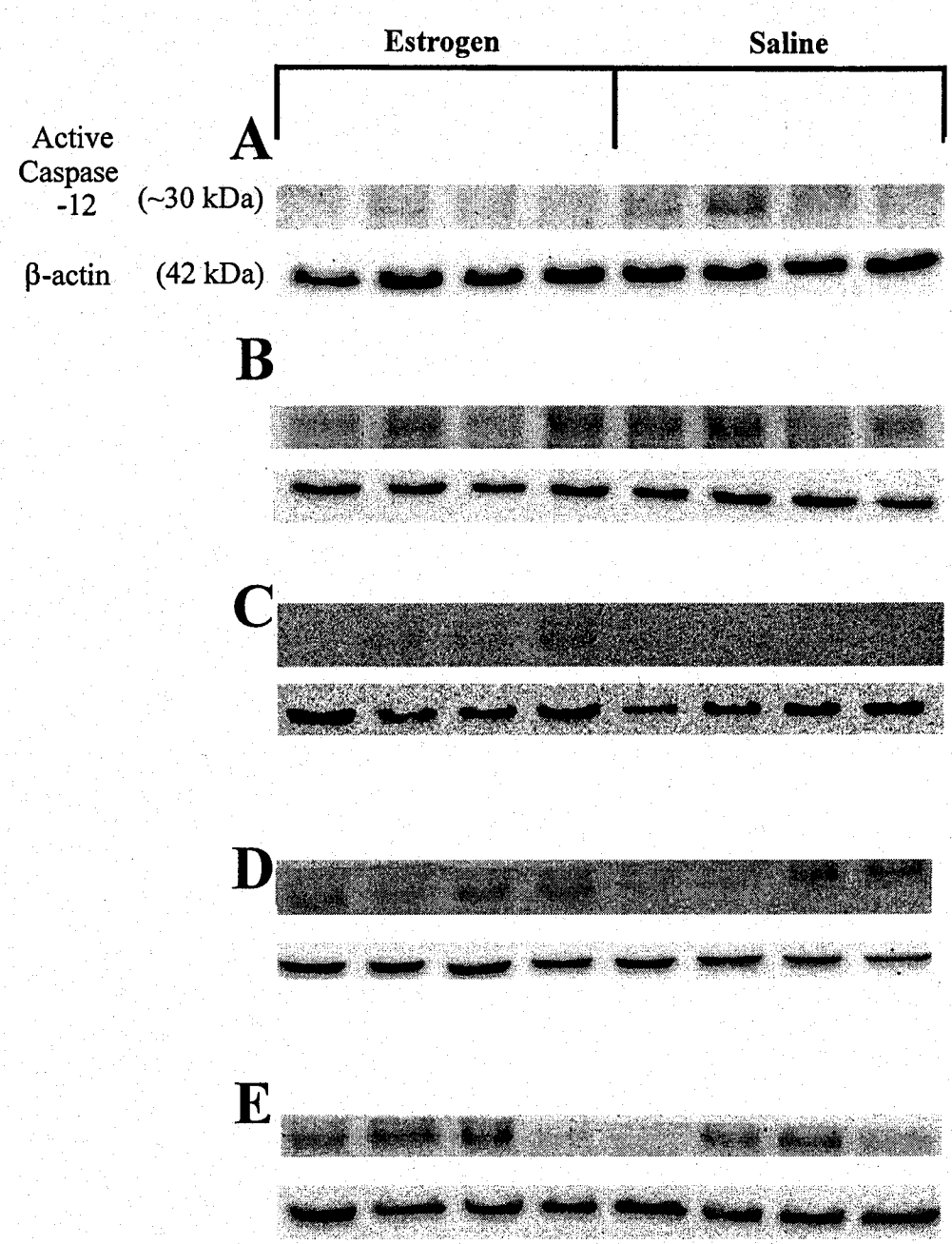

Figure 16. Western blots showing active caspase-12 and the corresponding β-actin levels in the peri-infarct region in both estrogen and saline treated animals. A: immediately following MCAO (0 hours), B: 1 hour post-MCAO, C: 2 hours post-MCAO, D: 3 hours post-MCAO, E: 4 hours post-MCAO.

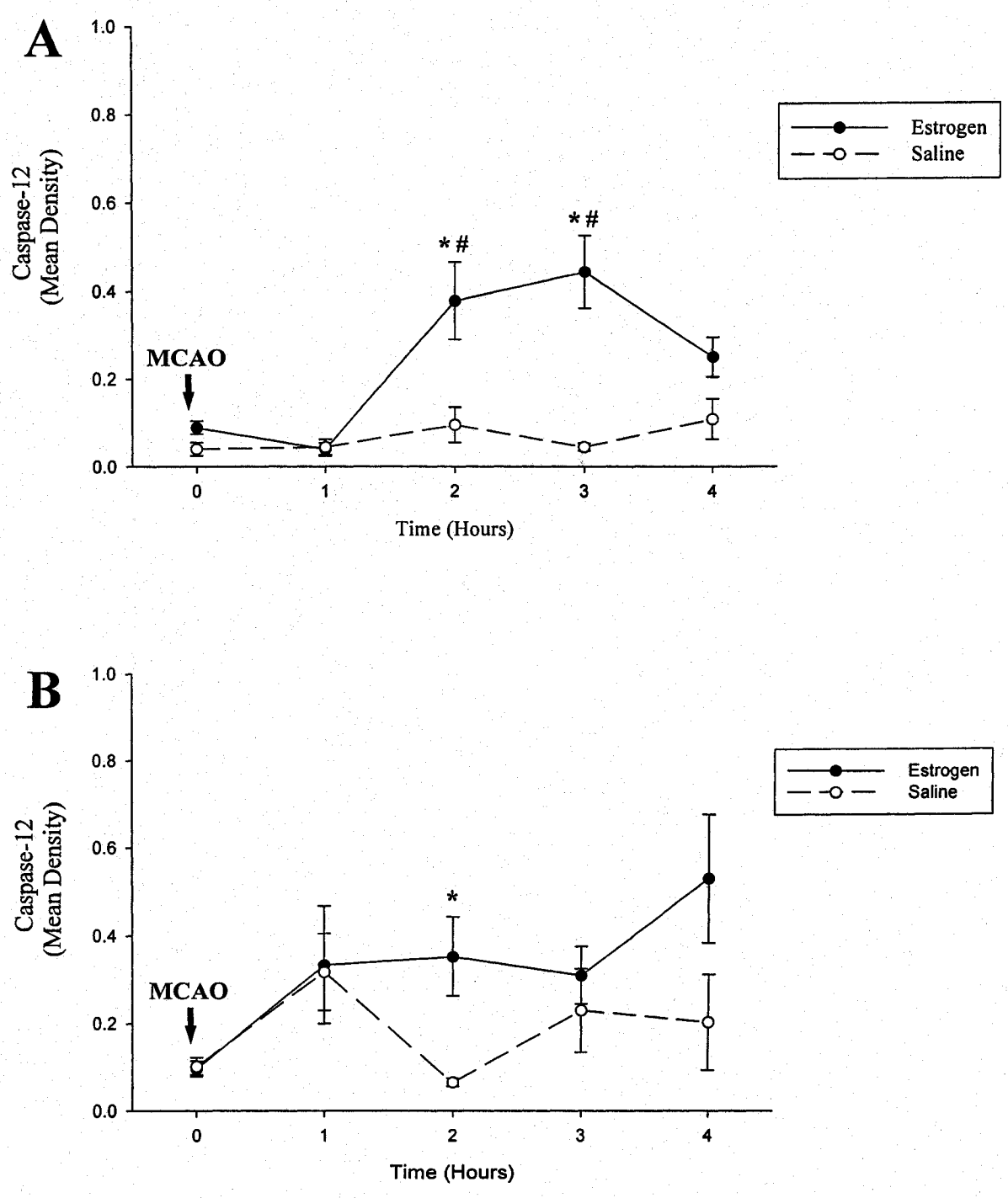

Figure 17. Active caspase-12 expression at 0, 1, 2, 3, and 4 hours post-MCAO with either estrogen or saline pretreatment. A: Infarct (4 mm punch), B: Peri-infarct (8 mm punch). * indicates significant difference ($p < 0.05$) between estrogen and saline treated animals at the same time point; # indicates significant difference ($p < 0.05$) from 0 hours post-MCAO within the same treatment group.

3.4 *Levels of m-calpain in estrogen and saline treated animals following MCAO*

Because caspase-12 activation was increased in estrogen treated animals, western blot analysis was performed to determine if changes in m-calpain, a well known regulator of caspase-12 activity, correlated with changes in procaspase-12 levels following MCAO. The level of m-calpain in both estrogen and saline treated animals was determined at 0, 1, 2, 3, and 4 hours post-MCAO. The representative western blots from each time point showing the level of m-calpain in the infarct, peri-infarct, and corresponding contralateral regions, are illustrated in Figure 18.

3.4.1 *Changes in m-calpain in the infarct region*

A paired t-test revealed that in comparison to saline, estrogen significantly increased ($p < 0.05$; $n = 3$-4; Figure 19A) the level of m-calpain in the infarct region 1 hour following MCAO. There were no significant differences ($p > 0.05$) in m-calpain levels in the infarct region at any other time point up to 4 hours post-MCAO when comparisons were made between estrogen and saline treated animals.

To determine if the level of m-calpain changed over the 4 hour time course in estrogen or saline treated animals, a one-way ANOVA was performed. No significant differences ($p > 0.05$) were observed over time within either the estrogen or saline treatment group.

3.4.2 *Changes in m-calpain in the peri-infarct region*

There were no significant differences ($p > 0.05$; $n = 3$-4; Figure 19B) in the level of m-calpain in the peri-infarct region between animals pretreated with estrogen compared to those pretreated with saline at any time point following MCAO.

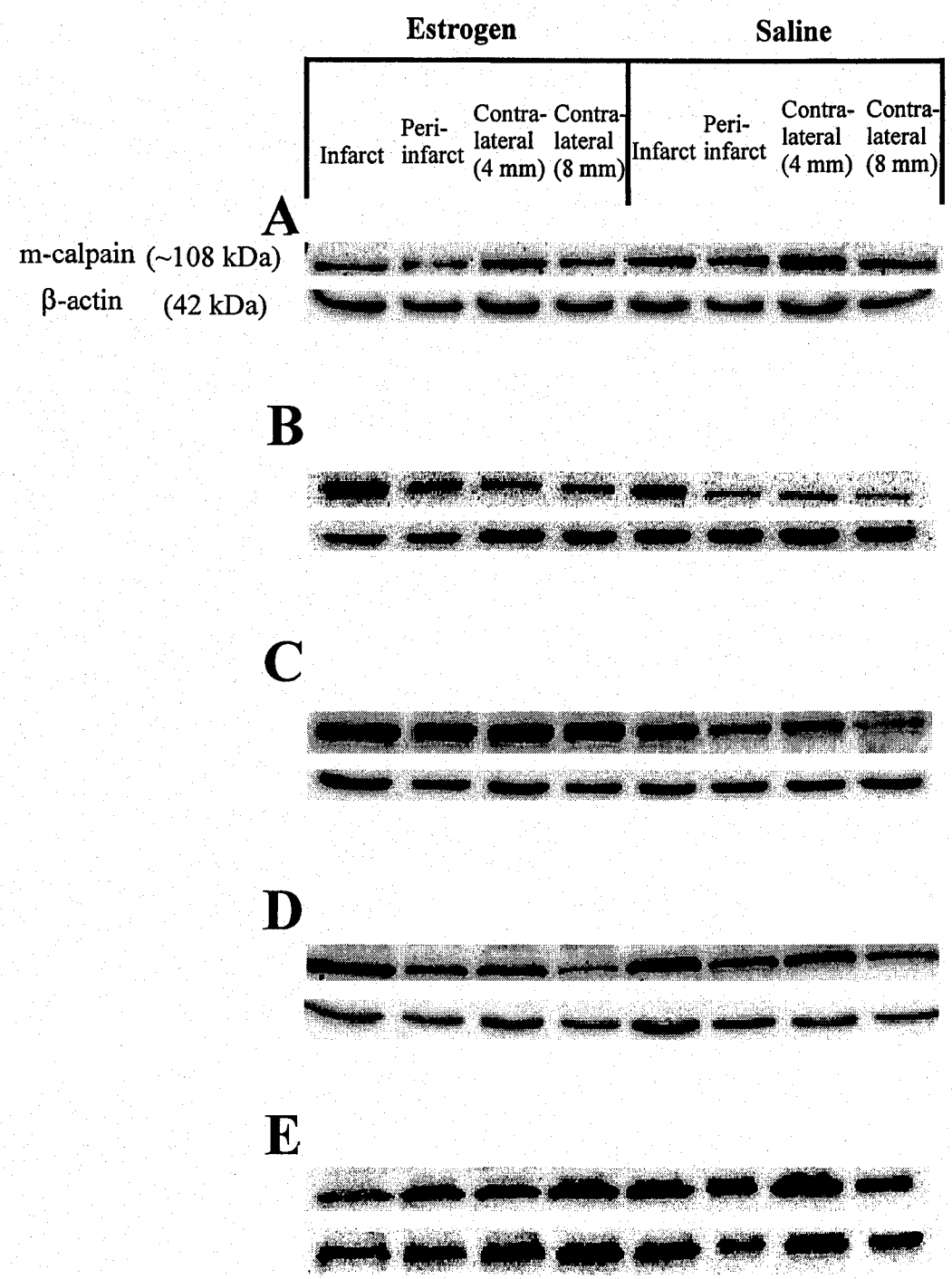

Figure 18. Representative western blots showing m-calpain and the corresponding β -actin levels in the infarct, peri-infarct, and corresponding contralateral regions in both estrogen and saline treated animals. A: immediately following MCAO (0 hours), B: 1 hour post-MCAO, C: 2 hours post-MCAO, D: 3 hours post-MCAO, E: 4 hours post-MCAO.

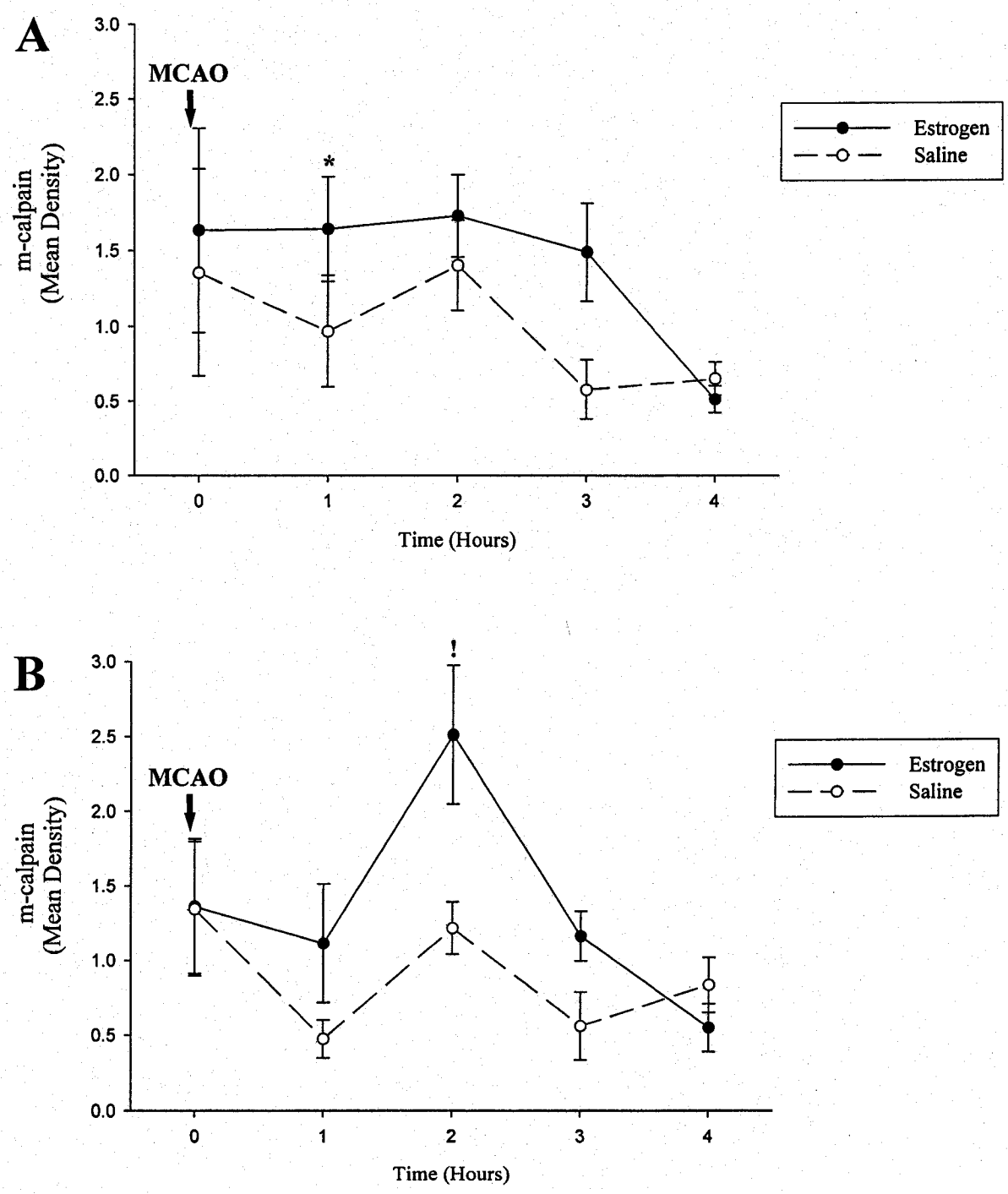

Figure 19. m-calpain expression on the ipsilateral side at 0, 1, 2, 3, and 4 hours post-MCAO with either estrogen or saline pretreatment. A: Infarct (4 mm punch), B: Peri-infarct (8 mm punch). * indicates significant difference ($p < 0.05$) between estrogen and saline treated animals at the same time point; ! indicates significant difference ($p < 0.05$) from 4 hours post-MCAO within the same treatment group.

In the peri-infarct region, a one-way ANOVA revealed that m-calpain expression significantly decreased ($p < 0.05$) at 4 hours post-MCAO compared to 2 hours following the stroke.

3.4.3 *Changes in m-calpain in the contralateral regions*

The level of m-calpain in the contralateral region corresponding to the infarct region (4 mm punch) in estrogen treated animals was found to be significantly lower ($p < 0.05$; $n = 3$-4; Figure 20A) at 4 hours post-MCAO compared to that in saline treated animals. There were no significant differences ($p > 0.05$) in m-calpain levels in this contralateral region between estrogen and saline treated animals at any other time point following the stroke.

A one-way ANOVA revealed that the level of m-calpain in the contralateral region (4 mm) in estrogen treated animals was significantly lower ($p < 0.05$; Figure 20A) at 4 hours post-MCAO compared to the time point immediately following the stroke (0 hours). No significant differences ($p > 0.05$) were observed in m-calpain levels over time in animals pretreated with saline.

When the level of m-calpain in the contralateral region corresponding to the peri-infarct region (8 mm) was compared between estrogen and saline treated animals at each time point following MCAO, no significant differences ($p > 0.05$; Figure 20B) were observed.

A significant difference ($p < 0.05$; Figure 20B) was observed in m-calpain expression in estrogen treated animals at 2 hours post-MCAO compared to the time point immediately following the stroke (0 hours). There were no significant differences ($p > 0.05$) in the level of m-calpain in saline treated animals over time following MCAO.

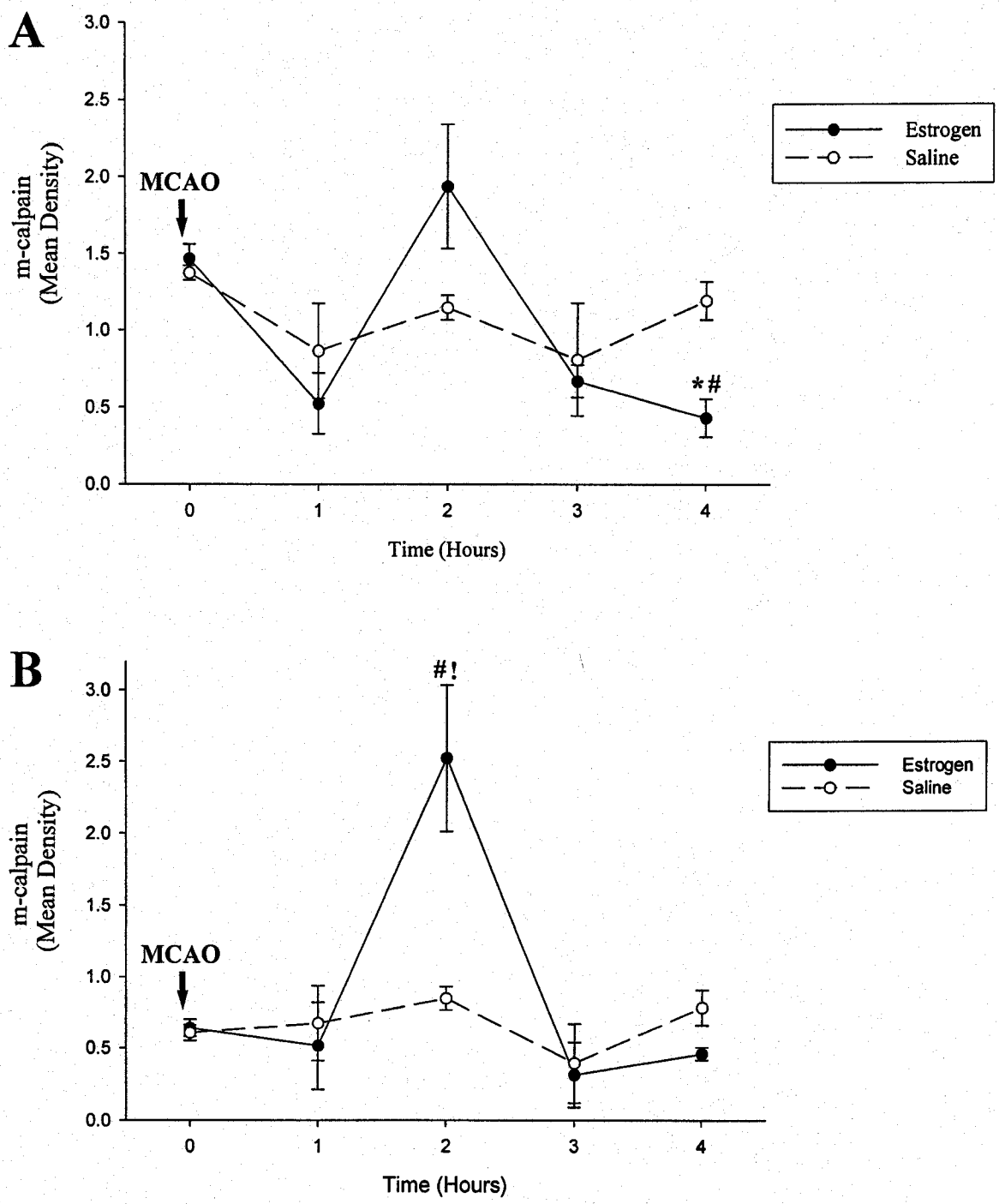

Figure 20. m-calpain expression at 0, 1, 2, 3, and 4 hours post-MCAO with either estrogen or saline pretreatment. A: Contralateral region corresponding to infarct (4 mm punch), B: Contralateral region corresponding to peri-infarct (8 mm punch). * indicates significant difference ($p < 0.05$) between estrogen and saline treated animals at the same time point; # indicates significant difference ($p < 0.05$) from 0 hours post-MCAO within the same treatment group; ! indicates significant difference ($p < 0.05$) from 4 hours post-MCAO within the same treatment group.

3.5 *Caspase-12 immunohistochemistry*

To confirm the western blot finding that estrogen causes an activation of caspase-12 following MCAO, caspase-12 immunohistochemistry was performed. Animals were pretreated with either estrogen or saline and subjected to MCAO for either 2 or 4 hours. The procedure was repeated multiple times using both paraffin-embedded sections and frozen tissue sections, and different caspase-12 antibodies. No immunostaining was detected under any conditions tested.

3.6 *TUNEL staining*

To determine if the increase in caspase-12 activation observed in estrogen treated animals following MCAO corresponded with an increase in apoptotic cell death, TUNEL staining was performed. Animals were administered estrogen or saline, and were subjected to MCAO for either 2 or 4 hours. In each experiment, both a positive control (DNase treatment) and a negative control (enzyme solution omission) were included. Figure 21 shows both positive and negative control sections, as well as the anatomical location of the tissue in the ipsilateral and contralateral cortices in which the number of positive cells was quantified. No staining was observed in the negative control sections.

3.6.1 *TUNEL staining in estrogen and saline treated animals at **2 hours** post-MCAO*

The number of TUNEL-positive cells in the ipsilateral and contralateral cortices was compared within animals pretreated with either estrogen or saline. Figure 22 shows representative digital photomicrographs of TUNEL-stained sections counterstained with hematoxylin at 2 hours post-MCAO. A paired t-test revealed no significant differences ($p > 0.05$; $n = 3$; Figure 23) in the number of stained cells between the ipsilateral and

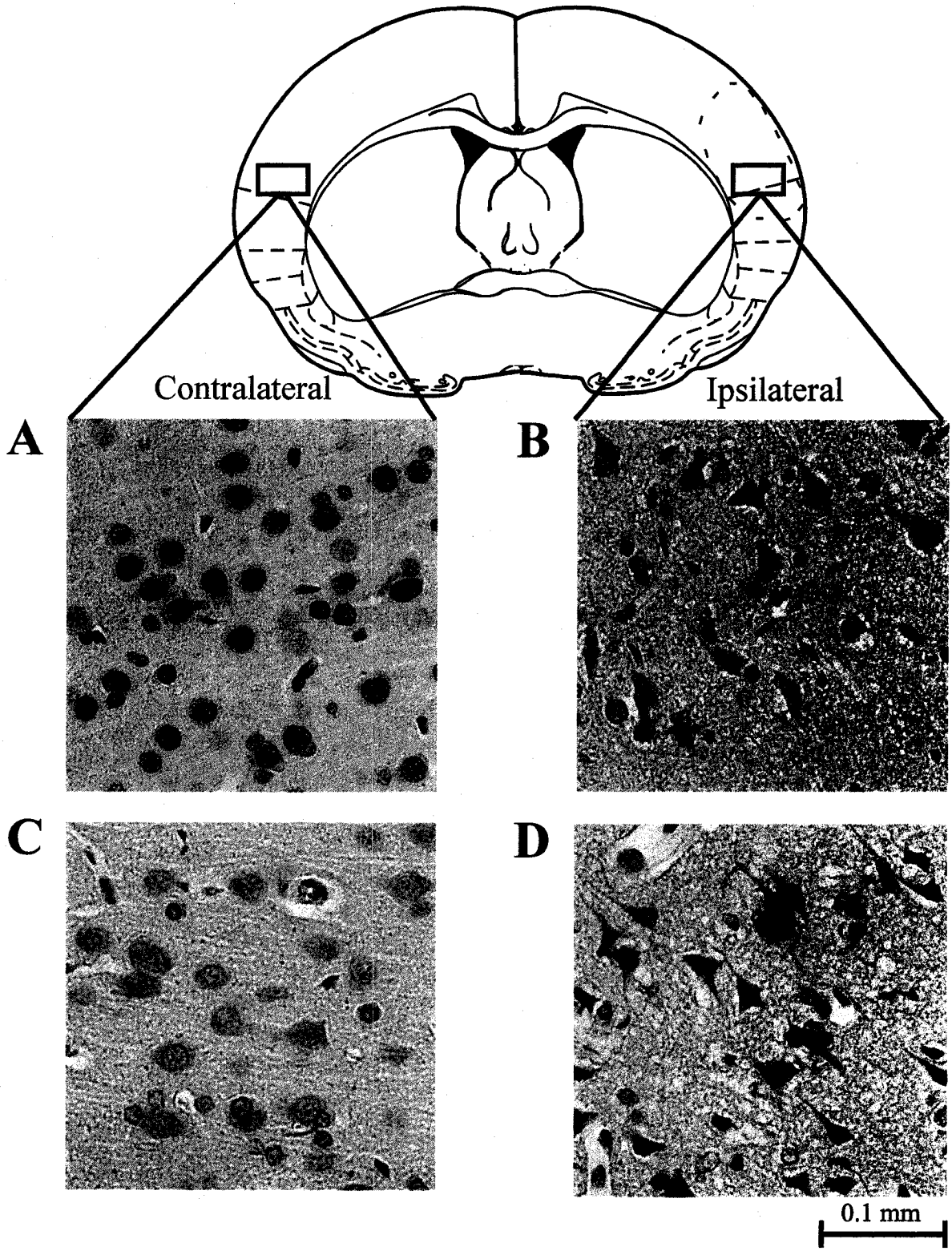

Figure 21. TUNEL staining in the ipsilateral and contralateral cortices. A: Positive TUNEL staining in the contralateral cortex induced with DNase, B: Positive TUNEL staining in the ipsilateral cortex induced with DNase, C: Negative control (contralateral cortex), D: Negative control (ipsilateral cortex). 80

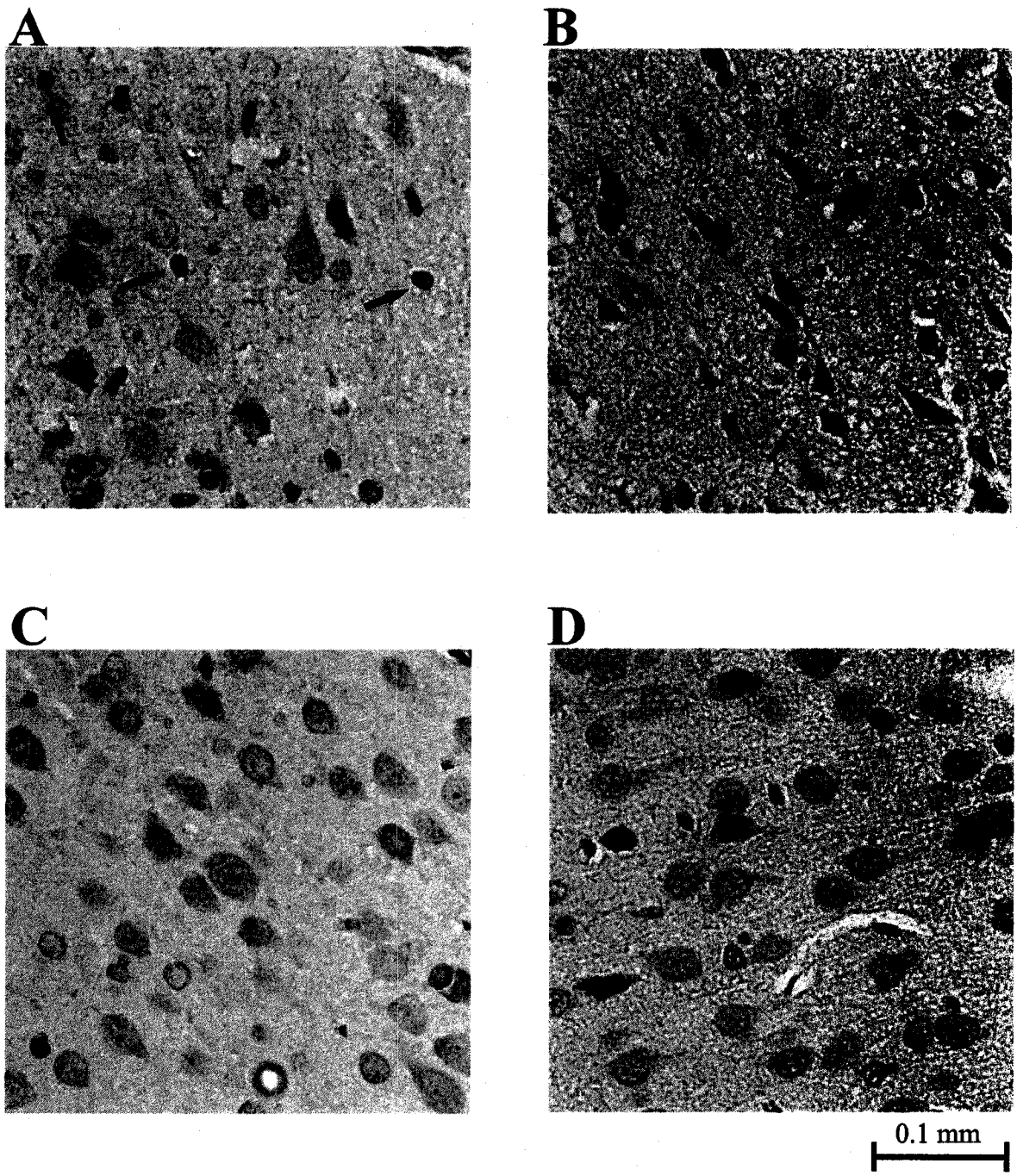

Figure 22. Representative tissue sections illustrating TUNEL staining in both estrogen and saline treated animals at 2 hours post-MCAO. A: TUNEL staining in the ipsilateral cortex at 2 hours post-MCAO with estrogen pretreatment, B: Contralateral cortex at 2 hours post-MCAO in an estrogen treated animal, C: TUNEL staining in the ipsilateral cortex at 2 hours post-MCAO with saline pretreatment, D: Contralateral cortex at 2 hours post-MCAO in a saline treated animal. Arrows indicate TUNEL positive cells.

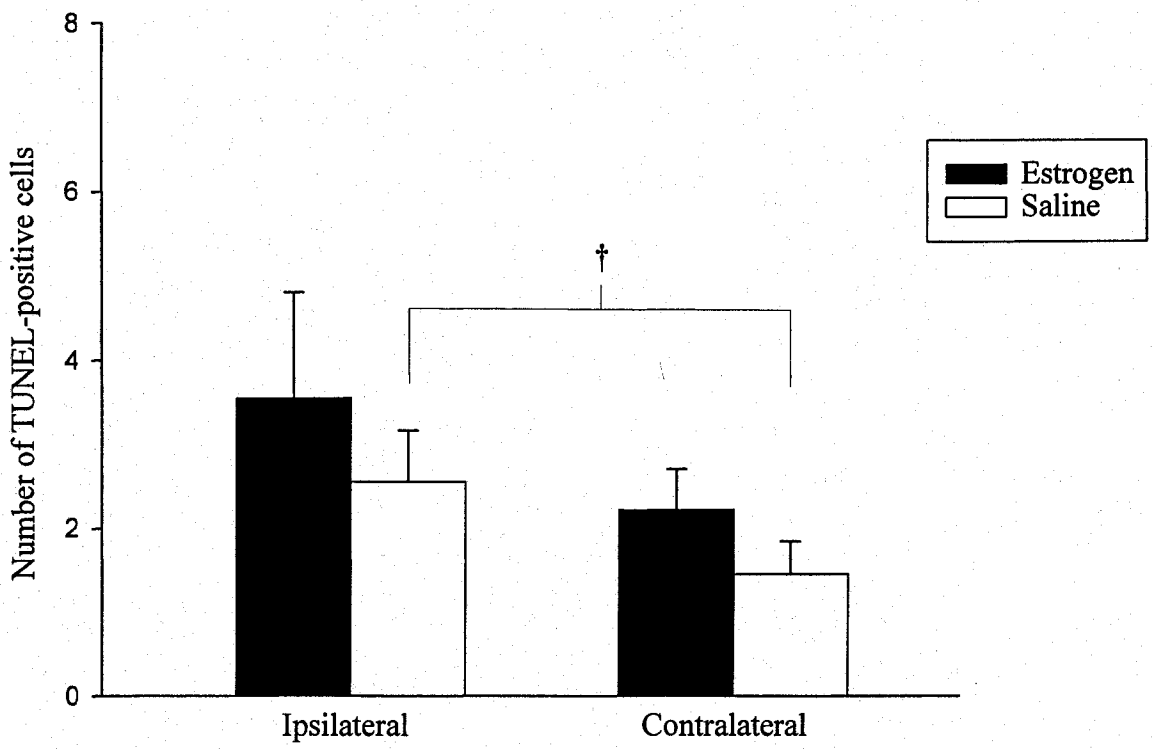

Figure 23. Number of TUNEL-positive cells in the ipsilateral and contralateral cortices from both estrogen and saline treated animals at 2 hours post-MCAO. † indicates significant difference ($p < 0.05$) between ipsilateral and contralateral cortices within the same treatment group.

contralateral cortices in estrogen treated animals at 2 hours post-MCAO. In saline treated animals however, the number of TUNEL-positive cells in the infarct region was significantly higher ($p < 0.05$) than that observed in the corresponding contralateral region. A bar graph summarizing these results is shown in Figure 23.

To determine if estrogen treatment resulted in an increase in apoptotic cell death, the amount of TUNEL staining in estrogen and saline treated animals was investigated. At 2 hours post-MCAO, there were no significant differences ($p > 0.05$; Figure 23) in the number of TUNEL-positive cells in the infarct region when estrogen treated animals were compared to those treated with saline. Similarly, no significant differences ($p > 0.05$) were observed in the contralateral regions between the two treatment groups at 2 hours post-MCAO.

3.6.2 *TUNEL staining in estrogen and saline treated animals at **4 hours** post-MCAO*

Figure 24 shows representative digital photomicrographs of TUNEL-stained sections counterstained with hematoxylin at 4 hours post-MCAO. A paired t-test revealed that the number of TUNEL-positive cells in the infarct region in estrogen treated animals was significantly higher ($p < 0.05$; Figure 25) than in the corresponding contralateral region. In saline treated animals, a similar result was observed: the number of positively stained cells was significantly elevated ($p < 0.05$) in the ipsilateral, compared to the contralateral, cortex.

The number of TUNEL-positive cells in animals administered estrogen was compared to those administered saline to determine the effect of estrogen on apoptotic cell death at 4 hours post-MCAO. An unpaired t-test revealed that estrogen significantly increased ($p < 0.05$; Figure 25) the number of positively stained cells in the infarct region

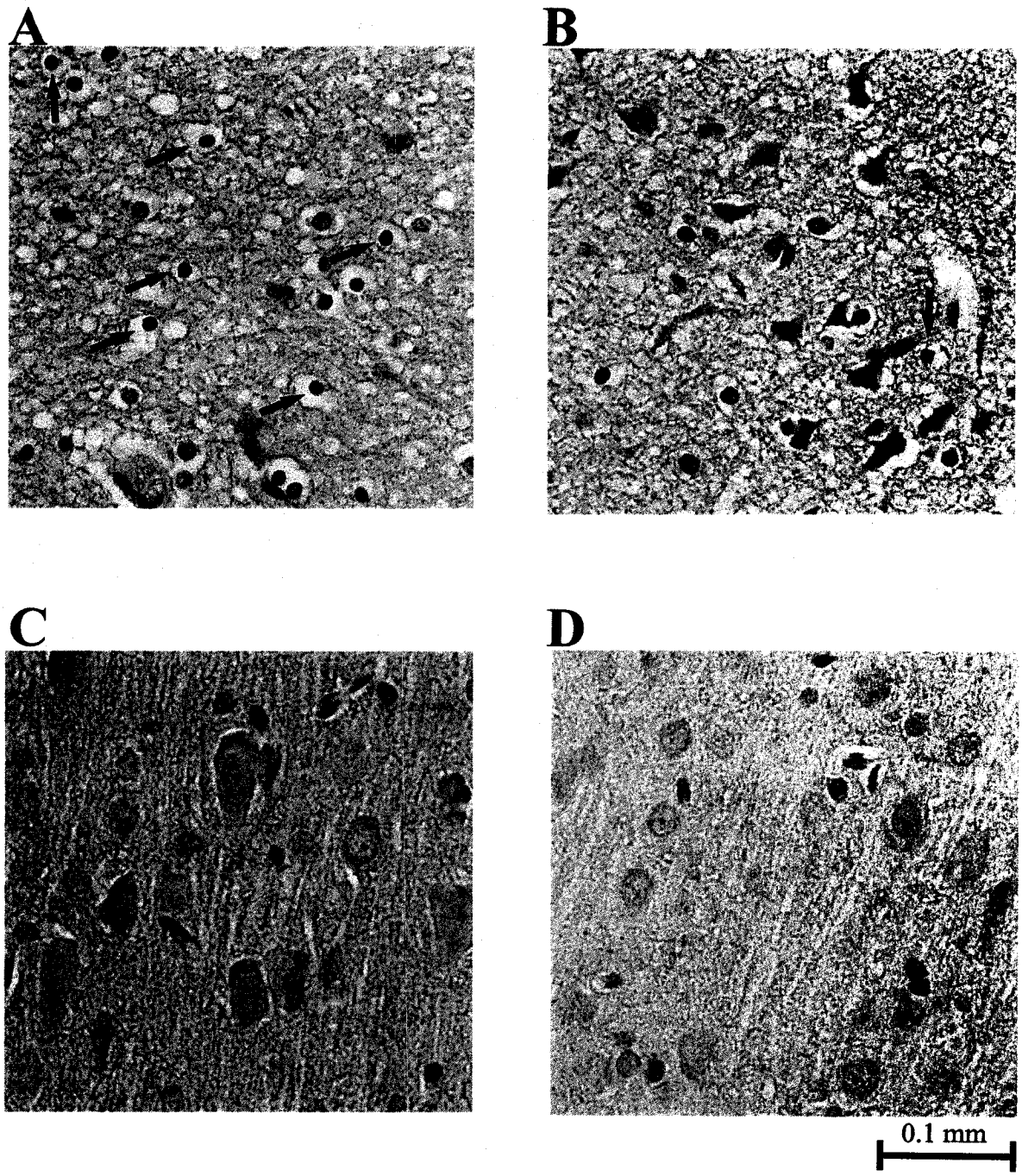

Figure 24. Representative tissue sections illustrating TUNEL staining in estrogen and saline treated animals at 4 hours post-MCAO. A: TUNEL staining in the ipsilateral cortex at 4 hours post-MCAO with estrogen pretreatment, B: Contralateral cortex at 4 hours post-MCAO in an estrogen treated animal, C: TUNEL staining in the ipsilateral cortex at 4 hours post-MCAO with saline pretreatment, D: Contralateral cortex at 4 hours post-MCAO in a saline treated animal. Arrows indicate TUNEL positive cells.

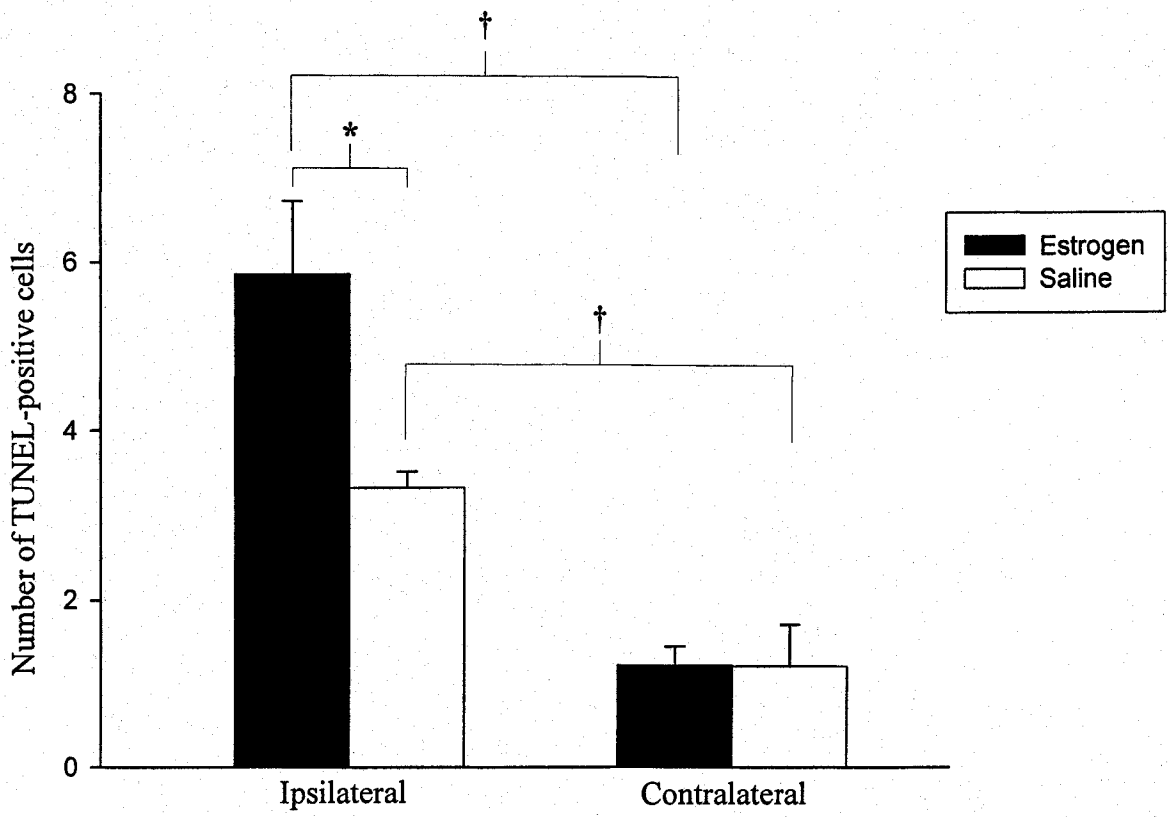

Figure 25. Number of TUNEL-positive cells in the ipsilateral and contralateral cortices from both estrogen and saline treated animals at 4 hours post-MCAO. * indicates significant difference ($p < 0.05$) between estrogen and saline treated animals; † indicates significant difference ($p < 0.05$) between ipsilateral and contralateral cortices within the same treatment group.

compared to saline. No significant difference ($p > 0.05$) in TUNEL staining was observed in the contralateral cortices between estrogen and saline treated animals. A bar graph summarizing these results is presented in Figure 25.

3.7 *DNA laddering and apoptotic cell death*

To provide further evidence for an estrogen-induced increase in apoptotic cell death, agarose gel electrophoresis was performed to assess DNA laddering. DNA from the ipsilateral and contralateral hemispheres from both estrogen and saline treated animals was isolated and DNA fragmentation was analyzed by gel electrophoresis. Figure 26 shows DNA agarose gel electrophoresis using isolated DNA from either estrogen or saline treated animals at 4 hours post-MCAO. The amount of DNA run on the gel was 3 μg per lane, except for in one lane where the amount was doubled (6 μg) to ensure there was a sufficient amount of DNA to be able to observe DNA laddering.

At 4 hours post-MCAO, no DNA laddering was observed in the ipsilateral or contralateral cortices from either estrogen or saline treated animals.

3.8 *Changes in the concentration of LDH post-MCAO in estrogen versus saline treated animals*

Microdialysis experiments were initially performed to determine the amount of LDH in the CSF as an indicator of necrotic cell death following MCAO in estrogen and saline treated animals. The dialysate samples were collected over the 4 hour time course at 20 minute intervals and assayed for LDH. The amount of LDH present in the CSF samples was below the detection threshold for the LDH assay, most likely reflecting the low recovery efficiency of the probe (~10 %). Push-pull perfusion was then performed as described in the Methods (section 2.1.2). Prior to the *in vivo* experiments, an *in vitro*

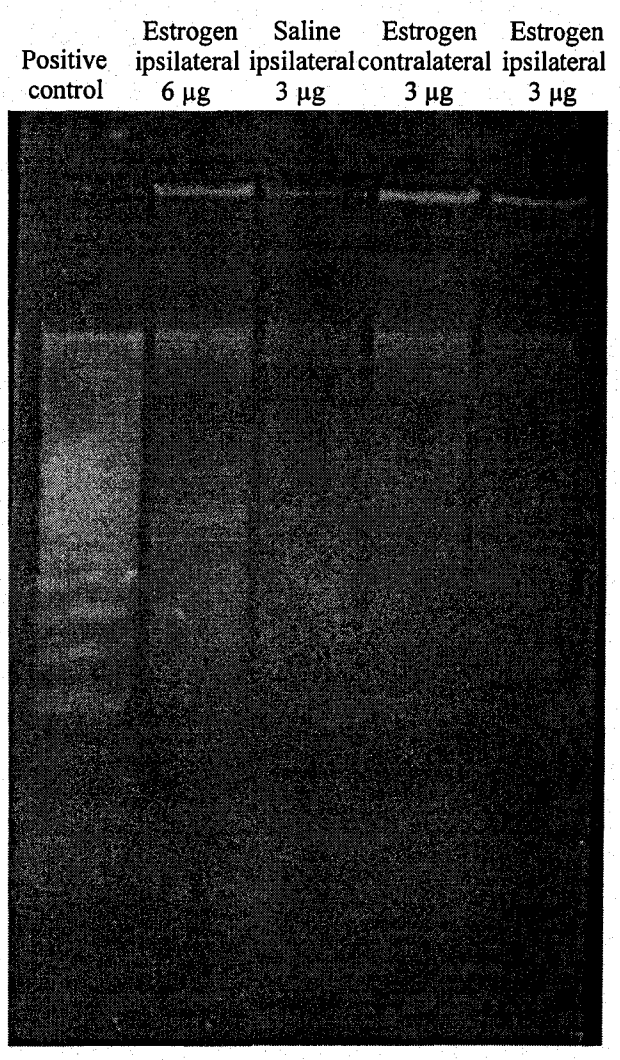

Figure 26. Agarose gel electrophoresis using DNA isolated from either estrogen or saline treated animals subjected to 4 hours MCAO.

recovery efficiency test was performed to determine the probe's ability to recover LDH. The push-pull probe utilized in these experiments was determined to have a recovery efficiency of ~ 75 %.

The LDH concentration present in the CSF in saline treated animals was compared between the MCAO and sham groups to determine if the concentration of LDH was higher following MCAO. A one-way ANOVA with repeated measures revealed a significant increase ($p < 0.05$; Figure 27A) in LDH concentration in MCAO treated animals at 160 minutes post-MCAO compared to sham treated animals at the same time point. There were no significant differences ($p > 0.05$) between the MCAO and sham groups at any other time point.

The area under the curve was calculated for both MCAO and sham occlusion groups in which animals were pretreated with saline. A t-test revealed a significant increase ($p < 0.05$; Table 4) in LDH concentration in the CSF in saline treated animals subjected to MCA occlusion compared to those subjected to sham occlusion.

A one-way ANOVA with repeated measures was performed to determine if significant differences existed over time in animals pretreated with saline and subjected to either MCAO or sham surgery. No significant differences ($p > 0.05$) were observed over time within either the MCAO or sham group in saline treated animals.

The concentration of LDH in the CSF from estrogen treated animals subjected to MCAO was compared to those undergoing sham surgeries. At various post-MCAO time points in saline treated animals, the concentration of LDH detected was significantly higher ($p < 0.05$; Figure 27A) in animals subjected to MCAO compared to those undergoing sham occlusion. These significant differences in the LDH concentration in

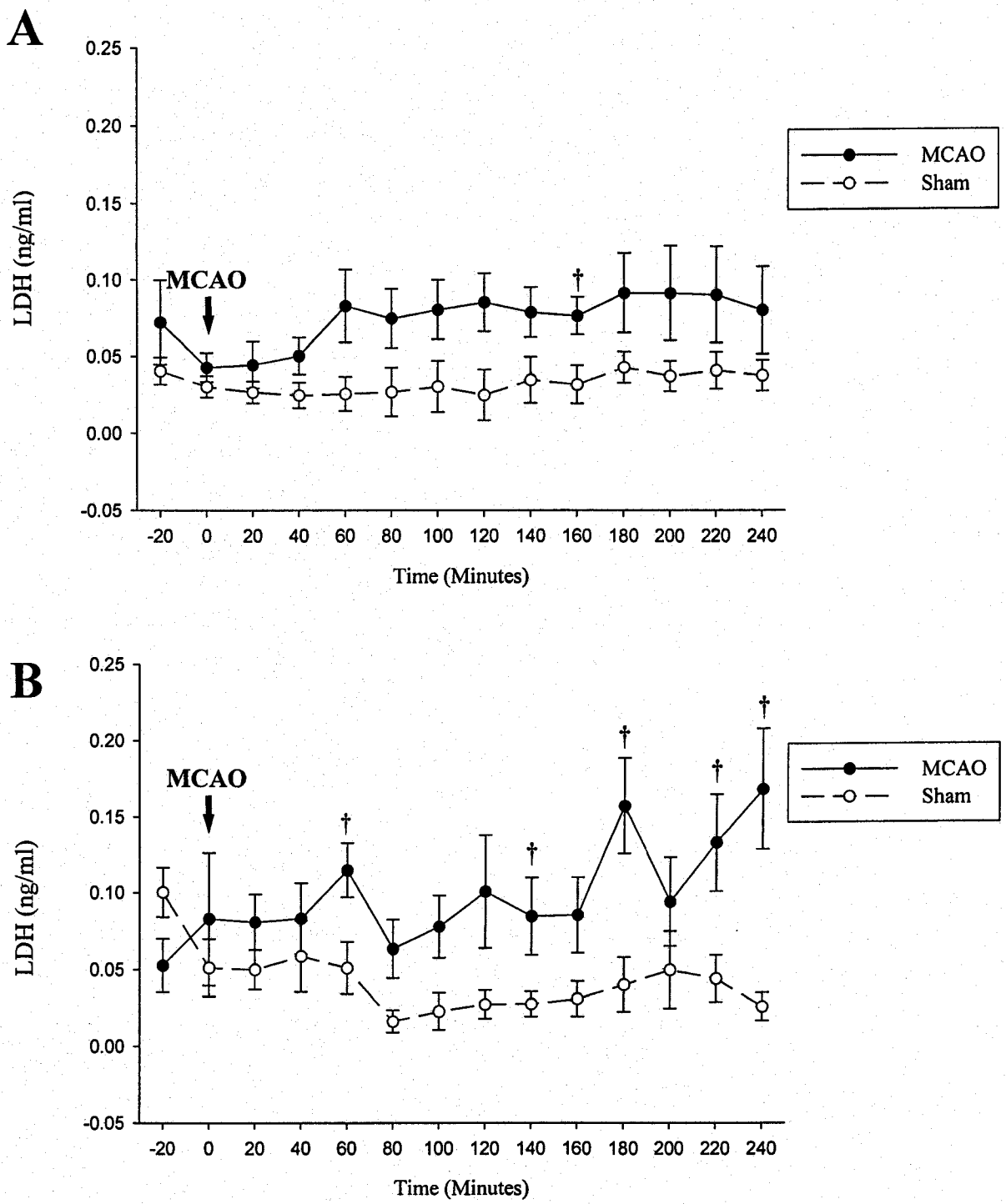

Figure 27. Lactate dehydrogenase concentrations in the cerebrospinal fluid sampled from the insular cortex prior to (-20 minutes) and at 20 minute intervals following either MCAO or sham in both saline (A) and estrogen (B) treated animals. † indicates significant difference ($p < 0.05$) between MCAO and sham at the same time point.

Table 4. Area under the curve calculations for the total concentration of LDH in the CSF in animals treated with either estrogen or saline and subjected to either MCAO or sham occlusion

Drug Treatment	Treatment	Mean Area Under the Curve ± Standard Error
Estrogen	MCAO	25.55 ± 5.86*
	Sham	10.08 ± 2.79
Saline	MCAO	18.73 ± 4.25*
	Sham	7.66 ± 2.03

* indicates significant difference from corresponding sham

the CSF between MCAO and sham treated animals (pretreated with estrogen) were observed at 60 minutes post-MCAO/sham, and again at 140, 180, 220, and 240 minutes post-MCAO/sham. No significant differences were observed at any other time points between MCAO and sham treated animals that had been pretreated with estrogen.

In addition, the values obtained from the area under the curve calculations for saline treated animals subjected to MCAO or sham occlusion indicated that the concentration of LDH in the CSF was significantly higher ($p < 0.05$; Table 4) overall in the MCAO group compared to the sham group.

As was observed in the saline treated animals, no significant differences ($p > 0.05$) were observed over time in saline treated animals subjected to either MCAO or sham occlusion.

3.8.1 *LDH concentration in the CSF following MCAO in estrogen versus saline treated animals*

To determine if the amount of necrotic cell death following MCAO was lower in animals pretreated with estrogen compared to those pretreated with saline, a one-way ANOVA with repeated measures was performed. This test revealed no significant differences ($p > 0.05$; Figure 28) in the concentration of LDH in the CSF at any time point up to 4 hours following MCAO between estrogen and saline treated animals.

In addition, values obtained using the area under the curve for both estrogen and saline treated animals were not significantly different ($p > 0.05$; Table 4).

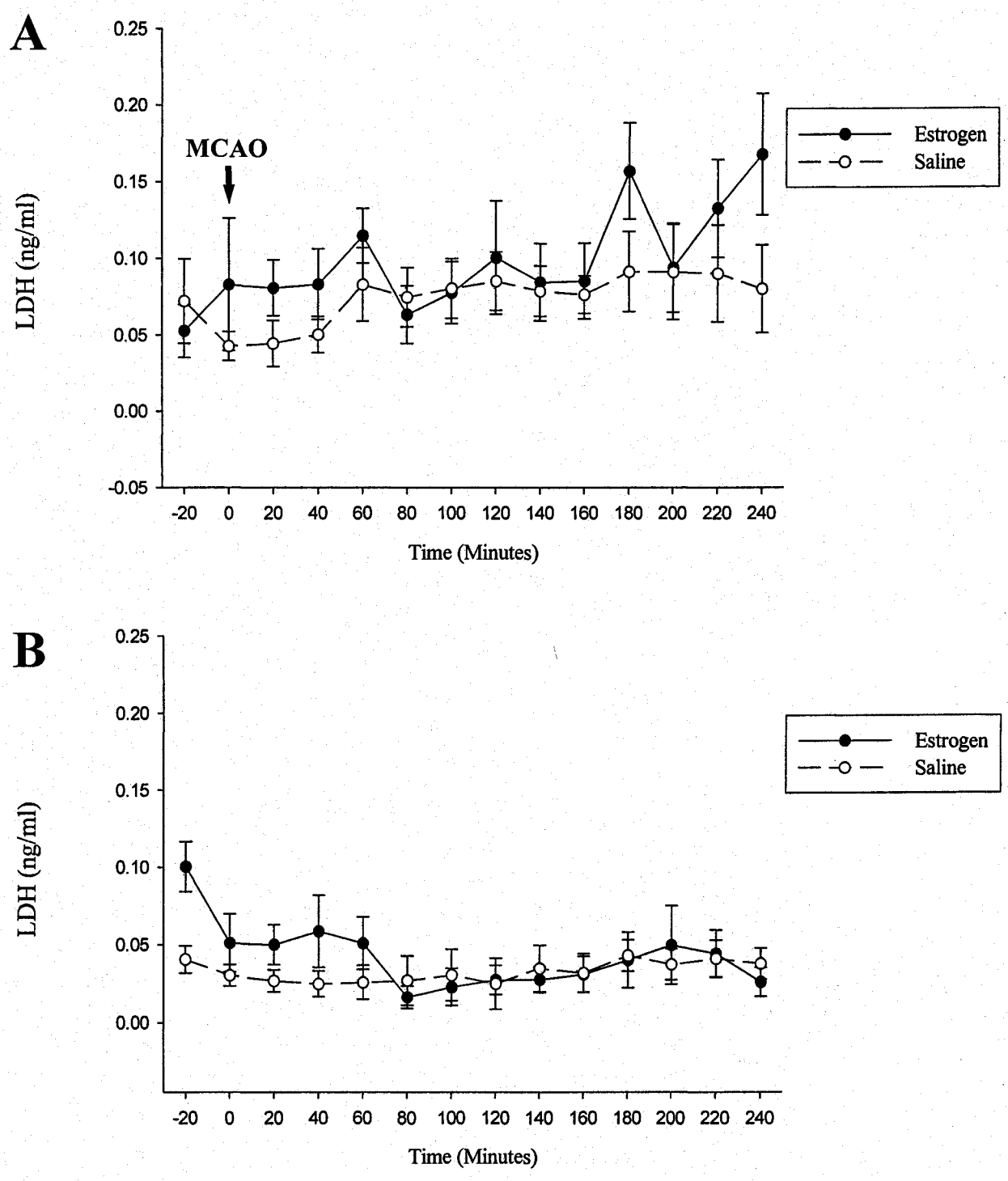

Figure 28. Lactate dehydrogenase concentrations in the cerebrospinal fluid sampled from the insular cortex prior to (-20 minutes) and at 20 minute intervals following either MCAO (A) or sham occlusion (B) in both estrogen and saline treated animals.

3.8.2 *LDH concentration in the CSF following sham occlusion in estrogen versus saline treated animals*

Estrogen treated animals subjected to sham occlusion were compared to saline treated animals undergoing sham surgery to determine if significant differences existed between these two groups. There were no significant differences ($p > 0.05$; Figure 28) between estrogen and saline treated animals subjected to sham occlusion at any time point up to 4 hours following the sham occlusion.

A t-test was performed to determine if significant differences existed in the area under the curve following sham occlusion between estrogen and saline treated animals. Again, no significant difference ($p > 0.05$; Table 4) was observed between these two groups.

Figure 29A shows a TTC stained coronal section illustrating the location of the probe tip within the cortex. Also illustrated is a schematic diagram indicating the placement of all probe tips within the cortex.

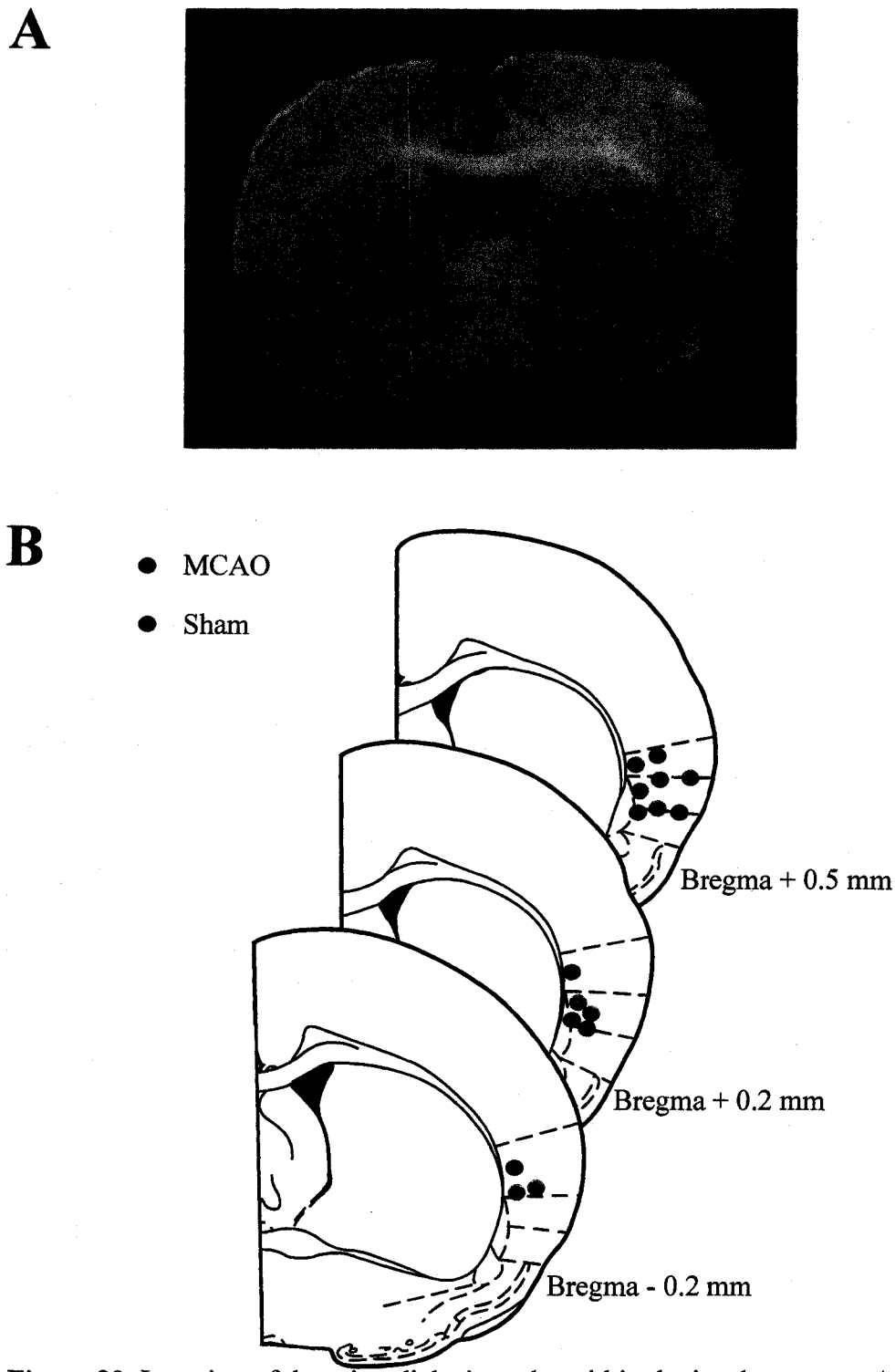

Figure 29. Location of the microdialysis probe within the insular cortex. A: TTC stained coronal section illustrating the placement of the probe 4 hours post-MCAO (the arrow indicates the tip of the probe), B: Schematic diagram illustrating the location of the tip of the probes within the insular cortex in either MCAO or sham treated animals.

CHAPTER 4. DISCUSSION

The experiments conducted in this thesis have provided evidence toward a potential molecular mechanism of estrogen-induced neuroprotection following permanent occlusion of the middle cerebral artery in male rats. The results from these studies suggest that the protective actions of estrogen are mediated by an increase in endoplasmic reticulum (EnR) stress-induced apoptosis via activation of caspase-12. Specifically, estrogen treatment was observed to decrease procaspase-12 expression in both the infarct and peri-infarct regions at 1 hour post-MCAO. This corresponded with an increase in activated caspase-12 at 2 hours post-MCAO in the both the infarct and peri-infarct region as well as at 3 hours post-MCAO in the infarct region. In addition, an estrogen-induced increase in the expression of m-calpain was observed at 1 hour post-MCAO in the infarct region, suggesting m-calpain may contribute to regulating caspase-12 activity following MCAO. At four hours post-MCAO, estrogen treatment resulted in an increase in DNA fragmentation, indicative of an increase in apoptotic cell death, as detected by TUNEL staining. The amount of necrotic cell death following MCAO was assessed by the presence of LDH in the CSF and the results indicated a significant elevation in necrotic cell death following MCAO compared to sham occlusion. However, estrogen treatment did not decrease the concentration of LDH in the CSF following MCAO when compared to saline treatment.

Taken together, these results provide evidence to support our hypothesis that the neuroprotective effects of estrogen are mediated by an increase in caspase-12-associated apoptotic cell death following MCAO.

4.1 *Estrogen-induced changes in caspase-12 expression following MCAO*

The first objective of this study was to determine if estrogen modulates the apoptotic pathway that results from EnR stress. To provide evidence for this objective, we first investigated the expression of procaspase-12 within the first 4 hours following MCAO. In both the infarct and peri-infarct regions, estrogen treatment was found to significantly reduce procaspase-12 levels at 1 hour post-MCAO compared to animals treated with saline. The mechanism behind the loss in procaspase-12 is likely through an induction in proteolytic cleavage to the active form of the enzyme. A reduction in the expression of a procaspase has been previously documented to correspond with proteolytic cleavage to generate the active caspase. Ryan and colleagues (178) reported a loss of procaspase-3 that coincided with the appearance of cleaved caspase-3 in a cell line exposed to an EnR stress-inducing agent. In vivo, caspase-12 cleavage products were observed following a decrease in the proenzyme in the spinal cord of amyotrophic lateral sclerosis (ALS) transgenic mice (179). In contrast, elevated levels of active caspase-12 have also been documented to be concurrent with an up-regulation in the expression of the proenzyme. Shibata et al. (124) reported that following cerebral ischemia, procaspase-12 was up-regulated at the same post-injury time points that caspase-12 activation was observed. However, this up-regulation was most prominent at 23 hours of reperfusion (which followed 1 hour of transient MCAO); therefore sufficient time was available for the induction of procaspase-12 to occur. Moreover, apoptotic cell death is more prominent in transient models of ischemia, compared to permanent occlusion models (180). Therefore, it makes sense that an induction in both the pro- and active form of the enzyme would occur in order to result in a significant amount of apoptosis.

A significant reduction in the expression of procaspase-12 was only observed at 1 hour post-MCAO (and not at any other post-MCAO time point) when estrogen treatment was compared to saline treatment. Therefore it is speculated that the reduction in procaspase-12 observed at 1 hour post-MCAO is responsible for the accumulation of active caspase-12 that reaches significance at 2 hours post-MCAO (to be discussed below).

Following estrogen administration, there were significantly lower levels of procaspase-12 at 1 hour post-MCAO in both the infarct and peri-infarct tissue compared to their corresponding regions on the contralateral side. This result provides further evidence that procaspase-12 is being cleaved to its active form on the ipsilateral side, which indicates that estrogen may be acting through a caspase-12 mediated apoptotic pathway.

To determine if the estrogen-induced reduction in procaspase-12 following MCAO corresponded with an increase in active products, we investigated the expression of active caspase-12 in estrogen versus saline treated animals. Significantly elevated levels of active caspase-12 were observed in the infarct region of estrogen treated animals at 2 and 3 hours post-MCAO. Furthermore, at these time points, caspase-12 levels were significantly higher than those measured immediately following MCAO (0 hours). Interestingly, caspase-12 activation was observed at 2 but not 3 hours post-MCAO in the peri-infarct region. As discussed in the Introduction, activation of caspases and subsequent apoptosis is typically more prominent in the peri-infarct (or penumbra) region (91). One of the main reasons for this spatial distribution appears to be the difference in energy levels between the two regions. Following ischemia, there is a profound energy

deprivation within the infarct core and as a result, apoptotic cell death is not as prominent in this region (91). However, energy-independent apoptotic pathways have been shown to occur within the infarct core (102) and DNA laddering has also been observed in the infarct core as early as 3 hours post-stroke (181). It is therefore reasonable that caspase-12 activation be observed in the infarct region in our model.

The above results suggest that the neuroprotective effects of estrogen are mediated through a caspase-12 specific pathway. Caspase-12 activation has been implicated in neuronal cell death resulting from both transient (124) and permanent (125) ischemia. Shibata et al. (124) observed activation of caspase-12 at 5-23 hours of reperfusion (after 1 hour of transient MCAO), but not at 2 hours of reperfusion. In the absence of estrogen treatment in the current investigation, there was also no apparent cleavage of caspase-12 within the acute phase (first 4 hours) of the stroke. However, estrogen administration was found to induce activation of caspase-12 within this time frame. Mouw and colleagues (125) assessed both caspase-12 mRNA and protein levels at 24 hours following permanent MCAO. At this time point, the authors reported an up-regulation in both the mRNA and active protein levels compared to those measured following sham occlusion.

Since estrogen-induced activation of caspase-12 was observed following MCAO, we subsequently attempted to determine if estrogen treatment had an effect on the expression of m-calpain, a well known upstream regulator of caspase-12 activity. In the infarct region, the expression of m-calpain was significantly higher with estrogen treatment at 1 hour post-MCAO compared to saline treatment. In the peri-infarct region however, estrogen treatment did not result in a significant elevation in m-calpain

expression. This was unexpected since procaspase-12 levels were significantly reduced and caspase-12 activation was observed in the peri-infarct region. Perhaps m-calpain is not the sole regulator of caspase-12 activity in this model. m-calpain is activated by a millimolar concentration of cytosolic calcium, and such a high concentration would be more likely be observed within the infarct region (91). As previously discussed, several proteases have been documented to activate caspase-12, including m-calpain, caspase-7, as well as TRAF2. Of these proteases, m-calpain appears to play a predominant role in activating caspase-12 in neuronal cell death (164). Nakagawa and colleagues (164) reported caspase-12 activation in primary cortical neurons exposed to conditions of oxygen and glucose deprivation (OGD) and this activation was prevented in the presence of an m-calpain inhibitor. Of the studies that investigated caspase-12 activation following cerebral ischemia, Shibata et al. (124) attempted to determine the mechanisms responsible for this activation. They concluded that caspase-7 was not likely to contribute to the cleavage of caspase-12 in their experimental MCAO model, because caspase-7 was not detected in the EnR fraction during the period of caspase-12 activation. There is also evidence for m-calpain-induced activation of caspase-12 in non-neuronal cells. Tan et al. (182) reported m-calpain was required for cleavage of caspase-12 in primary fibroblast cultures.

The increased m-calpain expression in our stroke model was observed at the same post-MCAO time point in the infarct region as the estrogen-induced decrease in procaspase-12, suggesting that m-calpain may play a role in cleaving procaspase-12 in this experimental model. However, additional experiments would be required to confirm the role of m-calpain in activating caspase-12. Specifically, administration of a calpain

inhibitor prior to MCAO would confirm if m-calpain is responsible for the cleavage of caspase-12 following MCAO.

The anti-m-calpain antibody utilized in these experiments recognized protein bands with a molecular weight of approximately 108 kDa, whereas in most tissues, m-calpain is typically detected at 80 kDa (169). According to the manufacturers' specifications, the anti-m-calpain antibody is directed at Domain III of the large (80 kDa) subunit. In kidney and liver, this antibody recognized an 80 kDa subunit, and when a kidney sample was included in our blots as an internal control, a strong band at 80 kDa was observed. However, to the best of our knowledge, m-calpain expression has not been assessed by western blotting in the rodent brain, therefore the molecular weight at which m-calpain is recognized in the brain is not precisely known. As previously mentioned, m-calpain consists of an 80 kDa subunit and a 28 kDa regulatory subunit (169), therefore it is likely that the band we recognized at about 108 kDa, was a combination of the large and small subunits. To confirm if this was the case, an alternative anti-m-calpain antibody that recognized the small (28 kDa) subunit was used. Using this antibody, protein bands were detected at the same molecular weight of approximately 108 kDa as those originally observed (unpublished observations). This result provides evidence that the bands we recognized were m-calpain in a complex consisting of the large and small subunit.

4.1.1 Do these changes in caspase-12 expression correspond with an increase in apoptosis?

To determine if the estrogen-induced activation of caspase-12 was associated with an increase in apoptotic cell death, DNA fragmentation was assessed through TUNEL staining of tissue from estrogen and saline treated animals subjected to MCAO. Some TUNEL-positive cells were observed with estrogen treatment at 2 hours post-MCAO, however, the number of positively stained cells was not significantly different from those observed with saline treatment. At 4 hours post-MCAO however, there was a significant elevation in the number of TUNEL-positive cells in estrogen treated animals compared to those treated with saline. In addition, the number of TUNEL positive cells in the ipsilateral cortex was significantly higher than those in the contralateral cortex in both estrogen and saline treated animals. Although TUNEL staining alone may not be definitive for apoptosis (because necrotic cells may also have DNA fragmentation) the increase in TUNEL positive cells with estrogen treatment along with caspase-12 activation provides strong evidence toward an estrogen-induced increase in apoptosis in the first 4 hours post-MCAO.

It has been very well documented that caspase-12 activation leads to apoptotic cell death. Nakagawa and colleagues (164) were the first to demonstrate that apoptosis results from activation of caspase-12. In their study, the number of apoptotic cells in the liver following treatment with tunicamycin (1 μg/ml) in wild-type and caspase-12 deficient mice was analyzed by TUNEL staining. A large number of TUNEL positive cells were observed in the wild-type mice, whereas significantly less TUNEL positive cells were found in the caspase-12 deficient mice (164). Following traumatic brain

injury, Larner et al. (158) reported an induction of caspase-12 in neurons, which was colocalized in cells showing apoptotic bodies. Caspase-12 activation has also been demonstrated to result in apoptosis following cerebral ischemia. Immunohistochemistry revealed caspase-12 positive cells that exhibited DNA fragmentation detected by TUNEL staining during reperfusion in a transient MCAO model of stroke (124). Aoyama and colleagues (174) demonstrated that activation of caspase-12 in the peri-infarct region following transient MCAO resulted in apoptosis detected by 4',6',-diamidino-2-phenylindole (DAPI) staining, which revealed chromatin condensation and the formation of apoptotic bodies. This evidence clearly demonstrates the association between caspase-12 activation and apoptotic cell death.

The results from the current investigation both agree with previous findings that caspase-12 activation leads to apoptosis and demonstrate a potential protective pathway used by estrogen following permanent cerebral ischemia. The time course of the molecular changes that lead to an increase in apoptosis in this study are in close correlation with the estrogen-induced reduction in infarct volume previously demonstrated in our laboratory (43). Our laboratory has previously shown that the infarct size in estrogen treated animals subjected to MCAO is significantly reduced at 3 and 4 hours post-MCAO. Therefore, the pathways involved in the mechanism of estrogen neuroprotection are likely activated within 1 to 2 hours following MCAO. In the current study, an increase in m-calpain (in the infarct region) and a decrease in procaspase-12 (in both the infarct and peri-infarct regions) expression were observed at 1 hour post-MCAO with estrogen treatment, and this corresponded with an increase in caspase-12 activation at 2 and 3 hours following MCAO. Although a significant difference in TUNEL positive

cells was not observed between estrogen and saline treated animals at 2 hours post-MCAO, there was a significantly greater number of TUNEL positive cells in estrogen treated animals by 4 hours post-MCAO. Caspase-12 activation was not observed at the same time point as the estrogen-induced elevation in TUNEL positive cells (4 hours post-MCAO), however, it has been reported to take anywhere from one to several hours to see signs of apoptotic cell death (such as DNA fragmentation) following activation of caspases (91). For a summary of the above results, refer to Table 5.

Several laboratories have attempted to determine the exact mechanism by which estrogen provides its protective effects in experimental models of stroke. Estrogen appears to provide neuroprotection through a mechanism that is independent of improvement in cerebral perfusion (183). Some studies have demonstrated an anti-oxidant effect of estrogen in experimental stroke, however, supraphysiological concentrations of estrogen were generally required to see the protective effect (184). Estrogen has anti-apoptotic effects that have been reported to be the mechanism of neuroprotection in both transient (185) and permanent (81) ischemia. However, these effects are generally based on observations with chronic estrogen treatment and at 24 to 48 hours following the stroke, whereas our interest is in the molecular events occurring in the first 4 hours post-stroke. In non-neuronal tissue, estrogen has also been shown to have proapoptotic effects. Tesarik and colleagues (186) demonstrated that estrogen stimulated apoptosis in breast cancer cells. However, upon exposure of these cells to vitamin E succinate (VES), a known proapoptotic agent, estrogen was found to inhibit the VES-induced apoptosis. Their study clearly demonstrates the ability of estrogen to increase or decrease apoptosis in the same tissue depending on the severity of the injury.

Table 5. Estrogen-induced changes on the ipsilateral side following MCAO compared to saline

Time Post-MCAO	Infarct Size	Procaspase-12	Active Caspase-12	m-calpain	TUNEL Staining
0					N/A
1		↓		↑	N/A
2			↑		No difference
3	↓		↑		N/A
4	↓				↑

In the current study, we are proposing that the protective actions of estrogen involve pro-apoptotic mechanisms in the acute phase of the stroke, and then based on the findings of Rau and colleagues (38), switch to anti-apoptotic mechanisms over the next 6-24 hours following the stroke.

There are several indications that estrogen interacts with the endoplasmic reticulum. As discussed in the introduction, estrogen binding proteins have been reported to be found within the EnR, suggesting estrogen may bind to a protein within the EnR and modulate specific EnR pathways. Estrogen has been observed to induce PDI, a molecular chaperone in the EnR, in vascular endothelial cells and provide antioxidant protection (187). Lacroix et al. (188) reported that XBP1, a transcription factor that plays a major role in the EnR unfolded protein response, is expressed in close association with the ER-α gene in breast cancer cells. The authors suggested that ER-α may recruit XBP-1 to the promoter region containing the ERE to stimulate gene transcription. These results indicate that estrogen can interact with and possibly modulate EnR specific pathways.

Apoptotic cell death was also assessed with DNA laddering by agarose gel electrophoresis. DNA smears were present on the gel but no specific DNA fragments were observed. The absence of DNA laddering may be due to a technical difficulty: the apoptotic DNA laddering kit was designed to detect large amounts of apoptosis in cell culture, and although the protocol was slightly modified for tissue, the amount of apoptosis occurring in the ischemic tissue may not have been sufficient for detection using this kit.

4.2 *Changes in LDH in the CSF in estrogen and saline treated animals subjected to MCAO or sham occlusion*

The second objective of this study was to determine if estrogen decreases necrotic cell death following MCAO. In both estrogen and saline treated animals, the amount of necrotic cell death, determined by the concentration of LDH in the CSF within the cortex, was significantly higher overall following MCAO compared to sham occlusion (as determined with area under the curve calculations). However, there were no significant differences in the concentration of LDH in the CSF between estrogen and saline treated animals subjected to MCAO. The presence of LDH in the extracellular fluid is a well established marker of necrotic cell death because it indicates rupture of the plasma membrane and subsequent release of intracellular contents. Numerous *in vitro* studies have assessed necrotic cell death by LDH release (88, 138-140), whereas only one *in vivo* study has investigated the extracellular concentration of LDH and related this to necrotic cell death in the brain. In this *in vivo* study, Kihara and colleagues (140) demonstrated a ten-fold increase in LDH activity following cold-induced brain injury compared to baseline values obtained prior to induction of the injury. The authors used a microdialysis probe with a molecular weight cut-off of 50 kDa, despite the fact that LDH has a molecular weight of 140 kDa (35 kDa/subunit). Therefore, Kihara and colleagues must have collected the individual subunits of LDH. In the current study, a microdialysis probe with a molecular weight cut-off of 3000 kDa was initially used to collect LDH from the CSF; however we were unable to recover a detectable concentration of LDH. Theoretically, this probe should have been satisfactory for dialysis of LDH, however the number of pores within most membranes that are capable of allowing the passage of large

molecules has been reported to be small, and therefore result in low recovery efficiencies (189). Removal of the semi-permeable membrane remedied the low recovery efficiency obtained with the intact membrane, but created an alternative problem: LDH was then only collected from a small diameter region surrounding the tip of the probe (approximately 1-2 mm in diameter). This may have accounted for the lack of significance in the LDH concentration between estrogen and saline treated animals subjected to MCAO because the concentration detected may not have been representative of the LDH found within the cortex. Furthermore, the location of the tip of the probe within the cortex may have also played a role. The placement of the probe was based on the coordinates for the insular cortex obtained from the stereotaxic atlas of the rat brain (-3.3 mm below Bregma) (176). Therefore, since the probe was inserted deep within the cortex, it may not have been located within the infarct over the 4 hour time course, whereas if the probe was inserted more dorsal in the cortex, perhaps a significant difference would have been detected.

Chapter 5. Summary and future perspectives

The results obtained from the experiments conducted in this thesis have provided evidence toward a potential unique molecular mechanism for the estrogen-induced neuroprotection that is observed in the first 4 hours following MCAO. Specifically, the results suggest that the early mechanism by which estrogen provides protection is mediated by an increase in endoplasmic reticulum stress-associated apoptosis via activation of caspase-12. The effects of estrogen on necrotic cell death however, are not completely clear. Based on the data obtained in the push-pull perfusion experiments, it appears that an alternative method for assessing necrotic cell death is necessary to accurately determine the effect of estrogen on this mode of cell death following MCAO.

In order to fully understand the mechanisms of the neuroprotective actions of estrogen in the first 4 hours following MCAO, additional experiments are necessary. While the results in this thesis suggest that m-calpain may be involved in regulating caspase-12 activity following MCAO, further work is required to confirm the role of m-calpain in this model. Furthermore, determination of the exact ratio of apoptotic to necrotic cell death at the progressive time points up to 4 hours post-MCAO will provide more insight on the precise temporal pattern of the mechanism of estrogen-induced neuroprotection following MCAO. Ultimately, an in depth understanding of the exact mechanisms by which estrogen provides protection following stroke may result in the development of a therapeutic strategy aimed at reducing the amount of ischemia-induced cell death.

References

(1) Heart and Stroke Foundation of Canada. Stroke. 2002. Ref Type: Report.

(2) Kandel ER, Scharwtz JH. Principles of Neural Science. 2nd ed. New York: Elsevier, 1985.

(3) Hutchins JB, Barger SW. (1998) Why neurons die: cell death in the nervous system. *Anat Rec* **253:** 79-90.

(4) Bullock BL. Pathophysiology: Adaptations and Alterations. 4th ed. Philadelphia: Lippincott, Williams and Wilkins, 1996.

(5) Heather SE, McCance KL. Understanding Pathophysiology. St. Louis: Mosby, 1996.

(6) Porth CM. Pathophysiology: Concepts of Altered Health States. 6th ed. Philidelphia: Lippincott, Williams and Wilkins, 2002.

(7) Xi G, Keep RF, Hoff JT. (2006) Mechanisms of brain injury after intracerebral haemorrhage. *Lancet Neurol* **5:** 53-63.

(8) Ture U, Yasargil MG, Al-Mefty O, Yasargil DC. (2000) Arteries of the insula. *J Neurosurg* **92:** 676-687.

(9) Ruggiero DA, Mraovitch S, Granata AR, Anwar M, Reis DJ. (1987) A role of insular cortex in cardiovascular function. *J Comp Neurol* **257:** 189-207.

(10) Cheung RT, Hachinski V. (2003) Cardiac rhythm disorders and muscle changes with cerebral lesions. *Adv Neurol* **92:** 213-220.

(11) Oppenheimer SM, Wilson JX, Guiraudon C, Cechetto DF. (1991) Insular cortex stimulation produces lethal cardiac arrhythmias: a mechanism of sudden death? *Brain Res* **550:** 115-121.

(12) Oppenheimer SM, Saleh TM, Wilson JX, Cechetto DF. (1992) Plasma and organ catecholamine levels following stimulation of the rat insular cortex. *Brain Res* **569:** 221-228.

(13) Cechetto DF, Wilson JX, Smith KE, Wolski D, Silver MD, Hachinski VC. (1989) Autonomic and myocardial changes in middle cerebral artery occlusion: stroke models in the rat. *Brain Res* **502:** 296-305.

(14) Smith KE, Hachinski VC, Gibson CJ, Ciriello J. (1986) Changes in plasma catecholamine levels after insula damage in experimental stroke. *Brain Res* **375:** 182-185.

(15) Hachinski VC, Smith KE, Silver MD, Gibson CJ, Ciriello J. (1986) Acute myocardial and plasma catecholamine changes in experimental stroke. *Stroke* **17:** 387-390.

(16) Butcher KS, Hachinski VC, Wilson JX, Guiraudon C, Cechetto DF. (1993) Cardiac and sympathetic effects of middle cerebral artery occlusion in the spontaneously hypertensive rat. *Brain Res* **621:** 79-86.

(17) Butcher KS, Cechetto DF. (1995) Insular lesion evokes autonomic effects of stroke in normotensive and hypertensive rats. *Stroke* **26:** 459-465.

(18) Hachinski VC, Oppenheimer SM, Wilson JX, Guiraudon C, Cechetto DF. (1992) Asymmetry of sympathetic consequences of experimental stroke. *Arch Neurol* **49:** 697-702.

(19) Goldstein DS. (1979) The electrocardiogram in stroke: relationship to pathophysiological type and comparison with prior tracings. *Stroke* **10:** 253-259.

(20) Oppenheimer S. (1992) The insular cortex and the pathophysiology of stroke-induced cardiac changes. *Can J Neurol Sci* **19:** 208-211.

(21) Cheung RT, Hachinski V. (2004) Cardiac Effects of Stroke. *Curr Treat Options Cardiovasc Med* **6:** 199-207.

(22) Meyer S, Strittmatter M, Fischer C, Georg T, Schmitz B. (2004) Lateralization in autonomic dysfunction in ischemic stroke involving the insular cortex. *Neuroreport* **15:** 357-361.

(23) Oppenheimer SM, Kedem G, Martin WM. (1996) Left-insular cortex lesions perturb cardiac autonomic tone in humans. *Clin Auton Res* **6:** 131-140.

(24) Larsen JA, Kadish AH. (1998) Effects of gender on cardiac arrhythmias. *J Cardiovasc Electrophysiol* **9:** 655-664.

(25) Barrett-Connor E, Grady D. (1998) Hormone replacement therapy, heart disease, and other considerations. *Annu Rev Public Health* **19:** 55-72.

(26) Medina RA, Aranda E, Verdugo C, Kato S, Owen GI. (2003) The action of ovarian hormones in cardiovascular disease. *Biol Res* **36:** 325-341.

(27) Kannel WB, Thorn TJ. (1994) The incidence, prevalence, and mortality of cardiovascular disease. *The Heart*: 185-197.

(28) The Changing Face of Heart Disease and Stroke in Canada 2000. Ref Type: Report

(29) Guyton AC, Hall JE. Textbook of Medical Physiology. *9th ed. Philadelphia: W.B. Saunders Company, 1996.*

(30) Liao S, Chen W, Kuo J, Chen C. (2001) Association of serum estrogen level and ischemic neuroprotection in female rats. *Neurosci Lett* **297:** 159-162

(31) Zhang YQ, Shi J, Rajakumar G, Day AL, Simpkins JW. (1998) Effects of gender and estradiol treatment on focal brain ischemia. *Brain Res* **784:** 321-324.

(32) Hurn PD, Macrae IM. (2000) Estrogen as a neuroprotectant in stroke. *J Cereb Blood Flow Metab* **20:** 631-652.

(33) Alkayed NJ, Harukuni I, Kimes AS, London ED, Traystman RJ, Hurn PD. (1998) Gender-linked brain injury in experimental stroke. *Stroke* **29:** 159-165; discussion 166.

(34) Carswell HV, Dominiczak AF, Macrae IM. (2000) Estrogen status affects sensitivity to focal cerebral ischemia in stroke-prone spontaneously hypertensive rats. *Am J Physiol Heart Circ Physiol* **278:** H290-294.

(35) Gibson CL, Gray LJ, Murphy SP, Bath PM. (2006) Estrogens and experimental ischemic stroke: a systematic review. *J Cereb Blood Flow Metab*. 1-11.

(36) Saleh TM, Cribb AE, Connell BJ. (2001) Reduction in infarct size by local estrogen does not prevent autonomic dysfunction after stroke. *Am J Physiol Regul Integr Comp Physiol* **281:** R2088-2095.

(37) Toung TK, Hurn PD, Traystman RJ, Sieber FE. (2000) Estrogen decreases infarct size after temporary focal ischemia in a genetic model of type 1 diabetes mellitus. *Stroke* **31:** 2701-2706.

(38) Rau SW, Dubal DB, Bottner M, Gerhold LM, Wise PM. (2003) Estradiol attenuates programmed cell death after stroke-like injury. *J Neurosci* **23:** 11420-11426.

(39) Shi J, Bui JD, Yang SH, et al. (2001) Estrogens decrease reperfusion-associated cortical ischemic damage: an MRI analysis in a transient focal ischemia model. *Stroke* **32:** 987-992.

(40) Dubal DB, Kashon ML, Pettigrew LC, et al. (1998) Estradiol protects against ischemic injury. *J Cereb Blood Flow Metab* **18:** 1253-1258.

(41) Yang SH, Shi J, Day AL, Simpkins JW. (2000) Estradiol exerts neuroprotective effects when administered after ischemic insult. *Stroke* **31:** 745-749; discussion 749-750.

(42) Saleh TM, Cribb AE, Connell BJ. (2001) Estrogen-induced recovery of autonomic function after middle cerebral artery occlusion in male rats. *Am J Physiol Regul Integr Comp Physiol* **281:** R1531-1539.

(43) Saleh TM, Connell BJ, Legge C, Cribb AE. (2004) Estrogen attenuates neuronal excitability in the insular cortex following middle cerebral artery occlusion. *Brain Res* **1081:** 119-129.

(44) Saleh TM, Cribb AE, Connell BJ. (2001) Reduction in infarct size by local estrogen does not prevent autonomic dysfunction after stroke. *Am J Physiol Regul Integr Comp Physiol* **281:** R2088-2095.

(45) Garcia-Segura LM, Azcoitia I, DonCarlos LL. (2001) Neuroprotection by estradiol. *Prog Neurobiol* **63:** 29-60.

(46) Shughrue PJ, Lane MV, Merchenthaler I. (1997) Comparative distribution of estrogen receptor-alpha and -beta mRNA in the rat central nervous system. *J Comp Neurol* **388:** 507-525.

(47) Nelson LR, Bulun SE. (2001) Estrogen production and action. *J Am Acad Dermatol* **45:** S116-124.

(48) Kong EH, Pike AC, Hubbard RE. (2003) Structure and mechanism of the oestrogen receptor. *Biochem Soc Trans* **31:** 56-59.

(49) Lin BC, Scanlan TS. (2005) Few things in life are "free": cellular uptake of steroid hormones by an active transport mechanism. *Mol Interv* **5:** 338-340.

(50) Edwards DP. (2000) The role of coactivators and corepressors in the biology and mechanism of action of steroid hormone receptors. *J Mammary Gland Biol Neoplasia* **5:** 307-324.

(51) Amantea D, Russo R, Bagetta G, Corasaniti MT. (2005) From clinical evidence to molecular mechanisms underlying neuroprotection afforded by estrogens. *Pharmacol Res* **52:** 119-132.

(52) McDonnell DP. (2004) The molecular determinants of estrogen receptor pharmacology. *Maturitas* **48 Suppl 1:** S7-12.

(53) Ho KJ, Liao JK. (2002) Non-nuclear Actions of Estrogen: New Targets for Prevention and Treatment of Cardiovascular Disease. *Mol Interv* **2:** 219-228.

(54) Honda K, Sawada H, Kihara T, et al. (2000) Phosphatidylinositol 3-kinase mediates neuroprotection by estrogen in cultured cortical neurons. *J Neurosci Res* **60:** 321-327.

(55) Migliaccio A, Di Domenico M, Castoria G, et al. (1996) Tyrosine kinase/p21ras/MAP-kinase pathway activation by estradiol-receptor complex in MCF-7 cells. *Embo J* **15:** 1292-1300.

(56) Wade CB, Robinson S, Shapiro RA, Dorsa DM. (2001) Estrogen receptor (ER) alpha and ER beta exhibit unique pharmacologic properties when coupled to activation of the mitogen-activated protein kinase pathway. *Endocrinology* **142:** 2336-2342.

(57) Toran-Allerand CD, Guan X, MacLusky NJ, et al. (2002) ER-X: a novel, plasma membrane-associated, putative estrogen receptor that is regulated during development and after ischemic brain injury. *J Neurosci* **22:** 8391-8401.

(58) Toran-Allerand CD. (2004) Minireview: A plethora of estrogen receptors in the brain: where will it end? *Endocrinology* **145:** 1069-1074.

(59) Govind AP, Thampan RV. (2003) Membrane associated estrogen receptors and related proteins: localization at the plasma membrane and the endoplasmic reticulum. *Mol Cell Biochem* **253:** 233-240.

(60) Parikh I, Anderson WL, Neame P. (1980) Identification of high affinity estrogen binding sites in calf uterine microsomal membranes. *J Biol Chem* **255:** 10266-10270.

(61) Monje P, Boland R. (1999) Characterization of membrane estrogen binding proteins from rabbit uterus. *Mol Cell Endocrinol* **147:** 75-84.

(62) Muldoon TG, Watson GH, Evans AC, Jr., Steinsapir J. (1988) Microsomal receptor for steroid hormones: functional implications for nuclear activity. *J Steroid Biochem* **30:** 23-31.

(63) Evans AC, Jr., Muldoon TG. (1991) Characterization of estrogen-binding sites associated with the endoplasmic reticulum of rat uterus. *Steroids* **56:** 59-65.

(64) Primm TP, Gilbert HF. (2001) Hormone binding by protein disulfide isomerase, a high capacity hormone reservoir of the endoplasmic reticulum. *J Biol Chem* **276:** 281-286.

(65) Zsarnovszky A, Belcher SM. (2001) Identification of a developmental gradient of estrogen receptor expression and cellular localization in the developing and adult female rat primary somatosensory cortex. *Brain Res Dev Brain Res* **129:** 39-46.

(66) Shughrue PJ, Merchenthaler I. (2001) Distribution of estrogen receptor beta immunoreactivity in the rat central nervous system. *J Comp Neurol* **436:** 64-81.

(67) Zhang JQ, Cai WQ, Zhou de S, Su BY. (2002) Distribution and differences of estrogen receptor beta immunoreactivity in the brain of adult male and female rats. *Brain Res* **935:** 73-80.

(68) Merchenthaler I, Dellovade TL, Shughrue PJ. (2003) Neuroprotection by estrogen in animal models of global and focal ischemia. *Ann N Y Acad Sci* **1007:** 89-100.

(69) Dubal DB, Zhu H, Yu J, et al. (2001) Estrogen receptor alpha, not beta, is a critical link in estradiol-mediated protection against brain injury. *Proc Natl Acad Sci U S A* **98:** 1952-1957.

(70) Dubal DB, Rau SW, Shughrue PJ, et al. (2006) Differential Modulation of Estrogen Receptors (ERs) in Ischemic Brain Injury: A Role for ER{alpha} in Estradiol-Mediated Protection against Delayed Cell Death. *Endocrinology* **147:** 3076-3084.

(71) Wang L, Andersson S, Warner M, Gustafsson JA. (2001) Morphological abnormalities in the brains of estrogen receptor beta knockout mice. *Proc Natl Acad Sci USA* **98:** 2792-2796.

(72) Zhao L, Wu TW, Brinton RD. (2004) Estrogen receptor subtypes alpha and beta contribute to neuroprotection and increased Bcl-2 expression in primary hippocampal neurons. *Brain Res* **1010:** 22-34.

(73) Gandy S. (2003) Estrogen and neurodegeneration. *Neurochem Res* **28:** 1003-1008.

(74) Vanderhorst VG, Terasawa E, Ralston HJ, 3rd. (2002) Axonal sprouting of a brainstem-spinal pathway after estrogen administration in the adult female rhesus monkey. *J Comp Neurol* **454:** 82-103.

(75) McEwen BS, Woolley CS. (1994) Estradiol and progesterone regulate neuronal structure and synaptic connectivity in adult as well as developing brain. *Exp Gerontol* **29:** 431-436.

(76) Behl C. (2002) Oestrogen as a neuroprotective hormone. *Nat Rev Neurosci* **3:** 433-442.

(77) Shughrue PJ, Dorsa DM. (1993) Estrogen modulates the growth-associated protein GAP-43 (Neuromodulin) mRNA in the rat preoptic area and basal hypothalamus. *Neuroendocrinology* **57:** 439-447.

(78) Wise PM, Dubal DB, Wilson ME, Rau SW, Liu Y. (2001) Estrogens: trophic and protective factors in the adult brain. *Front Neuroendocrinol* **22:** 33-66.

(79) Franklin TB, Perrot-Sinal TS. (2006) Sex and ovarian steroids modulate brain-derived neurotrophic factor (BDNF) protein levels in rat hippocampus under stressful and non-stressful conditions. *Psychoneuroendocrinology* **31:** 38-48.

(80) Garcia-Segura LM, Cardona-Gomez P, Naftolin F, Chowen JA. (1998) Estradiol upregulates Bcl-2 expression in adult brain neurons. *Neuroreport* **9:** 593-597.

(81) Dubal DB, Shughrue PJ, Wilson ME, Merchenthaler I, Wise PM. (1999) Estradiol modulates bcl-2 in cerebral ischemia: a potential role for estrogen receptors. *J Neurosci* **19:** 6385-6393.

(82) Won CK, Kim MO, Koh PO. (2006) Estrogen modulates Bcl-2 family proteins in ischemic brain injury. *J Vet Med Sci* **68:** 277-280.

(83) Singer CA, Figueroa-Masot XA, Batchelor RH, Dorsa DM. (1999) The mitogen-activated protein kinase pathway mediates estrogen neuroprotection after glutamate toxicity in primary cortical neurons. *J Neurosci* **19:** 2455-2463.

(84) Watters JJ, Dorsa DM. (1998) Transcriptional effects of estrogen on neuronal neurotensin gene expression involve cAMP/protein kinase A-dependent signaling mechanisms. *J Neurosci* **18:** 6672-6680.

(85) Pelligrino DA, Santizo R, Baughman VL, Wang Q. (1998) Cerebral vasodilating capacity during forebrain ischemia: effects of chronic estrogen depletion and repletion and the role of neuronal nitric oxide synthase. *Neuroreport* **9:** 3285-3291.

(86) Green PS, Simpkins JW. (2000) Neuroprotective effects of estrogens: potential mechanisms of action. *Int J Dev Neurosci* **18:** 347-358.

(87) Liao SL, Chen WY, Chen CJ. (2002) Estrogen attenuates tumor necrosis factor-alpha expression to provide ischemic neuroprotection in female rats. *Neurosci Lett* **330:** 159-162.

(88) Singer CA, Rogers KL, Strickland TM, Dorsa DM. (1996) Estrogen protects primary cortical neurons from glutamate toxicity. *Neurosci Lett* **212:** 13-16.

(89) Sribnick EA, Ray SK, Nowak MW, Li L, Banik NL. (2004) 17beta-estradiol attenuates glutamate-induced apoptosis and preserves electrophysiologic function in primary cortical neurons. *J Neurosci Res* **76:** 688-696.

(90) Ritz MF, Schmidt P, Mendelowitsch A. (2004) Acute effects of 17beta-estradiol on the extracellular concentration of excitatory amino acids and energy

metabolites during transient cerebral ischemia in male rats. *Brain Res* **1022:** 157-163.

(91) Lipton P. (1999) Ischemic cell death in brain neurons. *Physiol Rev* **79:** 1431-1568.

(92) Bullock BA, Henze RL. Focus on Pathophysiology. Philadelphia: Lippincott, Williams and Wilkins, 2000

(93) Mergenthaler P, Dirnagl U, Meisel A. (2004) Pathophysiology of stroke: lessons from animal models. *Metab Brain Dis* **19:** 151-167.

(94) Lee JM, Grabb MC, Zipfel GJ, Choi DW. (2000) Brain tissue responses to ischemia. *J Clin Invest* **106:** 723-731.

(95) Darwin M. (1995) The pathophysiology of ischemic injury. *Bio Preservation, Inc.*

(96) Szatkowski M, Attwell D. (1994) Triggering and execution of neuronal death in brain ischaemia: two phases of glutamate release by different mechanisms. *Trends Neurosci* **17:** 359-365.

(97) Saleh T. University of Prince Edward Island. Personal Communication

(98) Paschen W. (1996) Disturbances of calcium homeostasis within the endoplasmic reticulum may contribute to the development of ischemic-cell damage. *Med Hypotheses* **47:** 283-288.

(99) Fisher M, Garcia JH. (1996) Evolving stroke and the ischemic penumbra. *Neurology* **47:** 884-888.

(100) Dirnagl U, Iadecola C, Moskowitz MA. (1999) Pathobiology of ischaemic stroke: an integrated view. *Trends Neurosci* **22:** 391-397.

(101) McConkey DJ. (1998) Biochemical determinants of apoptosis and necrosis. *Toxicol Lett* **99:** 157-168.

(102) Onteniente B, Couriaud C, Braudeau J, Benchoua A, Guegan C. (2003) The mechanisms of cell death in focal cerebral ischemia highlight neuroprotective perspectives by anti-caspase therapy. *Biochem Pharmacol* **66:** 1643-1649.

(103) Verkhratsky A, Toescu EC. (2003) Endoplasmic reticulum Ca(2+) homeostasis and neuronal death. *J Cell Mol Med* **7:** 351-361.

(104) Groenendyk J, Michalak M. (2005) Endoplasmic reticulum quality control and apoptosis. *Acta Biochim Pol* **52:** 381-395.

(105) Zong WX, Thompson CB. (2006) Necrotic death as a cell fate. *Genes Dev* **20:** 1-15.

(106) Berridge MJ. (2002) The endoplasmic reticulum: a multifunctional signaling organelle. *Cell Calcium* **32:** 235-249.

(107) Shen X, Zhang K, Kaufman RJ. (2004) The unfolded protein response--a stress signaling pathway of the endoplasmic reticulum. *J Chem Neuroanat* **28:** 79-92.

(108) Hendershot LM. (2004) The ER function BiP is a master regulator of ER function. *Mt Sinai J Med* **71:** 289-297.

(109) Zhang K, Kaufman RJ. (2006) The unfolded protein response: a stress signaling pathway critical for health and disease. *Neurology* **66:** S102-109.

(110) Kleizen B, Braakman I. (2004) Protein folding and quality control in the endoplasmic reticulum. *Curr Opin Cell Biol* **16:** 343-349.

(111) Schroder M, Kaufman RJ. (2005) ER stress and the unfolded protein response. *Mutat Res* **569:** 29-63.

(112) Rao RV, Bredesen DE. (2004) Misfolded proteins, endoplasmic reticulum stress and neurodegeneration. *Curr Opin Cell Biol* **16:** 653-662.

(113) Harding HP, Calfon M, Urano F, Novoa I, Ron D. (2002) Transcriptional and translational control in the mammalian unfolded protein response. *Annu Rev Cell Dev Biol* **18:** 575-599.

(114) Jarosch E, Lenk U, Sommer T. (2003) Endoplasmic reticulum-associated protein degradation. *Int Rev Cytol* **223:** 39-81.

(115) Rao RV, Hermel E, Castro-Obregon S, et al. (2001) Coupling endoplasmic reticulum stress to the cell death program. Mechanism of caspase activation. *J Biol Chem* **276:** 33869-33874.

(116) Paschen W. (1996) Disturbances of calcium homeostasis within the endoplasmic reticulum may contribute to the development of ischemic-cell damage. *Med Hypotheses* **47:** 283-288.

(117) Rutkowski DT, Kaufman RJ. (2004) A trip to the ER: coping with stress. *Trends Cell Biol* **14:** 20-28.

(118) Kumar R, Azam S, Sullivan JM, et al. (2001) Brain ischemia and reperfusion activates the eukaryotic initiation factor 2alpha kinase, PERK. *J Neurochem* **77:** 1418-1421.

(119) Matsushita K, Matsuyama T, Nishimura H, et al. (1998) Marked, sustained expression of a novel 150-kDa oxygen-regulated stress protein, in severely ischemic mouse neurons. *Brain Res Mol Brain Res* **60:** 98-106.

(120) DeGracia DJ, Montie HL. (2004). Cerebral ischemia and the unfolded protein response. *J Neurochem* **91:** 1-8.

(121) Paschen W, Aufenberg C, Hotop S, Mengesdorf T. (2003) Transient cerebral ischemia activates processing of xbp1 messenger RNA indicative of endoplasmic reticulum stress. *J Cereb Blood Flow Metab* **23:** 449-461.

(122) Li F, Hayashi T, Jin G, et al. (2005). The protective effect of dantrolene on ischemic neuronal cell death is associated with reduced expression of endoplasmic reticulum stress markers. *Brain Res* **1048:** 59-68.

(123) Parsons JT, Churn SB, DeLorenzo RJ. (1997) Ischemia-induced inhibition of calcium uptake into rat brain microsomes mediated by Mg2+/Ca2+ ATPase. *J Neurochem* **68:** 1124-1134.

(124) Shibata M, Hattori H, Sasaki T, Gotoh J, Hamada J, Fukuuchi Y. (2003) Activation of caspase-12 by endoplasmic reticulum stress induced by transient middle cerebral artery occlusion in mice. *Neuroscience* **118:** 491-499.

(125) Mouw G, Zechel JL, Gamboa J, Lust WD, Selman WR, Ratcheson RA. (2003) Activation of caspase-12, an endoplasmic reticulum resident caspase, after permanent focal ischemia in rat. *Neuroreport* **14:** 183-186.

(126) Harwood SM, Yaqoob MM, Allen DA. (2005) Caspase and calpain function in cell death: bridging the gap between apoptosis and necrosis. *Ann Clin Biochem* **42:** 415-431.

(127) Rami A. (2003) Ischemic neuronal death in the rat hippocampus: the calpain-calpastatin-caspase hypothesis. *Neurobiol Dis* **13:** 75-88.

(128) Ziegler U, Groscurth P. (2004) Morphological features of cell death. *News Physiol Sci* **19:** 124-128.

(129) Barros LF, Hermosilla T, Castro J. (2001) Necrotic volume increase and the early physiology of necrosis. *Comp Biochem Physiol A Mol Integr Physiol* **130:** 401-409.

(130) Cribb AE, Peyrou M, Muruganandan S, Shneider L. (2005). The endoplasmic reticulum in xenobiotic toxicity. *Drug Metab Rev* **37:** 405-442.

(131) Unal-Cevik I, Kilinc M, Can A, Gursoy-Ozdemir Y, Dalkara T. (2004) Apoptotic and necrotic death mechanisms are concomitantly activated in the same cell after cerebral ischemia. *Stroke* **35:** 2189-2194.

(132) Linnik MD, Miller JA, Sprinkle-Cavallo J, et al. (1995) Apoptotic DNA fragmentation in the rat cerebral cortex induced by permanent middle cerebral artery occlusion. *Brain Res Mol Brain Res* **32:** 116-124.

(133) Saraste A, Pulkki K. (2000) Morphologic and biochemical hallmarks of apoptosis. *Cardiovasc Res* **45:** 528-537.

(134) Carini R, Autelli R, Bellomo G, Albano E. (1999) Alterations of cell volume regulation in the development of hepatocyte necrosis. *Exp Cell Res* **248:** 280-293.

(135) Liu X, Schnellmann RG. (2003) Calpain mediates progressive plasma membrane permeability and proteolysis of cytoskeleton-associated paxillin, talin, and vinculin during renal cell death. *J Pharmacol Exp Ther* **304:** 63-70.

(136) Lemasters JJ. (2005) Dying a thousand deaths: redundant pathways from different organelles to apoptosis and necrosis. *Gastroenterology* **129:** 351-360.

(137) Koh JY, Choi DW. (1987) Quantitative determination of glutamate mediated cortical neuronal injury in cell culture by lactate dehydrogenase efflux assay. *J Neurosci Methods* **20:** 83-90.

(138) Ioudina M, Uemura E, Greenlee HW. (2004) Glucose insufficiency alters neuronal viability and increases susceptibility to glutamate toxicity. *Brain Res* **1004:** 188-192.

(139) Carrier RL, Ma TC, Obrietan K, Hoyt KR. (2006) A sensitive and selective assay of neuronal degeneration in cell culture. *J Neurosci Methods* **154:** 239-244.

(140) Kihara T, Sakata S, Ikeda M. (1995). Direct detection of ascorbyl radical in experimental brain injury: microdialysis and an electron spin resonance spectroscopic study. *J Neurochem* **65:** 282-286.

(141) Zimmermann KC, Bonzon C, Green DR. (2001) The machinery of programmed cell death. *Pharmacol Ther* **92:** 57-70.

(142) Kerr JF, Wyllie AH, Currie AR. (1972). Apoptosis: a basic biological phenomenon with wide-ranging implications in tissue kinetics. *Br J Cancer* **26:** 239-257.

(143) Van Cruchten S, Van Den Broeck W. (2002) Morphological and biochemical aspects of apoptosis, oncosis and necrosis. *Anat Histol Embryol* **31:** 214-223.

(144) Remillard CV, Yuan JX. (2004) Activation of K+ channels: an essential pathway in programmed cell death. *Am J Physiol Lung Cell Mol Physiol* **286:** L49-67.

(145) L LVaI. (2001) What is necessary to know about apoptosis. *Biomedicine* **1:** 90-96.

(146) Hacker G. (2000) The morphology of apoptosis. *Cell Tissue Res* **301:** 5-17.

(147) Martelli AM, Zweyer M, Ochs RL, et al. (2001) Nuclear apoptotic changes: an overview. *J Cell Biochem* **82:** 634-646.

(148) Sgonc R, Gruber J. (1998) Apoptosis detection: an overview. *Exp Gerontol* **33:** 525-533.

(149) Schulze-Osthoff K, Walczak H, Droge W, Krammer PH. (1994) Cell nucleus and DNA fragmentation are not required for apoptosis. *J Cell Biol* **127:** 15-20.

(150) Zwaal RF, Comfurius P, Bevers EM. (2005) Surface exposure of phosphatidylserine in pathological cells. *Cell Mol Life Sci* **62:** 971-988.

(151) Lang F, Gulbins E, Szabo I, et al. (2004). Cell volume and the regulation of apoptotic cell death. *J Mol Recognit* **17:** 473-480.

(152) Kohler C, Orrenius S, Zhivotovsky B. (2002) Evaluation of caspase activity in apoptotic cells. *J Immunol Methods* **265:** 97-110.

(153) Nunez G, Benedict MA, Hu Y, Inohara N. (1998) Caspases: the proteases of the apoptotic pathway. *Oncogene* **17:** 3237-3245.

(154) Salvesen GS, Dixit VM (1999) Caspase activation: the induced proximity model. *Proc Natl Acad Sci USA* **96:** 10964-10967.

(155) Lamkanfi M, Kalai M, Vandenabeele P. (2004) Caspase-12: an overview. *Cell Death Differ* **11:** 365-368.

(156) Thornberry NA. (1999) Caspases: a decade of death research. *Cell Death Differ* **6:** 1023-1027.

(157) Czerski L, Nunez G. (2004). Apoptosome formation and caspase activation: is it different in the heart? *J Mol Cell Cardiol* **37:** 643-652.

(158) Larner SF, Hayes RL, McKinsey DM, Pike BR, Wang KK. (2004) Increased expression and processing of caspase-12 after traumatic brain injury in rats. *J Neurochem* **88:** 78-90.

(159) Stennicke HR, Salvesen GS. (1998) Properties of the caspases. *Biochim Biophys Acta* **1387:** 17-31.

(160) Cohen GM. (1997) Caspases: the executioners of apoptosis. *Biochem J* **326 (Pt 1):** 1-16.

(161) Boatright KM, Salvesen GS. (2003) Mechanisms of caspase activation. *Curr Opin Cell Biol* **15:** 725-731.

(162) Liou AK, Clark RS, Henshall DC, Yin XM, Chen J. (2003) To die or not to die for neurons in ischemia, traumatic brain injury and epilepsy: a review on the stress-activated signaling pathways and apoptotic pathways. *Prog Neurobiol* **69:** 103-142.

(163) Fan TJ, Han LH, Cong RS, Liang J. (2005) Caspase family proteases and apoptosis. *Acta Biochim Biophys Sin (Shanghai)* **37:** 719-727.

(164) Nakagawa T, Zhu H, Morishima N, et al. (2000) Caspase-12 mediates endoplasmic-reticulum-specific apoptosis and cytotoxicity by amyloid-beta. *Nature* **403:** 98-103.

(165) Momoi T. (2004) Caspases involved in ER stress-mediated cell death. *J Chem Neuroanat* **28:** 101-105.

(166) Rao RV, Peel A, Logvinova A, et al. (2002) Coupling endoplasmic reticulum stress to the cell death program: role of the ER chaperone GRP78. *FEBS Lett* **514:** 122-128.

(167) Yoneda T, Imaizumi K, Oono K, et al. (2001) Activation of caspase-12, an endoplastic reticulum (ER) resident caspase, through tumor necrosis factor receptor-associated factor 2-dependent mechanism in response to the ER stress. *J Biol Chem* **276:** 13935-13940.

(168) Nakagawa T, Yuan J. (2000) Cross-talk between two cysteine protease families. Activation of caspase-12 by calpain in apoptosis. *J Cell Biol* **150:** 887-894.

(169) Goll DE, Thompson VF, Li H, Wei W, Cong J. (2003) The calpain system. *Physiol Rev* **83:** 731-801.

(170) Huang Y, Wang KK. (2001) The calpain family and human disease. *Trends Mol Med* **7:** 355-362.

(171) Morishima N, Nakanishi K, Takenouchi H, Shibata T, Yasuhiko Y. (2002) An endoplasmic reticulum stress-specific caspase cascade in apoptosis. Cytochrome c-independent activation of caspase-9 by caspase-12. *J Biol Chem* **277**: 34287-94

(172) Fujita E, Kouroku Y, Jimbo A, Isoai A, Maruyama K, Momoi T. (2002) Caspase-12 processing and fragment translocation into nuclei of tunicamycin-treated cells. *Cell Death Differ* **9:** 1108-1114.

(173) Xu C, Bailly-Maitre B, Reed JC. (2005) Endoplasmic reticulum stress: cell life and death decisions. *J Clin Invest* **115:** 2656-2664.

(174) Aoyama K, Burns DM, Suh SW, et al. (2005) Acidosis causes endoplasmic reticulum stress and caspase-12-mediated astrocyte death. *J Cereb Blood Flow Metab* **25:** 358-370.

(175) Hong SC, Lanzino G, Goto Y, et al. (1994) Calcium-activated proteolysis in rat neocortex induced by transient focal ischemia. *Brain Res* **661:** 43-50.

(176) Paxinos G, Watson C. The Rat Brain in Stereotaxic Coordinates. New York: Academic Press, 1998.

(177) Loewy AD, Spyer KM. Central Regulation of Autonomic Functions. New York: Oxford University Press, 1990.

(178) Ryan PM, Bedard K, Breining T, Cribb AE. (2005) Disruption of the endoplasmic reticulum by cytotoxins in LLC-PK1 cells. *Toxicol Lett* **159:** 154-163.

(179) Wootz H, Hansson I, Korhonen L, Lindholm D. (2006) XIAP decreases caspase-12 cleavage and calpain activity in spinal cord of ALS transgenic mice. *Exp Cell Res* **312:** 1890-1898.

(180) Ford G, Xu Z, Gates A, Jiang J, Ford BD. (2006) Expression Analysis Systematic Explorer (EASE) analysis reveals differential gene expression in permanent and transient focal stroke rat models. *Brain Res* **1071:** 226-236.

(181) Yao H, Takasawa R, Fukuda K, Shiokawa D, Sadanaga-Akiyoshi F, Ibayashi S, Uchimura H. (2001) DNA fragmentation in ischemic core and penumbra in focal cerebral ischemia in rats. *Mol Brain Res* **91:** 112-118.

(182) Tan Y, Dourdin N, Wu C, De Veyra T, Elce JS, Greer PA. (2006) Ubiquitous calpains promote caspase-12 and Jnk activation during ER stress-induced apoptosis. *J Biol Chem* **281:** 16016-16024.

(183) Wang Q, Santizo R, Baughman VL, Pelligrino DA, Iadecola C. (1999). Estrogen provides neuroprotection in transient forebrain ischemia through perfusion-independent mechanisms in rats. *Stroke* **30:** 630-637

(184) Kii N, Adachi N, Liu K, Arai T. (2005) Acute effects of 17beta-estradiol on oxidative stress in ischemic rat striatum. *J Neurosurg Anesthesiol* **17:** 27-32.

(185) Bagetta G, Chiappetta O, Amantea D, et al. (2004) Estradiol reduces cytochrome c translocation and minimizes hippocampal damage caused by transient global ischemia in rat. *Neurosci Lett* **368:** 87-91.

(186) Tesarik J, Garrigosa L, Mendoza C. (1999) Estradiol modulates breast cancer cell apoptosis: a novel nongenomic steroid action relevant to carcinogenesis. *Steroids* **64:** 22-27.

(187) Ejima K, Nanri H, Araki M, Uchida K, Kashimura M, Ikeda M. (1999) 17beta-estradiol induces protein thiol/disulfide oxidoreductases and protects cultured bovine aortic endothelial cells from oxidative stress. *Eur J Endocrinol* **140:** 608-613.

(188) Lacroix M, Leclercq G. (2004) About GATA3, HNF3A, and XBP1, three genes co-expressed with the oestrogen receptor-alpha gene (ESR1) in breast cancer. *Mol Cell Endocrinol* **219:** 1-7.

(189) Clough GF. (2005) Microdialysis of large molecules. *Aaps J* **7:** E686-692.